Design and fabrication of a Planar Diffusion Chamber for bio-chemical applications

Final Year Project

by

Ivan Pérez Laka

Universitat Politècnica de Catalunya

New Jersey Institute of Technology

Advisor: Raquel Pérez Castillejos

Acknowledgment

I would like to take the opportunity to thank to all the people who have helped me during the development of this project. During this time I have grown as researcher but especially I have grown as person.

First of all, I would like to thank my family for their support during all these years of degree and because of understand my decision to travel so far from the beginning. Without them none of this would have been possible. I would also like to mention all the colleagues that I have been meeting during my period in UPC with who I spent a great time.

Especial gratitude to my advisor Raquel Pérez Castillejos, who always had time to help me and who after one year became a very good friend. Her support has been really helpful to carry out this project. I would also like to thank to all the people of the The Tissue Models Lab group of NJIT who helped me when I needed. They form a fantastic group and I will always remember the awesome time that we spent together; Isabel Burdallo, Anil B. Shrirao, Neha Jain and Olga Ordeig, part of this thesis has been possible thanks to you.

For their financial support I would like to thank *Fundación Vodafone España*, *Generalitat de Cataluña*, *Universitat Politècnica de Catalunya* and *Obra Social Bancaja*.

Finally I want to thank to *Escola Tècnica Superior d'Enginyeria de Telecumincació de Barcelona (ETSETB)* and *New Jersey Institute of Technology* for their institutional support and for gives me the opportunity to do this unforgettable journey.

Thanks to all of you.

Table of Contents

1 MOTIVATIONS AND OBJECTIVES 8

2 BACKGROUND INFORMATION 10

2.1 CELL COMMUNICATIONS FUNDAMENTALS 12
2.1.1 Basic concept of cell communication 12
2.1.2 Forms of intercellular signaling 13
2.1.3 Each cell responds to a specific extracellular signal molecules 15
2.1.4 Intracellular signal pathways 17
2.1.5 Shear stress phenomena 19
2.2 MOLECULAR COMMUNICATION SYSTEM 20
2.2.1 Nanotechnology 20
2.2.2 Overview of nanomachines 20
2.2.3 Communications among nanomachines 23
2.2.4 Communication systems 27
2.2.5 Conclusion and research challenges 31

3 MICROFLUIDICS 32

3.1 MEMS AND MICROFLUIDICS 34
3.1.1 History and context of microfluidics 35
3.1.2 Microfluidics and lab-on-chip devices 36
3.2 HYDRODYNAMICS OF MICROFLUIDIC SYSTEMS 37
3.2.1 The notion of the fluid particle and the viscosity 37
3.2.2 Reynolds numbers in microsystems 38
3.2.3 Flows in channels with rectangular cross-section 39
3.3 DIFFUSION 42
3.3.1 The origin of diffusion processes 42
3.3.2 Advection-diffusion equations and its properties 43
3.4 INTRODUCTION TO MICORFABRICATION 45
3.4.1 Current situation of microtechnologies 46
3.4.2 Photolithography 47
3.4.3 PDMS-Base molding 48
3.4.4 Sealing 49

4 FABRICATION AND CHARACTERIZATION OF A MICROFLUIDIC DEVICE: T-SENSOR 53

4.1 T-SENSOR 55
4.2 DESIGN 56
4.3 FABRICATION 57
4.3.1 Required materials 58
4.3.2 Fabrication process 58
4.4 EXPERIMENTAL CHARACTERIZATION 61
4.4.1 Data acquisition and image processing 64
4.5 THEORETICAL CHARACTERIZATION 66
4.5.1 1-Dimensional T-Sensor simulator 68
4.5.2 2-Dimensional T-Sensor simulator 71
4.6 RESULTS AND DISCUSSIONS 75
4.6.1 1-Dimensional simulator validation with theoretical results 76
4.6.2 1-Dimensional simulator validation with experimental results 79

5 FABRICATION AND CHARACTERIZATION OF A MICROFLUIDIC DEVICE: PLANAR DIFFUSION CHAMBER (PDC) 83

5.1 Microfluidic Diffusion Chamber 85
5.2 Design 86
5.3 Fabrication 87
5.3.1 Required materials 87
5.3.2 Fabrication process: chemical bonding 88
5.3.3 Fabrication process: mortar layer 90
5.4 Experimental Characterization 97
5.4.1 Data acquisition and image processing 99
5.5 Theoretical Characterization 102
5.5.1 2-Dimensional PDC simulator 105
5.5.2 1-Dimensional PDC simulator 106
5.6 Improving Device: PDC v2.0 107
5.6.1 Design 107
5.6.2 Fabrication: photolithography and surface oxidation by oxygen plasma 110
5.7 Results and Discussions 118
6 CONCLUSIONS AND FUTURE WORK 121
APPENDIX A 127
APPENDIX B 131
APPENDIX C 139
APPENDIX D 145
7 REFERENCES 157

1 MOTIVATIONS AND OBJECTIVES

Molecular communications are defined as those that use molecules as information carriers between transmitter and receiver. This type of communications is the one used by biological cells either in intra-cell communications or in inter-cell communications. In recent years there has been a growing interest by this type of communications driven by the development of nanotechnologies. Molecular communications is essential to communicate nodes and devices in networks at nanometric scale.

Molecular communications are a new investigation field with applications in biomedicine and in the development of technology at nano-level. For example a new treatment in the cure for cancer, specifically the metastases of it, is based on angiogenesis processes [1], which are based basically on molecular communications. Likewise, the future of the technology goes through the miniaturization of devices beyond the current micrometric scale. The next step is the nanotechnology, and a communication system that controls all devices of these sizes is needed. The current communication technologies such as electromagnetism or optics cannot be used on these scales; however molecular communications are intrinsically designed to this kind of sizes.

Useful systems to understand these molecular communication processes (either for technological or medical applications) are necessary. One of the motivations of this work is the interdisciplinary nature of this field that includes biology, chemistry, microfluidics or electronics. Understanding of cellular communications (which depends on bio-chemical processes) is a basic element in the study of molecular communications, because they are based on biological models. Technologies like microfluidics or microelectronic fabrication processes are the base of the fabrication of these systems.

The design and fabrication of devices capable to study these systems is the key to further progress in this promising field that molecular communications are.

The aim of this work is to fabricate a system based on diffusion molecular communications capable of supply different chemical signals at the same time to a culture cell avoiding unwanted issues due to the shear stress.

Javier Atencia in his work [2] designed a microfluidic device that was able to generate up to three different chemical gradients at the same time in a cellular culture cell. He could avoid all problems related with convective flows achieving very good

results. The main problem of this work was the complexity in the fabrication of the device (fabricated using glass wafers) and the difficulty to control its operation.

In this project we have proposed to fabricate a microfluidic device with the same conditions but using a completely different technology, being much easier its fabrication and its operation control. This multi chemical signal device could be used in analytical essays for medical applications or having an engineering point of view could be used to study the phenomenon of interferences in molecular communications.

This report is structured in seven sections. Firstly, in Chapter 2, the basic fundamentals of bio-cell communications and molecular communication systems are presented in order to clarify some concepts of systems that are based on molecular communications. The concepts defined in this section will be fundamental to understand the next sections.

Once this new scenario has been presented, in Chapter 3, the field of microfluidics is explained in detail. Fabrication of microfluidic devices is the main part of this work, so a complete understanding of the technology that describes their behavior and their fabrication processes is obviously necessary. In this section concepts about mechanical fluids or technologies of microfabrication are presented.

Since molecular communications are based on diffusion processes in Chapter 4, a microfluidic device, whose operating principle is the diffusion of particles, is presented, the **T-SENSOR**. In this section a T-Sensor is designed, fabricated and characterized in order to study the diffusion experimentally. This device is characterized either by experimental and theoretical results, showing different techniques of how this kind of systems have to be studied. A T-Sensor simulator is designed using MATLAB R2009 and validated using experimental results.

Chapter 5 is the most important section of this work. Since we have studied how to design, fabricate and characterize a microfluidic device such as a T-SENSOR, in this part the fabrication of the planar diffusion chamber. This chapter is divided in two parts; the first one consists in the design, fabrication and characterization of **PDC** in its simplest version. This device is made using a simple technique called “Scotch Tape Patterned Method” [3] used in Chapter 4. Although the results obtained with this device are very promising, we decided to improve it in the second part using more sophisticated techniques such as soft-lithography and oxygen plasma bonding. The process of master’s fabrication using photosensitive resists with lithography is explained in detail, and a theoretical characterization is made using the finite element solver COMSOL Multiphysics 4.0.

Finally the conclusions of this work are stated in Chapter 6.

2 BACKGROUND INFORMATION

In this section the basic concepts necessary to understand how molecular communications work is presented. The chapter is divided in three different sections. An overview of cell communications is explained in the first one that provides a biological perspective of molecular communications. The second section presents a point of view more technological, explaining the new field of nanonetworks that are strongly dependent on molecular communications.

2.1 Cell Communications Fundamentals

2.1.1 Basic concept of cell communication

Unicellular organisms have been present in the earth since long before multicellular organisms. The complexity of the mechanisms needed for the interaction in multicellular organisms is probably one of the reasons of their slow evolution. The cells have to be able to communicate with one other in a complex ways if they want to control their own behavior for the benefit of the unique organism.

The extracellular signal molecules are the fundamental piece in these communications. They are produced by cells which want to communicate with their neighbors or with cells further away. And also, an elaborate system of proteins that each cell contains enables it to react to a particular set of these signals in a specific way. Some of these proteins are the cell-surface receptor proteins, which bind the signal molecule; or the intracellular signaling proteins that distribute the signal to different parts in the cell. This distribution takes place through different intracellular signaling pathways, and at the end of each one there are target proteins, which react when the pathway is active changing the cell's behavior.

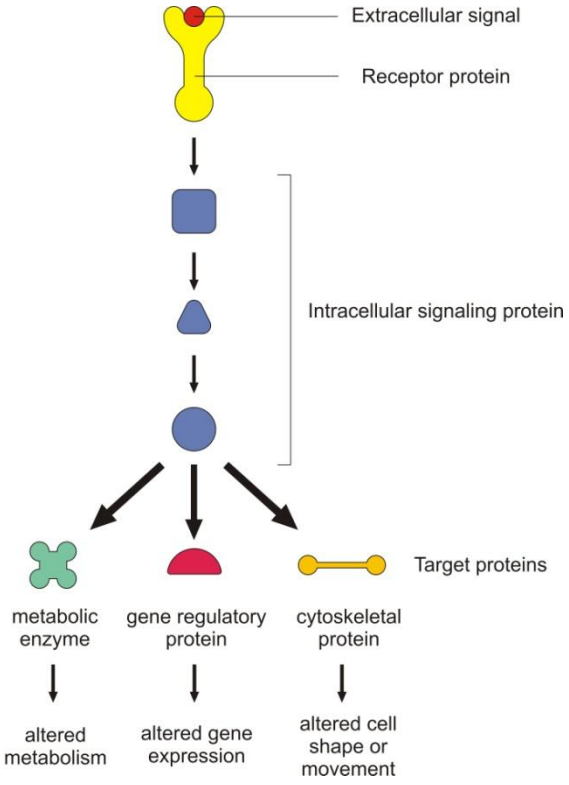

Fig. 2.1 Intracellular signaling pathway activated by extracellular signal.

Some unicellular organisms are able to communicate by secreting a few kinds of small peptides, but in higher multicellular organism communicate using hundreds of kinds of molecules. In most of the cases the signaling cell secretes the molecules to the

extracellular space by exocytosis (process by which a cell directs the contents of secretory vesicles out of the cell membrane). In other cases the molecules are released by diffusion through the plasma membrane, and in some others they are exposed to the extracellular space while remaining tightly bound to the signaling cell's surface.

The target cell detects the signal by means of receptors [4], a protein which binds specifically the signal molecule and this binding starts the reaction in the target cell. The extracellular signal molecules usually act at very low concentration and the receptor that detects them bind them with high affinity. In most cases this receptor proteins are on the target cell surface. The signal molecules (ligand) which are hydrophilic and then are unable to cross the plasma membrane directly, bind to cell-surface receptors, which in turn generate one or more signals inside the target cell that alter the behavior of the cell. Some small signal molecules can diffuse across the plasma membrane and bind to receptors inside the cell. This requires that the signal molecules be hydrophobic and sufficiently insoluble in aqueous solutions.

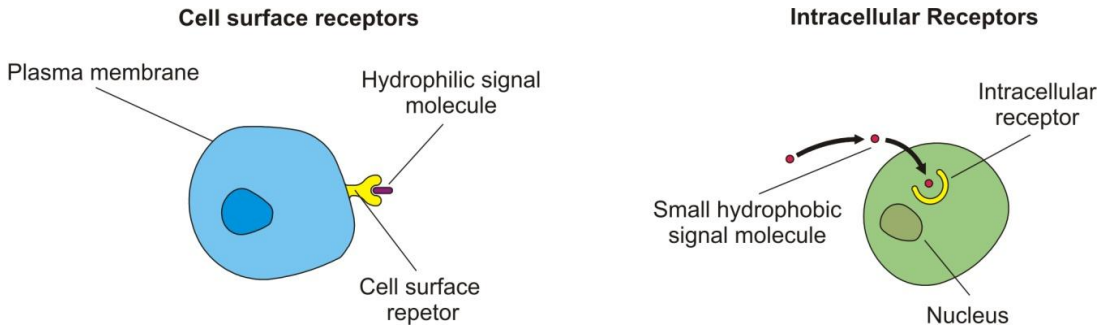

Fig. 2.2 The binding of extracellular signal molecules to either cell surface receptors (on the left) or intracellular receptors (on the right).

2.1.2 Forms of intercellular signaling

Cells have different ways to communicate [4]. In multicellular organism, the most "public" style of communication is the endocrine signaling. The signal molecules (called hormones in animal's cells) are secreted into the blood stream, which carries the information to the whole body. The cells that produce hormones are called endocrine cells. For example, part of the pancreas is an endocrine gland that produces the hormone insulin, which regulates glucose uptake in cells all over the body.

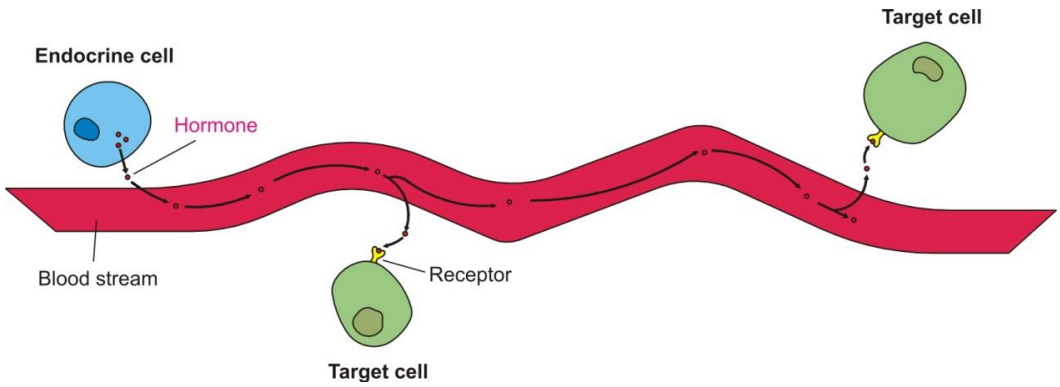

Fig. 2.3 Endocrine signaling.

The process known as paracrine signaling is less public than the endocrine signaling. In this case, signal molecules are secreted. The molecules secreted diffuse locally through the extracellular medium, affecting only cells in the immediate environment of the signaling cell. Thus they act as local mediators on nearby cells. The regulation of the inflammation process at the side on an infection is controlled using this kind of signaling.

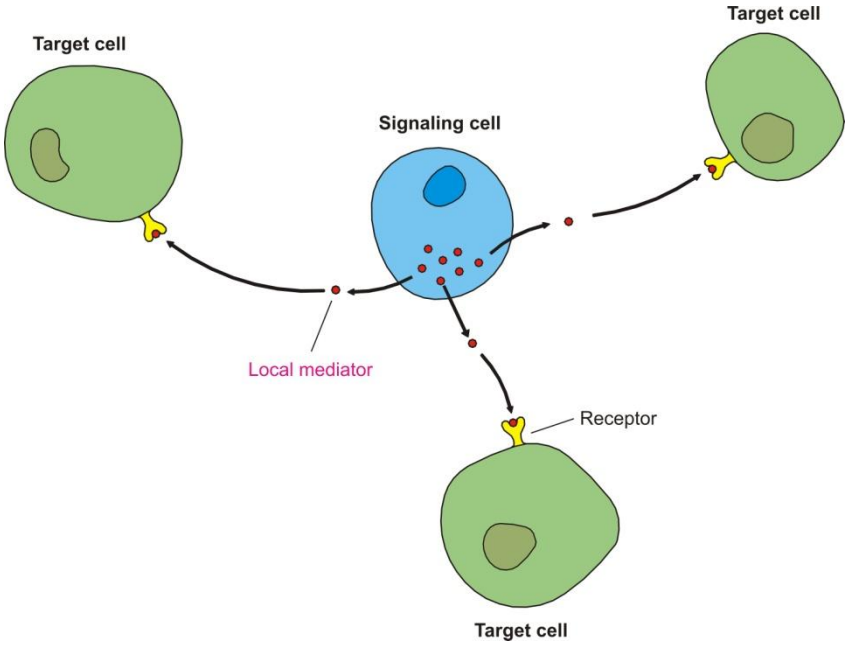

Fig. 2.4 Paracrine signaling.

The neuronal signaling is a sophisticated communication processes what such as happen in the endocrine signaling the message can be delivered across long distances. In this case, however, the message is delivered quickly to a specific target cell instead of broadcasted to the whole body. The specific cells called neurons, send electrical impulses rapidly along its axon (long part in the body of the neurons), and then, when the impulse reaches the end of the axon, it causes the secretion of a chemical signal

called neurotransmitter. This signal is secreted at specialized cell junctions called chemical synapse, which ensures that the neurotransmitter is delivered specifically to the postsynaptic target cell. The neurotransmitter diffuses across the gap between the axon-terminal membrane and the membrane of the target cell in less than 1 msec.

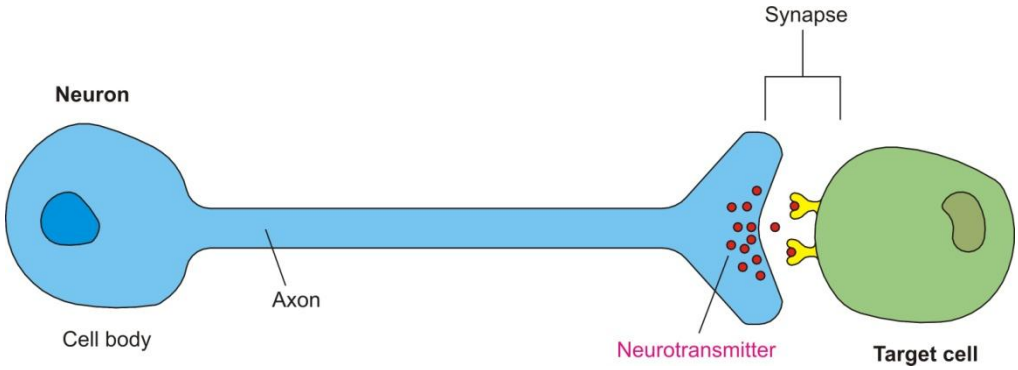

Fig. 2.5 Neuronal signaling.

Finally, when the cells are in physical contact it is not required the secretion of molecules to the extracellular medium. The message is delivered when the signal molecules are attached in the plasma membrane of the signaling cell, and they binds to a receptor embedded in the plasma membrane of the target cell. This process is called contact-dependent signaling and is important during development and in immune responses.

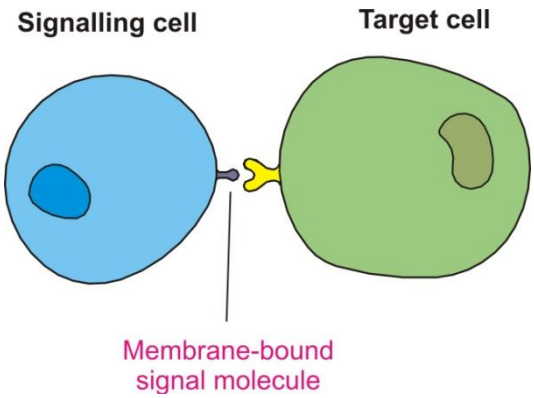

Fig. 2.6 Contact-dependent signaling.

2.1.3 Each cell responds to a specific extracellular signal molecules

In a multicellular organism the cells are exposed to a hundreds of different signals in its environment. These signals can be bound to the surface of a neighbor cell or they can be soluble in the extracellular fluid. Each cell must detect selectively some signals or ignoring others, according to their specialization function. A cell responds to a signal molecule if it has the specific receptor for that signal, otherwise the cell will ignore the presence of those molecules in the medium and will not react.

The cells restrict the amount of molecules that they can detect by producing a limited set of receptors out of the thousands that are possible. But even with this limited set of receptors, those signals are able to control the cell's behavior in a complex way. One signal binding to one receptor can cause many different effects in the target cell such as the movement of the cell or the alteration of the cell's shape. At the same time the cell's receptors can bind more than one molecule, and these signals, by acting together, can produce reactions that are more than the combination of the effects caused of each signals by their own. The intracellular transmission systems for the different signals interact, so the presence of one signal changes the reaction to another [4]. A cell may be programmed to respond to one combination of signals by differentiating, to another combination by multiplying, and to by doing a specialized task such as secretion or contraction. Even, most of the cells need the detection of a combination of signals simply to survive. In absence of these signals, the cells kill themselves; a process called apoptosis or programmed cell death.

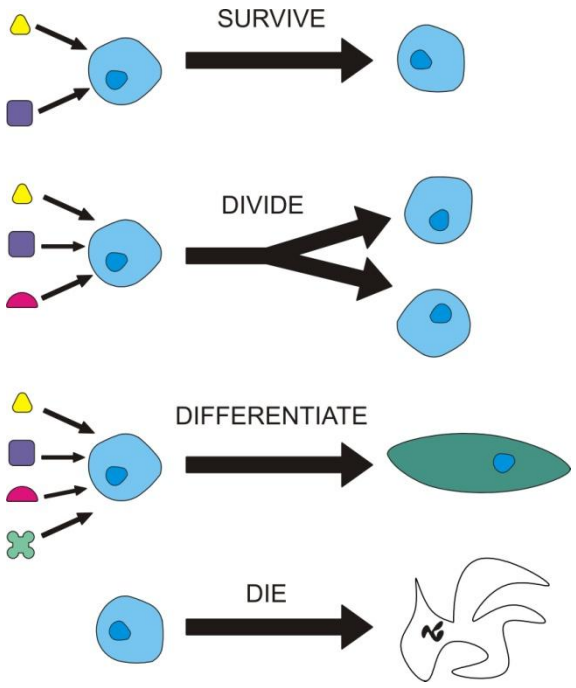

Fig. 2.7 Cell's dependence on multiple extracellular signals.

A cell can respond in many different ways to its environment. It depends on the set of receptor proteins the cell possesses, which determines the different set of signals that it is able to detect. And also it depends on the intracellular process, which understands the signals that it receives. Thus, a single molecule often has different effects on different targets cells. For example the neurotransmitter acetylcholine is detected by the skeletal muscle cells, they begin to contract. But when the heart muscle is exposed to the same neurotransmitter the rate and force of its contractions decrease. This happens because the acetylcholine receptor proteins on the heart muscle cell are different from those on the skeletal muscle cells. But these differences in the receptors are not the only reason

this success. It is perfectly possible that the same signal molecules binds to the same receptor proteins in two different types of target cell, and yet produce a very different responses. The receptor protein in the salivary gland is similar to the receptor protein presents in the heart muscle cells, but in this case, the gland secretes components of saliva instead of decrease the contraction.

2.1.4 Intracellular signal pathways

When a signal molecule binds with a receptor protein the signal reception begins. The receptor does the first transduction; it receives an external signal and generates a new intracellular response [5]. This is the first step in a chain in which the message passes from one intracellular signal to another, activating and generating the next intracellular signal, until arrive to a metabolic enzyme which execute some action, or to a gen regulatory protein, or to a cytoskeletal protein, changing the cell's configuration. This final result is called the response of the cell. These signaling cascades in the intracellular signaling have some important functions as:

- They are the responsible in the transduction of the signal into a molecular form appropriate to be transmitted through the cell.
- They relay the signal from the point where it is received to the point where the response will be produced.
- The signaling cascades can distribute the signal in order to affect different process at the same time. At any step in the pathway the signal can be relayed to other targets creating complex responses.
- The signal received can be amplified by the signaling cascades. With this few extracellular signal molecules are enough to start the intracellular response.
- All the steps in this cascade are susceptible to be modulated so the effects of the signal can be adapted to the conditions either inside or outside the cell.

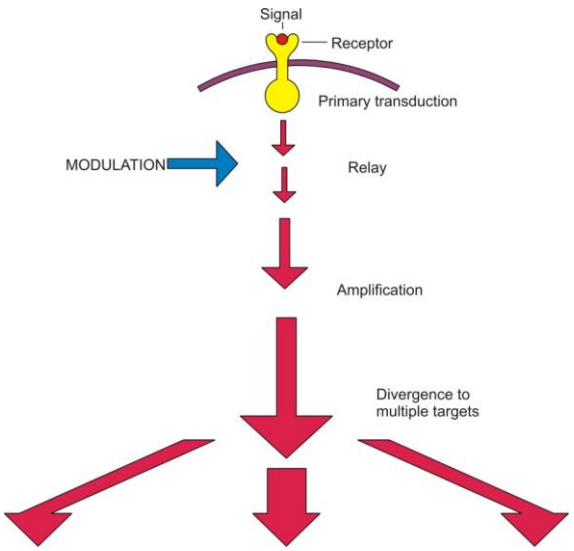

Fig. 2.8 Cellular signaling cascades.

Signaling pathways are usually long and with a lot of branches. Therefore, many intracellular parts are affected by the information received by the receptors at the cell surfaces. In these cases the molecules are too large or too hydrophilic to cross the plasma membrane of the target cell. Because of this they have to bind on the receptors at the cell surface to relay the message across the membrane. But it is also true that some signal pathways are more direct. This happens when the molecules are small enough and hydrophobic enough, they are able to cross the plasma membrane directly; Fig. 2.2.

2.1.4.1 Many intracellular signaling acts as molecular switches

One of the keys in the intracellular signal pathways lies in how fast an extracellular signal molecule evokes a response inside the cell. Some cellular responses are smoothly graded in simple proportion to the concentration of the molecule. This happens when the molecules bind to a single molecule receptor and the intracellular target reacts independently to each binding. As the concentration of molecules increases, the concentration of activated receptors increases proportionally, as does the number of complexes bound to specific intracellular targets. The response of the cell is then linear and gradual. Otherwise, in many cases, the responses to extracellular signal molecules begin more abruptly as the concentration of the molecules increases. Sometimes even occur almost as molecular switches, being undetectable below a threshold concentration and then reaching a maximum as soon as this concentration is exceeded. There are several reasons why this may happen; when an intracellular signaling molecule activates one enzyme and, at the same time, inhibits the enzyme which catalyzes the opposite reaction the responses become sharper. In other cases it is require more than one intracellular complex bind to some target macromolecule to induce a response. When this happen the responses become sharper as soon as the number of cooperative molecules increases, and as the number is getting larger responses like all-or-none type can be achieved.

All-or-none threshold responses usually depend on positive feedback mechanism; nerve and muscle cells generate all-or-none action potential in reaction to neurotransmitters.

These chemical switches can be in the active or inactive state. Once one of the steps in the pathway is activated it can turn on some other steps, and this activation can persist in an active state until some other process switches them off again.

2.1.4.2 Memory in cells. The cells can remember the effect of some signals

The effect of an extracellular signal on a target cell can persist well after the signal has disappeared [4]. The positive feedback process is one type of mechanism that represents this kind of persistence. If this system has been switched on by increasing the concentration above a threshold this system remains activated even after the disappearance of the signal; instead of reflecting the real level of signal, thus the

response system displays memory. Some of these changes can even persist for the rest of the life of the organism. They usually depend on self-activating memory mechanisms that operate in the last steps in the signaling pathway, at the level of gene transcription. For example, the signals that determine if a cell has to become a muscle cell turn on a series of muscle-specific gene regulatory proteins which produce many other muscle cell proteins. In this way, the decision to become a cell muscle is made permanent.

2.1.5 Shear stress phenomena

Most of cells are able by themselves to detect and react to mechanical forces. These may influence on the cell's behavior either in a good or in a bad way.

The blood vessels that conforms the cardiovascular system are made by endothelial cells. It unique location makes them able to detect and respond rapidly and sensitively to mechanical conditions created by blood flow and cardiac cycle. There is a strong correlation between endothelial cell dysfunction and areas with low mean shear stress [6].

Instead, autocrine and paracrine cells, may present unwanted effects under shear stress situations. This convective flux may remove the signals secreted by this kind of cells [2], and bias on the direction of the cellular migration [7] as well as to provoke asymmetrical mass transport [8].

The shear stress is always a phenomena that has to be token in care during experiments with cells.

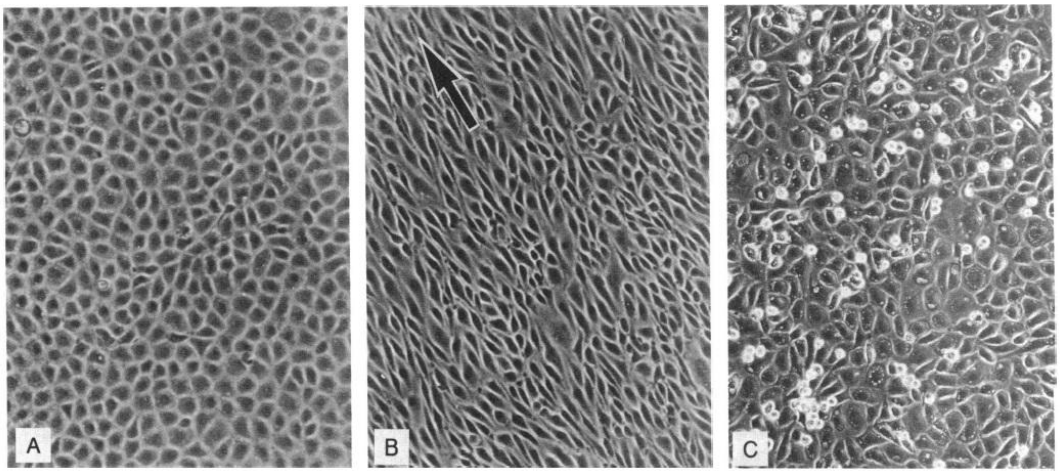

Fig. 2.9 Morphological changes in endothelial cell induced by exposure to shear stress. (A) Static culture under no flow conditions. (B) Alignment of cells following the direction of the flow (indicated with the arrow) under conditions of laminar shear stress. (C) No alignment of cells under condition of turbulent shear stress [9].

2.2 Molecular Communication System

2.2.1 Nanotechnology

The cell communication system exposed in the chapter above is one of the solutions for nano-scale communications scenarios. These systems based on the molecular signaling may be one of the keys for the development of the nanotechnologies. In this new situation appears the figure of the nanomachine, which is, at nano-scale, the most basic functional unit. Nanomachines represent tiny devices consisting in a group of molecules which are able to perform simple tasks such as computation, sensing or actuation. The interconnection between these nanomachines makes possible their cooperation and the exchange of information increasing the capabilities of a single nanomachine. Molecular communication provides a mechanism for one nanomachine to encode or decode the information into molecules and to send information to other nanomachines.

The interconnection of these nanomachines becomes in nanonetworks, and they improve their capacities in the following ways:

- Provides a larger workspace to the nanomachines, which is extremely limited for a single one. Nanonetworks will allow dens deployments of interconnected nanomachines. Thus, larger applications scenarios will be enabled.
- Allows the connection over large areas where the control of a specific nanomachine is difficult because of its small size. By means of broadcasting and multihopping nanonetworks can interact with remote nanomachines
- Nanomachines such as nano-valves, nano switches or nano memories, cannot execute complex task by themselves. The network performed by the connection between these nanomachines will allow them to work in a cooperative manner achieving more complex tasks.

Nanomachines cannot be built yet, but they exist in the nature in the form of biological cells and the chemical processes within those cells. The bionanotechnology is advancing quickly, until the actual point where engineering of biological systems is possible. It has been demonstrated [10] that the modification of the DNA can give a new functionality to a cell. As the bionanotechnology becomes more mature, the study of the molecular communications can be applied in the design of more complex nanomachine systems.

2.2.2 Overview of nanomachines

A nanomachine is defines as a device consisting of nanometer-scale components that performs a useful function at nano-level, such as communicating, data storing, sensing and actuation or computing. The tasks that a single nanomachine can achieve are very simple because of its low complexity and small size.

As it has said before, the fabrication of these nanomachines is still a very promising field in research, but with the exception of the found in the nature, it is not possible to built artificial nanomachines yet. There are three different approaches for their development; the top-down approach in which the nanomachines are developed by means of downscaling the already existing microelectronic technologies. The bottom-up approach consists in the design of nanomachines from molecular components, which are assembled using chemical principles of molecular recognition. Recently has appeared a third approach called bio-hybrid that is based on the use of existing biological nanomachines as models or components for the development of new nanomachines.

2.2.2.1 Nanomachine architecture

The architecture of a nanomachine depends strongly on its complexity. It can be from simple molecular switches up to complete nanorobots. In general a regular nanomachine should include the following architecture components [11]:

- Control unit. The control unit executes the instructions to perform the intended tasks, and all the components of the nanomachines can be controlled by this unit in order to achieve this purpose.
- Communications unit. The communications unit is a transceiver capable of transmitting and receiving messages at nano-scale.
- Power unit. The goal of the power unit is supply all the components of the nanomachine, by obtaining energy from external sources such as light or temperature and store it for a later distribution and consumption.
- Sensor and actuators. In the same way as the communications unit the sensors and actuators acts as interfaces between the environment and the nanomachine.
- Reproduction unit. In many applications the capability of replicate the nanomachine using external elements may be very useful. This is the aim of the reproduction unit. It fabricates each component of the architecture using external elements, and then assembles them to replicate it.

Currently such complex nanomachine cannot be built. However, systems found in the nature like living cells have similar architectures. According to the bio-hybrid approach, the biological cells have served as a template from which we are learning to build nanomachines. Similar to the architecture of a nanomachine, a cell contains the following components:

- Control unit. The chromosome within the nucleus contains all the instructions to realize the intended cell functions.
- Communications unit. The gap junctions and the receptor proteins located on the plasma membrane act as molecular transceivers for cell-cell communications.
- Power unit. For the power generation cells can include different nanomachines such as the mitochondria, that generate most of the chemical substances used as energy in the cellular processes, and the chloroplast, that converts sunlight into chemical fuel.

- Sensors and actuators. Several sensors and actuators are included in a cell such as the olfactory sensor (smell) or the flagellum which provides a method of locomotion to the cells.
- Reproduction unit. In the biological cells, the code of the nanomachine is stored in molecular sequences, which are duplicated in the cell division. The resulting cells contain a copy of the original DNA sequence.

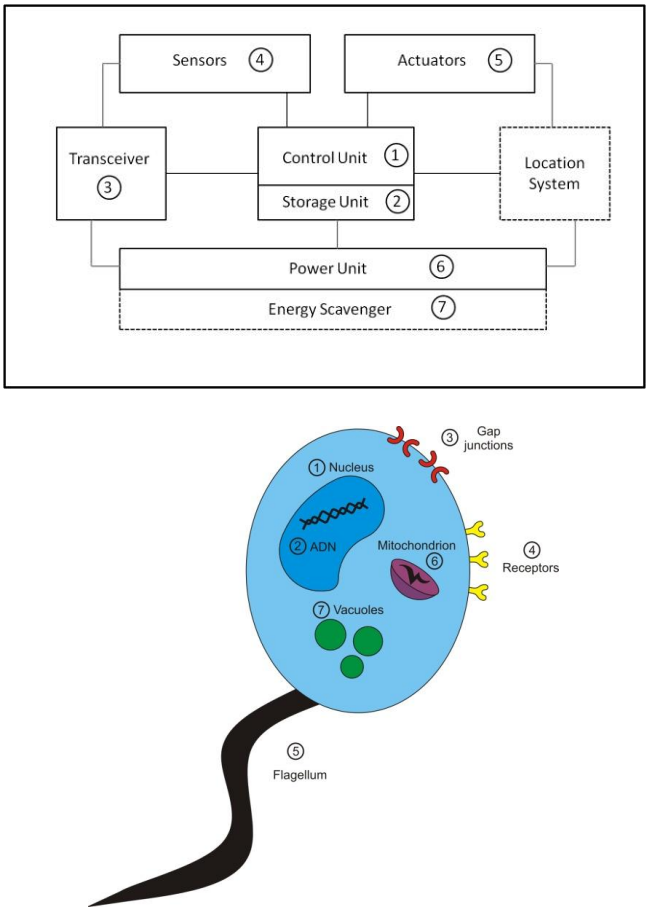

Fig. 2.10 On the top functional architecture of a nanomachine, on the bottom biological architecture of a cell.

The bio-hybrid approach, in addition to be used to develop nanomachines, is very useful as a means to understand their interactions. These interactions, controlled by molecular communication techniques, are essential because their understanding is the key to explore their capabilities to achieve more complex tasks in a cooperative manner.

2.2.2.2 Desirable features of nanomachines

As we have seen desirable features of nanomachines are presents in living cells. For example, nanomachines will have a set of instructions or code to realize specific tasks embedded in their molecular structure, or they will be able to read them from another molecular structure in which the instruction set is stored. The ability of a nanomachine could make a copy of itself would be interesting. In order to achieve this goal, a nanomachine would need the features of self-assembly and self-replication. Self-assembly is defined as the process in which several disordered elements form an

organized structure without external intervention. A nano-level this happens naturally due to the molecular affinities between two different elements. Self-replication is defined as the process in which a device makes a copy of itself using external elements. Self-maintenance is another feature very interesting to be considered as well as the locomotion, which would provide the ability to move from one place to another at a nanomachine. Communication among nanomachines is one of the most desired features. It is required to realize more complex tasks in a cooperative manner, and also a nano-to-macro interface with which to access and control the nanomachine.

From the point of view of communication, cells act as multi-interface devices. Cells have hundreds of receivers and are able to communicate using multiple unique channel access techniques such as ligand-recptors or gap junctions. Besides, the cells can be using these mechanisms simultaneously. All cells have a very sensitive transducing signal mechanism. The signal is detected by the receptor, which amplify the signal, integrate the signal with the input received by other receptors, and transmit the resulting signal to the cell. Therefore, a nanomachine should have these features that characterize signal transduction [12]:

- Specificity. Specificity is the ability to detect and react to a specific signal. The signal and the receptor are complementary. The specificity quantifies the precision with which a molecule fits in a complementary receptor, where other signals do not fit.
- Amplification. Amplification is the ability to increase the magnitude of a signal. Amplification by enzyme cascades can amplify a signal in several orders of magnitude within milliseconds.
- Desensitization. Desensitization is the ability to remove the molecules of the signal once this is received.
- Integration. Integration is defined as the ability of a system to receive multiple signals and integrate them into only one, producing the suitable response of the nanomachine.

2.2.3 Communications among nanomachines

Nanonetworks are communication networks which exist mostly at nano-level scale. The nanonetworks achieve the functionally and performance as the macro-scale networks using nodes of nanometers and channels physically separated by up to hundreds or thousands of nanometers. Besides, nodes are supposed to be rapidly deployable and mobile, and also are assumed to be self-powered.

Nanonetworks, such as all the other networks have all the features analogous communication networks. The information must be collected, coded, transmitted, received, decoded and delivered to the appropriate target. Thereby, all the concepts presented in the information theory apply in nanonetworks including bandwidth, compression, error detection and correction.

Since nanonetworks provides to the nanomachines a support on which establish a communication system, two different bidirectional scenarios appear:

- Communications between two or more nanomachines.
- Communications between a nanomachine and a larger system such as electronic micro-device.

Different communication technologies have been proposed to approach each scenario [13] electromagnetic, acoustic or molecular.

The electromagnetic waves have been used for communications since long time, and actually are the most common technique to interconnect microelectronic devices. The losses for these waves are minimal along wires or through air. However, in the nano-scale scenario, wiring large quantity of nano-machines is unfeasible. In this case, wireless technology could be an alternative. In order to establish bidirectional communication, a radiofrequency transceiver would have to be integrated in the nanomachine. Nano-scale antennas can be built for very high frequency communications, but due to the size and the complexity of the transceivers, they cannot be easily integrated in nanomachines yet. In addition, even if this integration could be realized, the nanomachine could not have enough output power to establish a bidirectional communication. Because of that, electromagnetic communication could be used to transmit information from a micro-device to a nanomachine, but not in the opposite direction.

Acoustic communications are based in the transmission if ultrasonic waves, air pressure waves. In the same way to the electromagnetic communications, the acoustic communication would need the integration of ultrasonic transducers in the nanomachines. These transducers are obviously needed to sense the variations of pressure produced by the ultrasonic waves and also to emit acoustic signals. The issue in this case is exactly the same that in the previous case, the size of these transducers makes impossible their integration in the nanomachines.

Molecular communication is established when the information is encoded using molecules. Molecular communication is a new and interdisciplinary field which includes knowledge in nano, bio and communication technologies. Unlike previous communication techniques, in this case the integration of transceivers in the nanomachine is not an issue because of the intrinsic size of the molecular transceivers. These transceivers are nanomachines which are able to react to specific molecules, and to release others as a response to an internal command. Molecular communications can be used to interconnect different nanomachines, resulting in nanonetworks which increase the capabilities of a single nanomachine.

2.2.3.1 Features of molecular communication

The nanonetworks, as it has said previously, expand the capabilities of a single nanomachine, but in addition, represent a potential solution for some applications

where the current communication networks are not suitable. Compared to actual communication network technologies, nanonetworks have the following advantages [12]:

- Biocompatibility: This is defined as the capacity of a device to operate in biological environments without affecting them negatively. Inserting nanomachines into the human body for medical applications requires nanomachines that are biologically friendly. Functions as receiving, interpreting, and releasing molecules would provide to biological nanomachines a mechanism to interface directly with natural processes. Thus, it would not be necessary to include harmful inorganic chemicals. In addition, nanomachines and molecular messages may also be programmed to be broken down after use to avoid procedures for removal or cleanup of devices
- Scale: The reduced size of the nanomachines and the resulting nanonetwork components are a very interesting goal in systems where the dimensions of the system are critic.
- Information representation: Molecules can represent the information using different ways, such as their chemical structure, relative positioning or concentration. Thus, molecular information provides different methods for manipulating and interacting with the information since operation performed are non-binary.
- Energy efficiency: In terms of energy consumption, chemical reactions are highly efficient. These reactions could power nanonetwork nodes and processes. In addition, chemical reaction can represent computation and decision processes, which usually take multiple operations.

2.2.3.2 Traditional communication networks and nanonetworks

The emergence of nanonetworks has implied the development of a new paradigm which is much more complex than a simple extension of the traditional communication networks. Especially due to the size, most of the communication processes are inspired by biological systems found in nature and because of that there are some differences between nanonetworks and traditional communication networks [11]:

- In nanonetworks the message is encoded using molecules instead of electromagnetic, acoustic or optical signals which are used by the traditional communication networks. There are two different and complementary techniques to encode the information in nanonetworks. The first, called molecular encoding, uses internal parameters of the molecule -such as chemical structure, polarization or relative positioning- to encode the information. In this case the receiver has to be able to detect these parameters in order to decode the information. This technique is similar to the use of encrypted messages, in which only the specific receivers are able to decode the information. The second technique uses temporal sequences to encode the information, such as the

temporal concentration of a specific molecule in the medium. Depending on the concentration, the receiver decodes the information in one way or another. This technique is similar to those used in traditional communication where the information is encoded in time-varying sequences.

- Most of the processes in nanonetworks are chemical reactions with low power consumption. In traditional networks, the communication processes consume electrical power which comes from batteries or from external sources such as electromagnetic induction.
- In traditional communication networks, the noise is known as an unwanted perturbation overlapped with the wanted signals. In nanonetworks, according to the molecular encoding techniques the noise can be described in two different ways. The first, as occurs in traditional communication systems, is an overlapping of the molecule signal with some other molecules of the same type. This means, another source emits the same molecules used to encode the message, affecting the concentration sensed by the receiver. The second source of noise in nanonetworks can be understood as undesirable reaction between the information molecules and other molecules present in the medium. Those reactions can modify the structure of the information molecules and then the receiver would not be able to detect the message.
- The propagation speed of signals used in traditional communication networks is much faster than the propagation of molecular messages. In nanonetworks, the information molecules have to be physically transported from the transmitter to the receiver. In addition, molecules can be subjected to random diffusion processes and environmental conditions, such as temperature, that affects the propagation of the molecular message.

Type of communication	***Traditional***	***Molecular***
Signal type	*Electronic or optical*	*Chemical*
Communication carrier	*Electromagnetic waves*	*Molecules*
Noise	*Electromagnetic fields and signals*	*Molecules in medium*
Encoded information	*Voice, video, text, images...*	*Chemical states, phenomena, processes..*
Propagation speed	*Light (3e8 m/s)*	*Very low*
Medium conditions	*Wired: Almost immune* *Wireless: Affect communication*	*Affect communication*
Energy	*High energy consumption*	*Low energy consumption*

Table 2.1 Main differences between traditional communication networks and nanonetworks enabled by molecular communication [14].

2.2.4 Communication systems

Several solutions for molecular communications have been proposed depending on the distance between emitter and receiver. Different approaches have been taken in order to cover distances spanning from nanometers to tenths of meters [12].

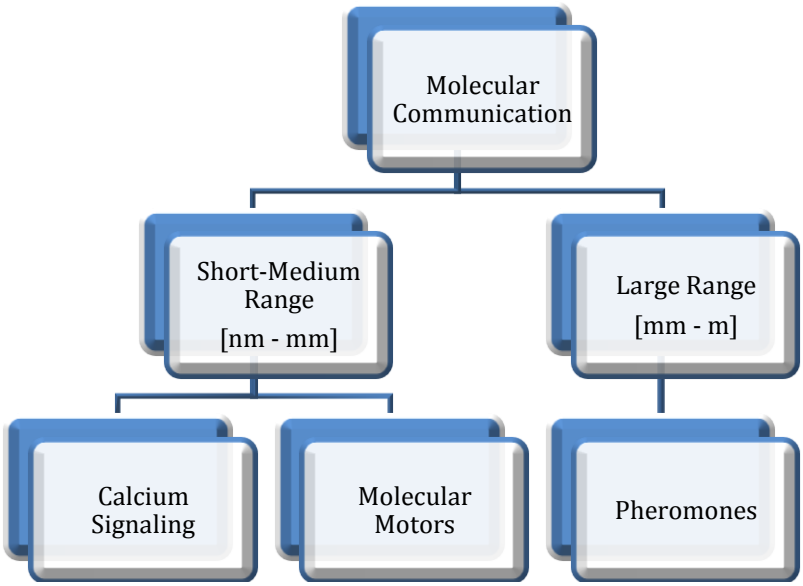

Fig. 2.11 Molecular Communication Systems.

2.2.4.1 Calcium signaling

Cell-cell communication based on calcium signaling is one of the most important molecular techniques [15, 16]. It is responsible for many coordinated cellular task, such as, contraction, secretion or fertilization**.** This signaling process is used in two different scenarios, when two cells are in physical contact, or when there is not this physical dependence.

The propagation of the signal is driven by a chemo-signal pathway, in which one messenger transports the information until certain point in the pathway where the information is transferred to another messenger. This transmission from one messenger to another continues until the information reaches its destination. This process is explained in more detail in the previous chapter “Intracellular signal pathways”. As it is presented there, this system has some important advantages, especially the possibility to amplify the information at different levels of the chemo-signal pathway. The ligand-receptor binding principle is the most important process in this information transfer between messengers. As it is explained before, this process consists in the bounding between to molecules (the information molecule, or ligand, and the protein receptor) resulting in a local reaction, which in turn can trigger other process.

When cells are physically separated the information molecule binds to the receptors placed on the cell membrane. This binding generates an internal signal which can be decoded by cell components.

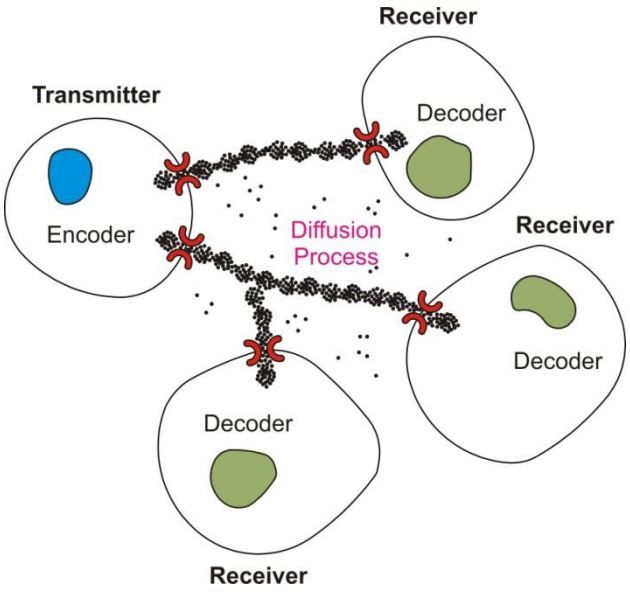

Fig. 2.12 Signal propagation in calcium signaling communication systems by diffusion.

In this case the information molecule is considered as the first messenger, while the internal signal is considered as the second messenger. The first messenger in the signal that transports the information outside the cell while the second messenger is the signal which transports the information inside the cell. Membrane receptors transforms first messenger into second messengers by chemical reactions.

If cells are located next to each other, existing physical contact between them, they can be connected through gap junctions. These biological gates allow molecules and ions to pass from one cell to another.

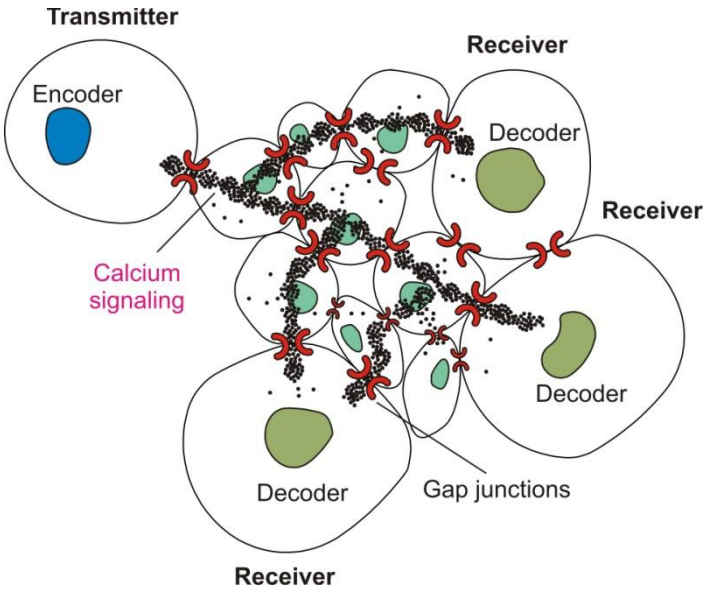

Fig. 2.13 Signal propagation in calcium signaling communication systems by gap junctions signal forwarding.

In this case the information travels along cells using only second messengers such IP3 (inistor 1,4,5-triphosphate) without intervention of first messengers. IP3 is a messenger that propitiates the secretion of calcium ions (Ca^{2+}) by cell organelles. Therefore, diffusion of IP3 through gap junctions propagates waves of Ca^{2+} along the interconnected cells.

The propagation of Ca^{2+} is very complex task in which several cell components participate in order to make this signal propagation possible. Ca^{2+} buffers or reservoirs are needed inside the cell when it needs to release molecules to the medium, or when it is passing those molecules through the gap junctions to the next cell. These buffers can be certain proteins of the cytoplasm and organelles such as the endoplasmatinc reticulum. Also ion channels located on the cell membrane are involved in this process, maintaining this finite resource.

Calcium signaling provides a method to maintain neighboring cells interconnected. Using calcium signaling surrounding nanomachines can receive a message sent it only from one nanomachine, in a similar way that is done in traditional communication networks in processes such as multicasting or broadcasting.

2.2.4.2 Molecular motors

Similar to the calcium signaling, the communication systems based on molecular motors are used in tiny scenarios. They cover the necessities in short-ranges from nm to a few μm. Molecular motors are used in most of the intra-cellular communications and they are proteins that converts chemical energy into mechanical work at nano-scale [17].

The information molecule is carried on the motor, in this move directionally along cytoskeletal tracks. Inside the cells, molecular motors are aimed to transport molecules among organelles. They travel along molecular rails performs a complete railway network inside the cell for intra-cell substance transportation.

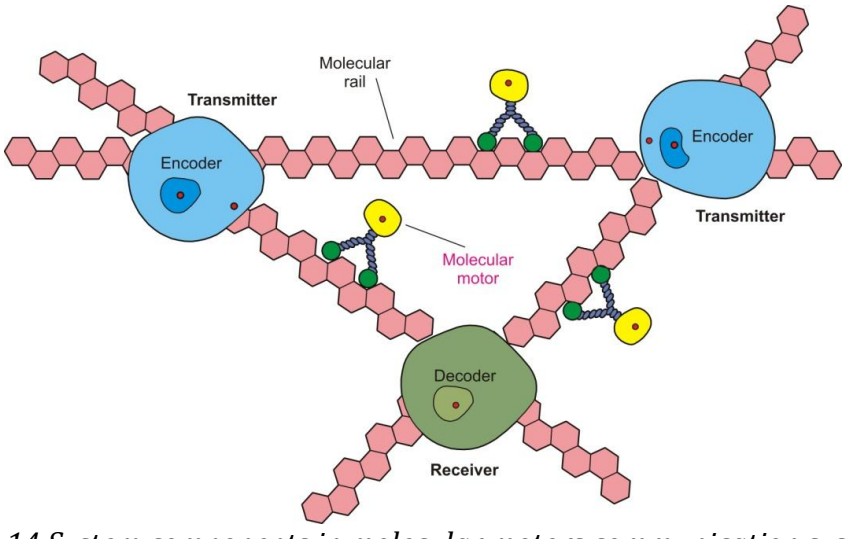

Fig. 2.14 System components in molecular motors communication systems.

This communication system includes one transmitter and only one receiver. The ability to move molecules makes molecular motors a feasible way to transport information packets. But this system applied in nanonetworks should be able to adapt to more complex scenarios. In this case techniques as multi-hoping would be needed and because of that the nanomachines should be able to amplify, decode and redirect the information.

2.2.4.3 Pheromones

Pheromones are a system very useful when the distance between transmitter and receiver nanomachines ranges from mm up to km. Nanonetworks in long-range scenario are also inspired in biological systems found in nature. Many animals such as butterflies, bees, many mammals or ants use pheromones in their communications. Butterflies use pheromones and molecular messages can reach the range of a few kilometers [12].

Communication using pheromones is similar to the techniques based on the release molecules that can be detected by a receiver. Once the molecules are released to the medium, they can be affected by factors, temperature, medium flow, antagonist agents, and the can be considered as noise sources.

Probably, the most important feature in this kind of log-range communication system is the coding system. In the nature only the animals of the same species can detect the pheromones in the air. While in traditional communication networks, the information is usually encoded in a binary system, in pheromone systems the information is encoded in the molecule itself. The messages can be encoded using different molecules which imply more combinations to encode the information.

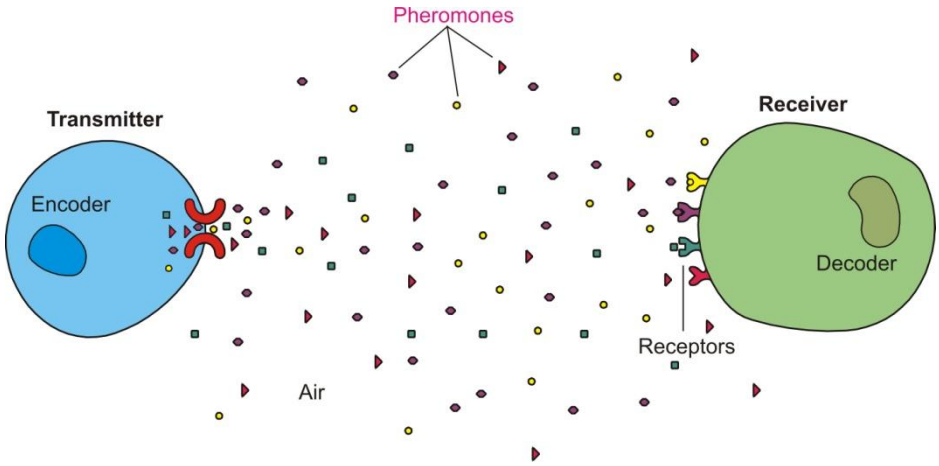

Fig. 2.15 System components in pheromone communication systems.

The reception of the transmitted molecules is realized by molecular receptors located on the receiver. In a similar way to the calcium signaling scenarios, the process is based on the ligand-receptor binding. In molecular communication using pheromones, the receptor proteins can be considered as the receiver nanomachine antenna, which transforms energy contained in the message into a reaction at the receiver.

2.2.5 Conclusion and research challenges

The study of cellular communications is basic in the development of reliable communication techniques at nano-scale. Sciences such as biology, chemistry, electronics or communication sciences converge in nanotechnology, creating a new multidisciplinary science. Biology and chemistry describe the processes in the nature which yield in the development of functions at nano-scale. Engineers should be able to model such processes with the purpose of create devices with the same characteristics.

Paracrine communications used by cells, and especially those driven by mean of calcium ions signaling, are an interesting point of study to understand the communications at nanometric scales. This work pretends to design a microfluidic system based on the process of diffusion of particles. This study could be highly useful in the developing of communication systems in nanomachines or at the same time their medical applications are very promising.

3 MICROFLUIDICS

In this chapter it is presented in detail the field of microfluidics, a science that will be needed in the understanding of all this work. Here are explained concepts related with mechanical fluids and micro technologies techniques.

Microfluidics is the study of flows that are simple or complex which are circulating in artificial microsystems [18].

In the recent years, important progress has been made in the field of miniaturization. Nowadays is completely feasible to miniaturize many kind of systems – e.g. mechanical, electromechanical, fluidic or thermal- to micrometric scales. In the 1980s, due to these achievements, a new field known as MEMS (microelectronic-mechanical systems) showed up. Later in 1990s these systems began to be used in many different fields, being manufactured MEMS for chemical, biological and biomedical applications. These systems utilized fluid flows operating in unusual and unexplored conditions, which inevitable led to the creation of a new discipline known as microfluidics.

In microfluidics the systems manipulate small amounts of liquids, from 10^{-18} to 10^{-9} liters, using channels with dimensions of tens to hundreds of micrometers [19]. It takes advantage of its most obvious characteristic, small size, but also it exploits a less obvious characteristic of fluid in microchannels, the laminar flow.

Microfluidics offers a number of interesting capabilities such as the ability to use very small quantities of samples, low cost or short time of analysis which are very useful in analysis applications. It offers fundamentally new capabilities in the control of concentration of molecules in space and time.

3.1 MEMS and Microfluidics

Miniaturization and MEMS gave birth to microfluidics in the 1990s and today still constitute a large portion of this young discipline. MEMS are electromechanical systems whose total size varies between 1 and 300μm. Since sixteenth century with the invention of the optical microscope the world at micrometric scale has been studied hardly. The microscope allowed many scientific discoveries such as Brownian motion, chromosomes, and protozoa However is far more difficult to act at microscopic scale, which is exactly what MEMS technology allows us to do. Many discoveries and technical inventions have been made possible thanks to the MEMS.

Sometimes these advances became large industrial successes such as the usage of MEMS in airbag activation. MEMS for airbags appeared in the 1980s, and they consist of an integrated system on a silicon wafer that is just a few millimeters long. The detection of the physical impact is made by a portion which is only a few hundreds of micrometers large and constitutes the heart of the chip.

A second major industrial success came in the 1990s with the advent of MENS usage for inkjet printer heads.

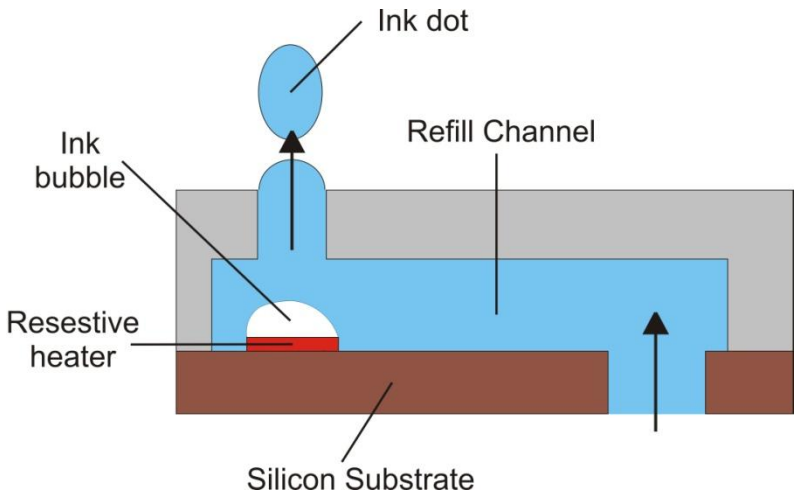

Fig. 3.16 Printed head of a commercial inkjet made using MEMS technology.

The printer head consists of a portion microfabricated from silicon that serves as an ink reservoir, a heating element to put the fluid in motion and a nozzle. The fluid is pushed through the nozzle due to the formation of a bubble near the heating element; this bubble is generated by the vaporization of the ink.

The volume of MEMS activity is estimated to be worth in several tens of billions of dollars. It was expected in 2010 that would have at least five MEMS devices per person in use in the United States. Today, there are a numerous industries involved in MEMS.

3.1.1 History and context of microfluidics

In the period when silicon-based MEMS began to take off, there were no technical obstacles in making simple microfluidic systems [20]. Thus, the first miniaturized gas chromatography system was created around 1975 [21].

This remarkable device circulated gas through microchannels etched in silicon. This achievement was an isolated one, most likely because the science community was not ready to develop silicon technologies for its own needs.

It was only after 1991 that the advantages of miniaturization reach the application of chromatography, and all sorts of microfluidic systems began to be fabricated. Appearing chronologically were electrophoretic separation systems [22], electro-osmotic pumping systems [23], diffusive separation systems [24], micromixers [25], DNA amplifiers [26] and chemical microreactors [24] just to cite a few examples.

During this period of time, microfluidics was being used to deal with fundamental physical questions. In 1993 the first experiments involving the stretching of DNA [27] were made using a microfluidic system to control the viscous stretching force applied to the molecule. This experiment founded a new domain of fundamental research, the study of the single molecule.

The first microfluidic product commercializes on a large scale was the inkjet printer head described before. Today tens of millions of inkjet printers use MEMS and billions of documents are printed thanks to microfluidics. By parallelizing ejection heads, it is possible to construct droplet dispensers, which are strongly used for chemical and biological analyses.

Droplet dispensers at this time are a substantial part of commercial activity in the field of microfluidics. Chips are produced massively allowing a large number of test running in parallel that provides a large amount of data achieving precise characterization of products.

Microfluidic systems do not normally use moving parts (micropumps and microvalves are a rare counterexample) and this is a significant simplification with respect to non-microfluidic MEMS. Microfluidic systems have become simpler technologies, faster and less expensive than silicon technology. Due to the absence of moving parts and the relative ease and accessibility of many of these technologies, it has become possible to integrate several elements on the same chip and to create **lab-on-chip** devices. Microfluidic MEMS and related technologies that have no moving parts, the integration of different components has since opened a wide range of possibilities.

3.1.2 Microfluidics and lab-on-chip devices

The possibility of integration has made possible the rapid expansion of the field of microfluidics. The ultimate objective is to be able to detect biological molecules, and transport, mix and characterize a raw sample, all with only one device. Achieving this would require miniaturizing systems such as cytomers, separators, and bioreactors, and then connecting them together. This field of integrated analysis systems is known as μTAS (*micro-total-analysis-systems*), or also lab-on-chip systems.

In 1994 a group of researchers achieve the integration in a single chip of three different functions: the mixing of reactants, enzymatic reaction, and separation [28]. During the last few years researchers have come up with all sorts of solutions to improve and simplify the manipulation of fluids on-chip. Some devices have been already commercialized. In 1998 the company Biosite commercialized the system “Triage Cardiac” which could take a drop o blood from a patient and diagnoses whether or not the patient had suffered a heart attack. The system transported the blood by capillary force across a filter and analyzed the blood in a functionalized microchannel. The principle of the test is based on the detection of three proteins that are produced in abnormal quantities once a heart attack has taken place.

Lab-on-chip devices have become in a basic element in the research of physical phenomena that occur at micrometric scale. Miniaturization have permitted that these devices are able to integrate several components into a single chip, have provide the capability to fabricate portable devices, have allowed their mass fabrication reducing their production cost and have increased their rapidity of getting results. For the first

Biosite chip, a diagnosis was achieved in 15 minutes, while traditional systems needed several hours.

3.2 Hydrodynamics of Microfluidic Systems

In microfluidics, systems present unique problems in hydrodynamics due to the significant role of surfaces, the presence of Brownian motion, and more generally, the unusual force balances. We are presenting below some of the most important aspects of the physics involve in microfluidics that will be helpful to understand the work done in this project.

3.2.1 The notion of the fluid particle and the viscosity

At small scales spatial fluctuations in density take place due to the molecular structure of the fluid; while at the scale of the system, density can evolve with respect to the spatial position, the presence of temperature variations or the presence of a system with inhomogeneities.

The **fluid particle** is defined as a volume containing a large number of molecules. For simple fluids one can assume that the fluid particle has a size of a few nanometers. Thus this fluid particle is typically much smaller than a microchannel, and fundamental hypothesis of hydrodynamics can be applied without difficulty. For nanochannels with a transverse dimension of just a few tens of nanometers, this situation must be re-considered. In this case we enter in the field of nanofluidics that is still a very new research field.

The physical representation of **viscosity** is that of trucks filled with sacks of coal, circulating around at slightly different velocities. The drivers continually exchange sacks between the two trucks. Due to the exchange of momentum, the two trucks will have a tendency to adopt identical speeds, just as if they exerted a “friction” force on one another.

For liquids, the situation is quite different. Liquids possess the effect of having a certain crystalline order over short distances (smaller than a nanometer) while still remaining disordered over large distances. Molecules must cross an energy barrier to leave from the “cage” formed by their immediate neighbors, and exchange momentum with a fluid layer moving at a different velocity. The calculation leads to the following form the viscosity of simple liquids:

$$\mu = A \cdot e^{\left(\frac{E}{kT}\right)} \qquad (3.1)$$

Where A is a constant and E is energy. This reasoning assumes that the idea of viscosity only applies to liquids confined in systems whose size is many times the size of the intermolecular distance; many times greater than a nanometer. We find here another nanofluidic problem.

3.2.2 Reynolds numbers in microsystems

In fluid mechanics, the Reynolds number is the ratio between the inertial forces and the viscous forces, and quantifies the relative importance between these two types of forces.

$$Inertial = \frac{\rho \bar{v}^2}{d} \qquad (3.2)$$

$$Viscous = \frac{\mu \bar{v}}{d^2} \qquad (3.3)$$

Where ρ is the density of the fluid (kg/m^3), $\bar{v}$ is the mean velocity of the fluid (m/s), d is the characteristic length of the flow (m) and μ is the dynamic viscosity of the fluid (kg/m·s).

This dimensionless number can be used to characterize different flow regimes, such as laminar flow or turbulent flow. For low values of the Reynolds number (less than 2300 [29])the fluid flows in a laminar way, on the other hand for large values of this number (more than 10000 [29]) the behavior of the fluid is turbulent. Laminar flow is characterized by smooth, constant fluid motion. The motion of the particles of fluid is very orderly with all particles moving in straight lines parallel to the pipe walls [30], while turbulent flow tend to create vortices, chaotic eddies and other flow instabilities.

$$\mathrm{Re} = \frac{\rho \bar{v} d}{\mu} = \frac{\bar{v} d}{\upsilon} \qquad (3.4)$$

Where υ is the kinematic viscosity (m2/s). The characteristic length of closed channel flow is the hydraulic diameter of the channel:

$$d_h = \frac{4A}{P} \qquad (3.5)$$

Where A is the cross-sectional area and P is the wetted perimeter, the perimeter of the channel which is wetted by the fluid.

In microfluidic systems, typical fluid velocities do not exceed a centimeter per second and widths of canal are on the order of tens to hundreds of micrometers; therefore, in general, Reynolds number in microfluidic systems do not exceed 10e-1. In fact, we can say that a microfluidic system whose channels have one of the three dimensions (height, width or depth) lower than 100μm, always will work in laminar regime.

3.2.3 Flows in channels with rectangular cross-section

In the situation of two parallel planes close together filled with fluid the gap space between them. In fluid dynamics there are two ways of provoke movement in the fluid between the planes: by applying shear stress through the channel or by a playing a pressure gradient along the channel [31].

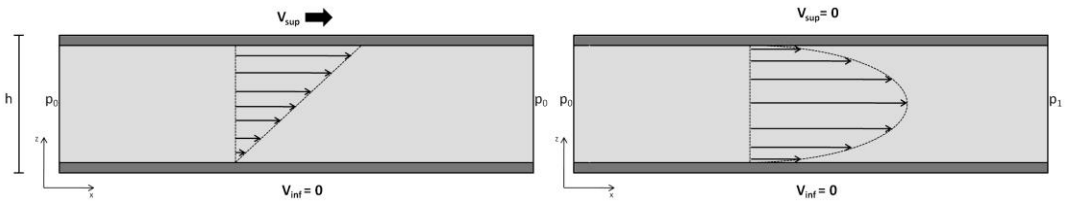

Fig. 3.17 On the left velocity profile applying shear stress of the superior plane. On the right, velocity profile applying a pressure gradient along the channel.

The second one, which is called *Poiseuille* flow, is the most common situation in microfluidic systems because in these systems the walls are usually resting in the same position.

The flow forced by a hydrodynamic pressure gradient is called Pressure-Driven Flow (PDF) and it is conditioned by the velocity of the channel walls. As it has been said before, in pressure-driven flow the walls are at rest forcing the velocity of the fluid at the channels walls is zero. On the other hand, the pressure applied to the fluid volume generates a uniform force over the whole cross-sectional area of the channel. The combination of the no-slip condition at the walls and the uniform force applied to the entrance provokes a parabolic velocity profile of the flow, that is, zero velocity at the walls and maximum a velocity at the center of the channel.

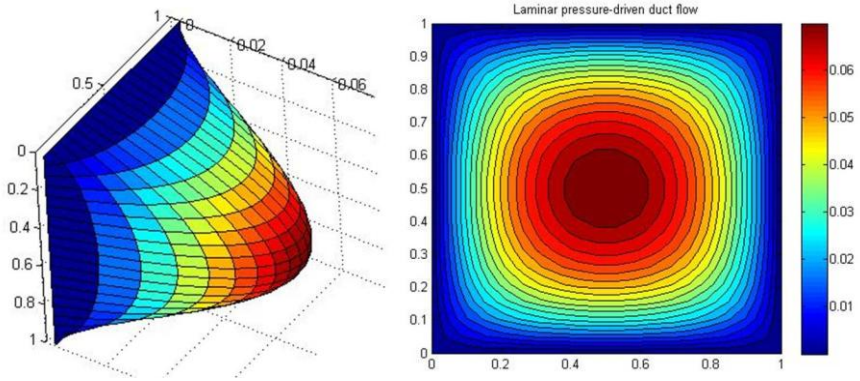

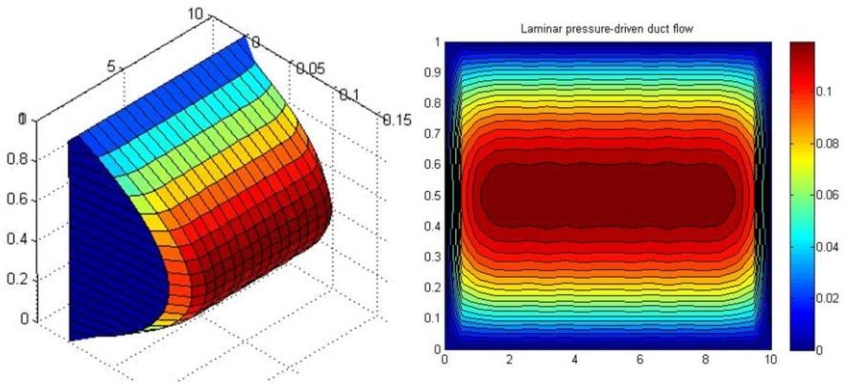

Fig. 3.18 Fluid velocity profiles within two rectangular ducts of different height:width ratios. On the top aspect ratio AR=1, on the bottom AR=10.

In laminar flow the particles of the fluid follow straight paths, so they do not cross each other. Thus, the flow may be considered as a series of concentric cylinders flowing over each other.

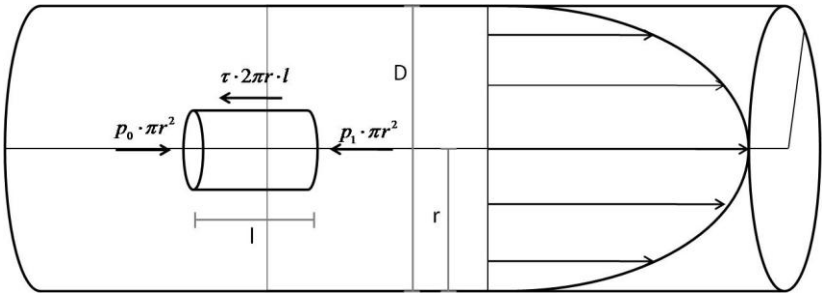

Fig. 3.19 Steady flow in a circular pipe.

The forces applied to a steady state laminar flow are in equilibrium conditions. In a horizontal pipe, the pressure force in the flow is balances by the shear stress force on the wall.

The shear stress is defined as an inertial force which is applied parallel to the liquid.

$$\tau = \frac{F}{A} \qquad (3.6)$$

Where τ is the shear stress (N/m2), F is the force applied (N) and A is the cross-sectional area (m2).

By the Newton's law of viscosity, the shear stress for laminar flow is linearly related to the fluid viscosity:

$$\tau = \mu \frac{\partial v}{\partial r} \qquad (3.7)$$

Hence, in equilibrium conditions:

$$F_0 - F_1\big|_{\text{Pressure}} = F_{Shear} \tag{3.8}$$

$$-\Delta P \cdot \pi r^2 = \tau \cdot 2\pi r \cdot l \rightarrow \tau = -\frac{r}{2} \cdot \frac{\Delta P}{l} \tag{3.9}$$

Combining the equations (3.7) and (3.9):

$$\mu \frac{\partial v}{\partial r} = -\frac{r}{2} \cdot \frac{\Delta P}{l} \tag{3.10}$$

And solving this simple differential equation, the velocity is:

$$v(r) = -\frac{1}{4\mu} \frac{\Delta P}{l} r^2 + C \tag{3.11}$$

And the integration constant C can be found using the no-slip at the walls condition v(r)=0 when r=R.

$$\begin{aligned} v(R) = 0 &= -\frac{1}{4\mu} \frac{\Delta P}{l} R^2 + C \rightarrow C = \frac{1}{4\mu} \frac{\Delta P}{l} R^2 \\ v(r) &= \frac{1}{4\mu} \frac{\Delta P}{l} \left(R^2 - r^2 \right) \end{aligned} \tag{3.12}$$

We can observe that the velocity has a parabolic relationship with the distance. Re-arranging the equation above:

$$v(r) = \frac{1}{4\mu} \frac{\Delta P}{l} \cdot R^2 \left(1 - \left(\frac{r}{R} \right)^2 \right) \tag{3.13}$$

The equation (3.13) shows that the velocity at the walls, $v\left(r = R\right)$, is 0, while the velocity at the center of the pipe, $v\left(r = 0\right)$ is maximum:

$$v_{\max} = \frac{1}{4\mu} \frac{\Delta P}{l} \cdot R^2 \tag{3.14}$$

Similar to the *Poiseuille* flow, the velocity profile in a pipe is also parabolic. Actually, the three dimensional flow has a velocity profile which a form of a paraboloid, having its maximum at the axis of the pipe, and its zeros at the walls. For non-circular three dimensional channels, the solution is not analytical so microfluidic devices have to be studied through simulation tools.

3.3 Diffusion

In lab-on-chip systems, it is usually necessary to mix reactants. For example, in biology in order to identify proteins in an unknown sample proteins are fragmented by mixing them with enzymes. Proteins can then be characterized using spectrometry analysis of the resulting fragments. But as we saw before, in microchannels the Reynolds number is always small so hydrodynamic instabilities and turbulences are practically non-existing. According to this, may seem difficult to mix fluids in a microchannel, but one of the solutions to solve this issue is based on the diffusion process.

3.3.1 The origin of diffusion processes

3.3.1.1 Brownian motion

In 1827 a botanist named Robert Brown showed for the first time the erratic behavior of the movement of pollen grains on the surface water. He had just discovered the Brownian motion. He suggested that this phenomenon might be related to the collisions between pollen grains and water molecules. The theory of Brownian motion and of molecular diffusion was studied much later, at the beginning of the twentieth century, for Langevin, Smoluchowshi and Einstein [32].

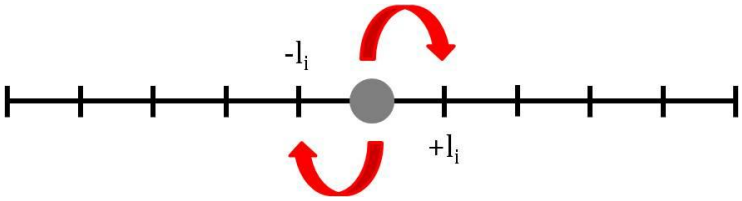

Fig. 3.20 Brownian particle along a line. The particle can take random steps of length l.

One dimensional Brownian motion can be explained by means of a particle moving in a line, taking steps of length $\mp l$ in a random way. This particle occupies a position $X(N)$ from the origin equal to the sum of all the steps, N that it has made:

$$X(N) = \sum_{1}^{N} l_i \qquad (3.15)$$

Where l_i is a random variable that can take the values $+l$ or $-l$ with the same probability. The squared value of the displacement of the particle would be:

$$X^2(N) = \sum_{1}^{N} l_i^2 = N \qquad (3.16)$$

The number of steps can be considered of a function of the time by means of a coefficient that specifies how easy is for this particle moving, the number of steps per time unit.

$$X^2(N) = N \approx Dt \qquad (3.17)$$

This coefficient D is known as **Diffusion Coefficient** or **Diffusivity**. This particle could do a large number of steps, but on average it would remain in the same place all the time.

In a two dimensional case the Central Limit Theorem establish that for long times, the distribution of particles in space would be Gaussian.

3.3.1.2 The Stokes-Einstein law

The Brownian model describes the behavior of molecules in a free environment, where the relevant events are collisions at localized sites. This model is useful to describe the process of diffusion of one gas into another. However, when the molecules are immersed in a dense environment (for example a liquid with a viscosity μ) the problem must be formulated in a different way. In this case the diffusing molecules can be described by the Langevin equation as follows:

$$\frac{\partial v_i}{\partial t} - \beta v_i = f(t) \qquad (3.18)$$

Where v_i is one of the three velocity components of the diffusing molecule, and β is a friction coefficient representing the friction exercised by the fluid on the particle. The function $f(t)$ includes in it the friction forces, its own inertia and stochastic forcing (translating to the presence of collisions).

The Stokes-Einstein law provides an estimation of the diffusion coefficient based on the size of the diffusing molecule. Usually this estimation is more accurate than the 30%. For example, the diffusivity of oxygen in water, taking 1.73 Å as the radius of the oxygen molecule has a value of $1.3e10^{-5}$ cm^2/s at 25°C [33]. This value is only 30% lower than the measured value, and thus the order of magnitude is well determined.

The Stokes-Einstein law is determined by the next formula [32]:

$$D = \frac{kT}{6\pi R\mu} \qquad (3.19)$$

Where R is the radius of the diffusing molecule assuming spherical shape and μ is the viscosity of the fluid. The formula becomes imprecise in highly concentrated solutions and in non-Newtonian fluids, such as polymers.

3.3.2 Advection-diffusion equations and its properties

3.3.2.1 Fick's first laws of diffusion

In microfluidics is very common to find situations where the particles in the liquid move inside it following diffusion processes.

Molecular diffusion is the thermal motion of all molecules at temperatures above absolute zero. This principle establishes that when in a certain point exists a non-uniform distribution of particles, then they tend to diffuse away in order to reach

uniform concentration through all the space [34]. Molecular diffusion can be also considered a specific case of random walk or Brownian motion, which is used to model the movement of particles suspended in a fluid.

Molecular diffusion is typically described using the Fick's laws of diffusion. The Fick's first law permits relate the net flux of particles to the concentration of particles, establishing that the flux goes from regions of high concentration to regions of low concentration, with a value proportional to the concentration gradient.

$$J\left(\bar{x},t\right) = -D\nabla C\left(\bar{x},t\right) \qquad (3.20)$$

J represents the net flux of particles in a specific position x and at a specific time t ($mol/m^2 \cdot s$). C is the concentration of particles (mol/m^3) and D is the diffusion coefficient or diffusivity (m^2/s). The diffusion coefficient is a parameter which specifies how "easy" is for a particle to move in a fluid. It provides the idea of the speed at which the particles move from positions with high concentration to positions with low concentrations. This coefficient depends strongly on the size of the particles. Small particles have high values of diffusivity while big particles provide low values of this parameter.

3.3.2.2 Fick's second law: Advection-Diffusion equation

The advection-diffusion equation formalizes the law of conservation of mass for an elementary volume. It predicts how diffusion causes the change of the concentration with the time. This law depends on the combination of the Fick's first law and the law of conservation of mass. The law of conservation of mass states that the particles cannot be created or destroyed, and thus, all the particles entering or leaving the global system must be the same.

In a first approximation, the variation of the particles concentration in time must be opposite to the gradient of the particle flux in the same location.

Hence:

$$\frac{\partial C\left(\bar{x},t\right)}{\partial t} = -\nabla J\left(\bar{x},t\right) \qquad (3.21)$$

And then, substituting the expression of the first Fick's law (3.20) into the law of conservation of mass (3.21) the Fick's second law is obtained:

$$\frac{\partial C\left(\bar{x},t\right)}{\partial t} = D \cdot \nabla^2 C\left(\bar{x},t\right) \qquad (3.22)$$

A more detailed expression for the Fick's second law takes into account two more terms that can affect in the ratio of appearance of disappearance of particles in the system.

The four terms are [35]:

- Rate of increase of particles per unit volume:

$$\frac{\partial C\left(\bar{x},t\right)}{\partial t} \qquad (3.23)$$

- Net rate of addition of particles per unit volume by convection:

$$\bar{v}\cdot\nabla C\left(\bar{x},t\right) \qquad (3.24)$$

- Rate of addition of particles per unit volume by diffusion:

$$-\nabla J\left(\bar{x},t\right)=D\cdot\nabla^2 C\left(\bar{x},t\right) \qquad (3.25)$$

- Rate of production or elimination of particles per unit volume by reactions:

$$R\left(\bar{x},t\right) \qquad (3.26)$$

Then, the variation of particles concentration is the result of the addition of molecules by convection, by diffusion or by reaction:

$$\frac{\partial C\left(\bar{x},t\right)}{\partial t}=-\left(\bar{v}\cdot\nabla C\left(\bar{x},t\right)\right)-\left(\nabla J\left(\bar{x},t\right)\right)+R\left(\bar{x},t\right) \qquad (3.27)$$

Arranging the previous equation and assuming the simplification that the diffusion coefficient is constant [35]:

$$\frac{\partial C\left(\bar{x},t\right)}{\partial t}+\bar{v}\cdot\nabla C\left(\bar{x},t\right)=D\cdot\nabla^2 C\left(\bar{x},t\right)+R\left(\bar{x},t\right) \qquad (3.28)$$

Where $\bar{v}$ is the velocity and R is the production or elimination (source or sink) of particles. There are two important: when the velocity is zero, then, the system works in a pure diffusion mode, while if the velocity is not zero, then, is the system is produces the dispersion phenomena.

The equation (3.28) is also known as the **Diffusion Equation**. It provides the value of the future concentration of particles in one point if the concentration in that point and in its vicinities is known.

3.4 Introduction to Micorfabrication

The most common technique of microfabrication of microfluidic systems is the one known as Soft-Lithography. It is based in two steps, the fabrication of a master using

lithography techniques, and the replica of this master by casting of some plastics or polymers.

The use of microelectronic techniques such as photolithography over silicon wafer to fabricate the master is especially due to two reasons. The first one is that the microelectronic fabrication techniques are a very well known source of knowledge in the fabrication of all kind of devices at micrometric scale. The second one is because of the low roughness of the silicon wafers (around 2nm [36]), which is essential in the replication of structures. The use of glass substrates is being used more frequently due to its characteristics of softness and its lower cost.

3.4.1 Current situation of microtechnologies

3.4.1.1 Different scales and their associated fabrication techniques

Ordinary fabrication or machining techniques produce objects of a size between 1 mm and a few decimeters. Currently, we have entered in the domain of traditional mechanical machining, whose precision is on the order of tens of μm. There are even machines that allow the production of metallic objects with a precision of tens of nanometers. The fact that these machines are dedicated exclusively to be used on metals reveals a significant limitation. Metal is not an appropriate material for analytical chemistry or biology, fields that prefers materials such as Teflon, glass or plastic. These machines are a great technological feat, but unfortunately they have a very limited usage in practice.

The domain of microfabrication involves scales such as a fabrication of a micrometer and the millimeter. These technologies can be divided in two categories: silicon technologies and “soft” technologies, which use materials like elastomers or plastics.

Nanometric scale can currently be obtained using variety of rapidly developing techniques. We know today how to isolate molecules and to use the, to achieve a specific function. Nanomanipulation techniques constitute the base for the approach bottom-up.

3.4.1.2 Hard, plastic, and soft microtechnologies

Currently we can differentiate between two different types of microtechnologies used in microfluidics, those technologies based on etching, lithography and deposition; and those based on “plastic MEMS”. The figure below represents the different types of microtechnologies depending on the size.

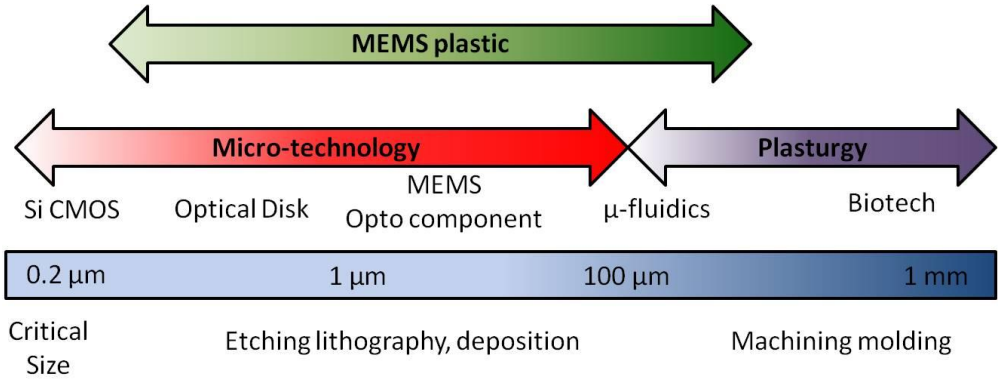

Fig. 3.21 Different types of microtechnologies.

Technologies based on etching, lithography and deposition can be applied in the range of scales between 0.2 and 500 µm. These are "hard" technologies, because they use hard materials such as silicon or glass. The combination of etching, lithography, and deposition techniques makes it possible to obtain complex microfluidic devices.

Plastic MEMS involves the range between 0.5 and 500 µm. These are the "soft" technologies. As materials they use elastomers such as PDMS (polydimethylsiloxane) or plastic materials lime PMMA (polymethylmetharylate). Depending on the material, plastic MEMS are made using a direct method or by replication methods.

Plastic technologies are attractive from the point of view of cost: by unit weight, current plastics are about 100 times less expensive than silicon. They are also attractive because of the possibility of fast prototyping. Some of them allow the development of a microfluidic circuit in just few hours, while silicon technologies require times typically on the order of a week.

3.4.2 Photolithography

One process that plays a central role in microfabrication is photolithography. It consists in the exposition of a photosensitive resist through a mask, which has been deposited on a substrate.

The photolithography **masks** are generally plates of quartz on which deposits of chrome form the pattern that is desired to replicate. Obviously is not possible to fabricate objects with geometric precision superior to that of the mask. These masks are often made using electron beams with a precision on the order of a fraction a micrometer. When this high precision is not required methods like high quality printout on a transparency can be used.

The mold will appear when the light through the mask cure the photosensitive resist. This resist is **deposited** in a thin layer on a solid substrate of silicon or glass. The deposit is made using a spin coater.

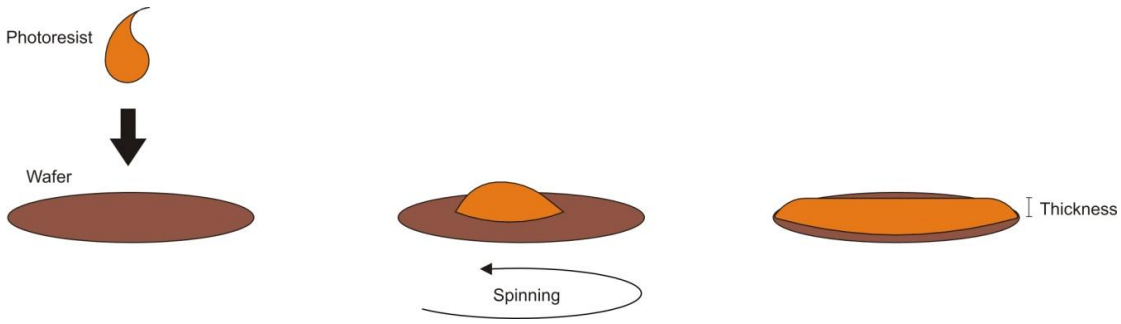

Fig. 3.22 Spinning process. Firstly a droplet of photoresist is poured over the wafer, after that the wafer starts turn obtaining finally the photeresist uniformly spreaded on the wafer.

This piece of equipment consists in a disk that turns at high velocities and allows the spreading of a drop of liquid initially deposited in the center of the disk. The thickness of the layer spread can be controlled changing the rotation speed of the disk. Over the last few years, highly photosensitive polymers such as SU-8 or AZ-series resists have been selected to create structures on glass or silicon substrates.

Once the resist is deposited, the film is **exposed** to a luminous flux produced by a source crossing the mask. In this way dark and light zones appear on the polymer, forming the same pattern that had been designed on the mask. Basically, the light initiates chemical reactions in the polymer, which modify the solubility in certain solvents. There are two types of resists, positive and negative.

- **Positive resist**. The light zone become soluble in a particular solvent, the other zones remain insoluble. That means, the zones affected by the luminous flux are susceptible to be dissolved in presence of a specific solvent, while the zones that have been protected of the luminous flux remain without changes in presence of the same solvent.
- **Negative resist**. The light zones become insoluble in a particular solvent, while the other zones can be dissolved in that same solvent.

Thus, for positive resists, radiation across a mask defines the zones that will form holes in the resist film after the immersion in the solvent (this process is known as development), leaving the other parts of the film permanently polymerized. On the other hand, for negative resists, radiation across the mask defines zones that will remain after the immersion in the solvent, erasing the rest of the polymer that has not exposed.

3.4.3 PDMS-Base molding

Molding is one of the three methods of replication, molding, casting and microinjection. In this study only the molding method is described. A mix containing a catalyst and a polymer is poured on a mold and heated. After curing, the structure is peeled off the mold and it contains the pattern of the mold.

PDMS is a polymer thermo curable that plays a very important role in the fabrication of microfluidic structures. This polymer, when is heated beyond its polymerization temperature and in presence of a curing agent, forms a transparent elastomeric. There are three basic steps in the fabrication of a replica using PDMS-based molding: fabrication of the mold, pouring and curing and separation.

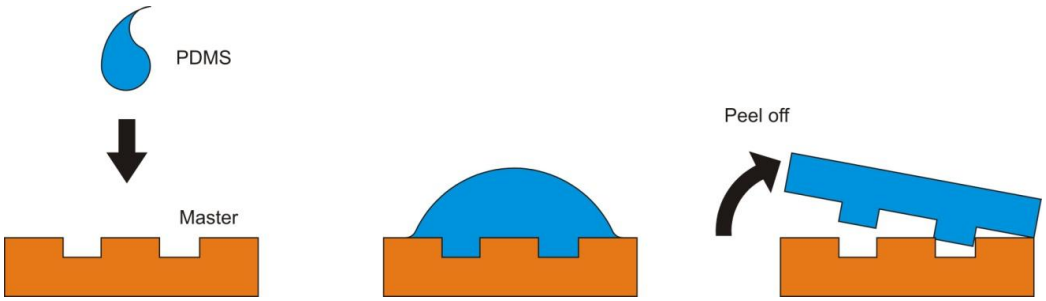

Fig. 3.23 Molding process. Firstly a droplet of polymer is poured over the master, after that the polymer is cured and finally the replica is separated from the master.

The mold is usually made using soft-lithography techniques, such as it is explained previously. A mix of PDMS and curing agent is poured onto the mold. The system is taken to a moderately elevated temperature (on the order of 65°C). During this phase the PDMS polymerizes, cures, and the mix becomes solid. After peeling off the PDMS and object representing the negative of the mold structure is obtained.

Some of the specific properties of PDMS are:

- Its transparency, which allows the visualization of flows.
- The elasticity of the material, which allows the fabrication of micro-valves or micro-pumps using flexible membranes.
- Hydrophobicity in untreated PDMS. It becomes hydrophilic after oxidation of the surface by oxygen plasma. Oxidized PDMS adheres by itself to glass, silicon or polyethylene, as long as those surfaces were themselves exposed to oxygen plasma.
- Permeability to gases such as oxygen or carbon dioxide.
- Non-toxic.

All of these characteristics have made PDMS the most used polymer in lab-on-chip systems.

3.4.4 Sealing

To form enclosed channels, we seal a PDMS replica containing a network of channels irreversibly to a flat surface. The sealing of microfluidic devices made using PDMS to substrates such as glass, silicon or other PDMS devices is a delicate process that has to be studied in detail.

There are sealing processes based on thermal or chemical processes, but the most used is the sealing by means of surface oxidation with oxygen plasma. In this section it will be presented the sealing methods PDMS-PDMS and glass-PDMS by surface oxidation and the PDMS-mortar sealing PDMS-PDMS because them are the two used in this work.

3.4.4.1 Plasma oxidizer

Polymers as PDMS can be bonded to glass or to other polymers by means of a surface activation using oxygen plasma. This bonding involves the oxidation of the two surfaces in contact, which increases the concentration of hydroxyl groups (-OH), making easier the formation of strong intermolecular bonds.

- **PDMS - PDMS**

PDMS belongs to a family of polymers that notably contain silicon oils. The formula of PDMS is $(-Si(CH_3)_2O)$. After the exposition, the surface activated with oxygen plasma changes its molecular structure, and the hydroxyl groups combined with the silicon present in the PDMS form silanol groups (SiOH).

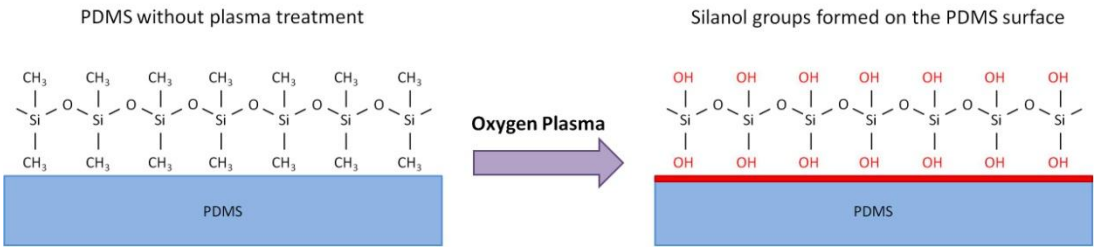

Fig. 3.24 Formation of silanol groups on the surface of PDMS after oxygen plasma treatment.

Once the two surfaces are treated with plasma they are put in contact, and with the appropriate conditions of temperature, a condensation reaction between the two PDMS surfaces is produced forming a covalent siloxane (Si-O-Si) bonds.

$$SiOH + SiOH \rightarrow (Si - O - Si) + H_2O$$

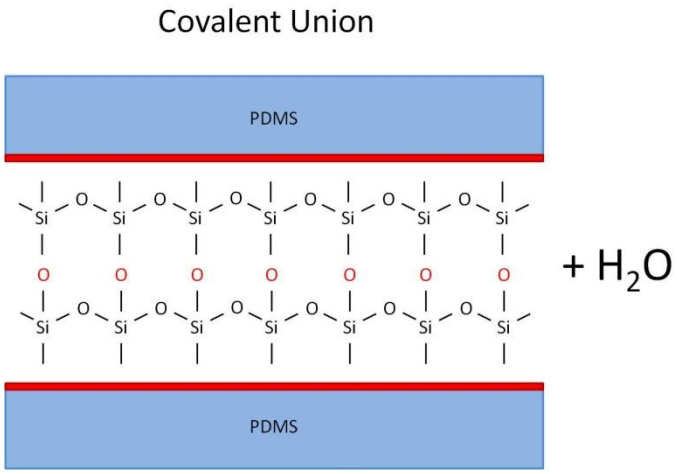

Fig. 3.25 PDMS-PDMS bonding by formation of siloxane groups (Si-O-Si).

This molecular union is irreversible, and an excessive force trying to separate the two pieces only would break the PDMS.

- **Glass – PDMS**

Silicate glass is non-crystalline solid material, which chemical composition is SiO_2. As it happened with the PDMS, the exposition to oxygen plasma would increase the concentration of hydroxyl groups, which combined with the silicon, would form silanol groups.

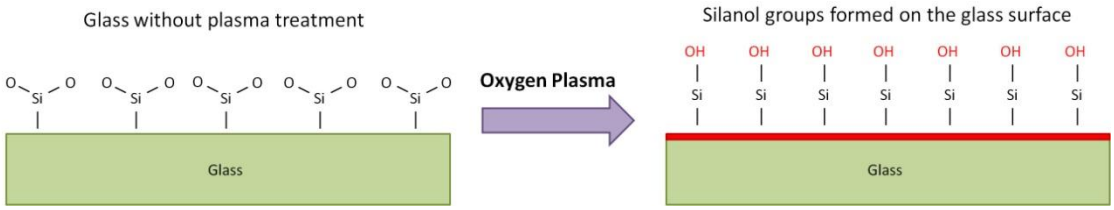

Fig. 3.26 Formation of silanol groups on the surface of glass after oxygen plasma treatment.

Treating glass and PDMS with oxygen plasma we form silanol groups in both surfaces, and putting in contact them we achieve a covalent siloxane bonding by means of the condensation reaction.

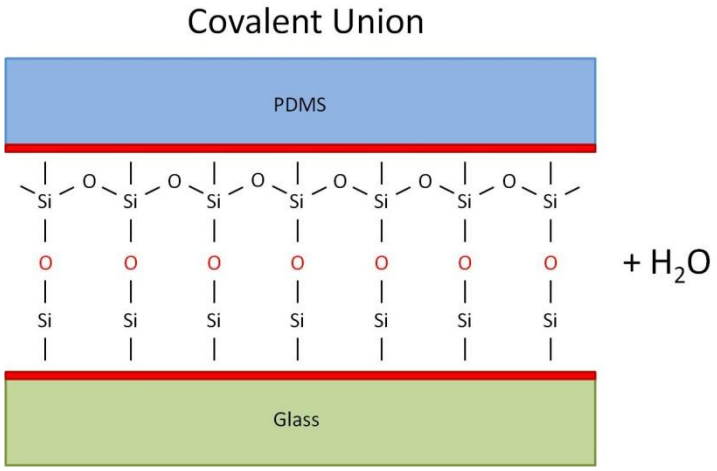

Fig. 3.27 Glass-PDMS bonding by formation of siloxane groups (Si-O-Si).

Once again, the molecular union between the PDMS and the glass is irreversible. This type of union is perfect in order to avoid leakage from the microchannels.

3.4.4.2 PDMS-mortar sealing

This method is useful when the bonding between two layers of PDMS must be done without a plasma oxidizer. It consists in using a thin layer of uncured PDMS as mortar layer between the two pieces of PDMS. Once this layer is cured, the molecular structure inside the PDMS is repeated taking molecules from the mortar layer. It acts as "glue" providing a strong bonding [37].

This mortar is usually done spreading uncured PDMS on a flat surface such as glass slide or a silicon wafer, using a spinner. The angular velocity imposed in the spinner controls the thickness of the mortar layer, which controls the bonding quality. Usually the best adhesion is achieved for bigger thickness, while for small thickness the union tends to be reversible. A lot of care has to be token choosing the thickness, because too large values of it can produce the opposite effect. Very large thickness of mortar layer provokes the apparition of air bubble between the two pieces, and at the same time makes difficult the uniform spreading of the mortar layer. This yields in a soft bonding that can be broke infusing fluids with a low flows.

4 FABRICATION AND CHARACTERIZATION OF A MICROFLUIDIC DEVICE: T-SENSOR

The aim of this chapter is to fabricate a microfluidic device known as T-SENSOR whose operating principle is basically the same of the one that governs the molecular communication systems. In the first part of this chapter a T-SENSOR is fabricated and experimentally characterized. In the second part of this chapter a finite differences simulator is programmed in order to characterize theoretically this device.

4.1 T-SENSOR

The T-Sensor [24] is a microfluidic analytical device which uses the low Reynolds numbers to ensure laminar flow inside it. It has two inlets for which are introduced different fluids that flow together side-by-side, and one outlet which drop the mixed fluid. The mixing between them is only due by diffusion process because of the flow is strictly laminar. Diffusion of molecules between streams flowing side-by-side may be observed directly and monitored optically through the downstream direction.

The T-Sensor is a microfluidic analytical device which uses the low Reynold numbers to ensure laminar flow inside it. It has two inlets channels that join in a one main channel. Two different fluids are introduced for the inlets and when they converge in the main channel flow together side-by-side mixing only by diffusion process. Diffusion of molecules between streams flowing side-by-side may be observed directly and monitored optically through the downstream direction.

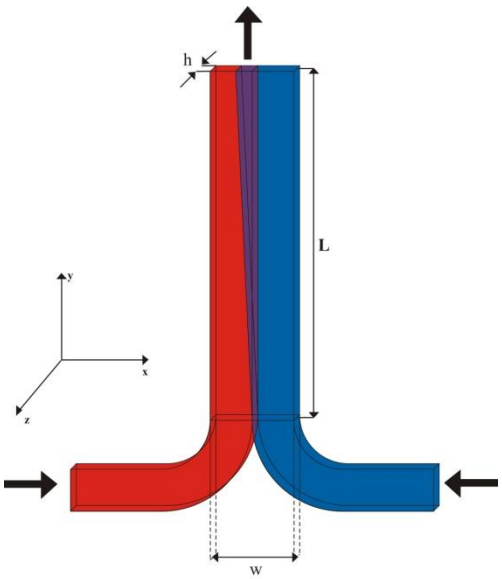

Fig. 4.28 Schematic representation of the T-Sensors shape. Two fluid enter for the channels at the bottom and one mixed fluid drop for the outlet at the top.

The T-SENSOR is the most common passive mixer. The two fluid mix along the main channel, and if this channel was long enough a fluid with uniform concentration would be achieved.

The zone where the two fluids are mixes is called "interdiffusion zone" and it is very dependent of the flow velocity. When the velocity is slow, it takes more time to the particles to travel along the whole channel, and during this time these particles can diffuse a through the interdiffusion direction $\vec{x}$. Otherwise, when the fluid is fast the particles leave the main channel before they can diffuse.

The T-Sensor is a microfluidic device which is fabricated using the known as "Soft Lithography" process. The soft-lithography process can be separated in two parts:

fabrication of an elastomeric element and use of this element to pattern the geometric features defined by a relief structure. The structure from which the stamp is derived is called 'master'. It can be fabricated by any method which is capable to reproduce a well defined structure of relief on a surface. Commonly the regular lithography technique is used to define a master. The elastomeric element is generated by casting a polymer against the master. The most common elastomeric used is the Polydimethylsiloxane or PDMS which is a heat curable polymer.

In this work a much easier way to fabricate the master was used [3]. The main idea is the fabrication of a master made by Scotch Tape. It is easier, quicker and more inexpensive than a master made it by lithography.

4.2 Design

In order to study the diffusion process of particles in a fluid the microfluidic device T-SENSOR will be fabricated and characterized.

The basic features for this device are:

$$w = 2mm$$
$$h = 60\mu m$$
$$L = 3cm$$

This dimensions have been chosen because the device will be fabricated using a hand-made technique, and the features must be easy to handle using regular tools such as scalpels or rulers.

Even being big features in microfluidics, because of the height is lower than 100μm we can ensure that the flux will be laminar. The equations (3.4) and (3.5) allows us to calculate the Reynolds number.

w	*2000 μm*
h	*60 μm*
Re	$\frac{\bar{v}d}{\upsilon}$
d	$\frac{4A}{P} = 4\frac{h \cdot w}{2(h+w)}$
υ_{water}	$1.13 \cdot 10^{-6}\ m^2/s$

Table 4.2 Parameters to calculate the Reynolds number

It has been assumed that the channels have a rectangular cross-sectional shape and that the fluids used in this scenario are dissolutions in water.

Following the specifications in the Table 4.2 the Reynolds number will be:

$$\mathrm{Re} = 2\frac{h \cdot w}{h+w} \cdot \frac{\bar{v}}{\upsilon} \approx 2h \cdot \frac{\bar{v}}{\upsilon} \qquad (4.29)$$

As it was said in the **Chapter 2** values below 2300 of the Reynolds number ensure laminar flow. The velocity needed to comply this limit is:

$$\mathrm{Re} = 2\frac{h \cdot w}{h+w} \cdot \frac{\bar{v}}{\upsilon} \approx 2h \cdot \frac{\bar{v}}{\upsilon}$$
$$\mathrm{Re} < 2300 \Leftrightarrow \bar{v} < \frac{2300 \cdot \upsilon}{2h} = 21.7\, {}^{m}\!/_{s} = 78.12\, {}^{km}\!/_{h} \qquad (4.30)$$

This is a huge velocity in terms of microfluidics, so we can state that the system's dimensions ensure laminar flow inside the device.

Some drawing software can be used to design the device's layout. Corel DrawX4 was used in order to achieve these layouts.

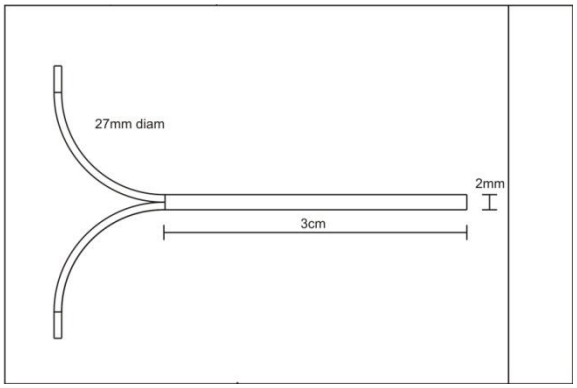

Fig. 4.29 T-Sensor Layout.

4.3 Fabrication

Usually the fabrication of microfluidic devices is limited to people who have access to a clean room that allows the fabrication with features of micrometers. For the features needed in the device presented in Fig. 4.29, a much easier technique can be used without the need of accessing to the clean room. The soft lithography techniques are base on the replication of masters in some curable polymers. How this master is fabricated is up to the designer. The adhesive tape can be used as a powerful tool in the fabrication of masters for microfluidic applications due to its features.

Scotch tape presents a uniform height of ~ 60 μm, so cutting this tape following the shape of the device required will yield a relief structure completely useful to be replicated. As it has been demonstrated in the condition (4.30) the height that Scotch tape has ensures laminar flow inside the channels.

Next are detailed the all the steps in the fabrication of devices using the Scotch tape patterned method.

4.3.1 Required materials

One of the most important advantages of the master fabricated using Scotch tape is its low cost. This is due especially to two factors, firstly only bench-top tools are required for the fabrication of these masters, and secondly accessing to the clean room is not required.

The needed materials for the fabrication of microfluidic devices are presented below:

- Glass slides, pre-cleaned from Manufacturer (Fisher Scientific, 75mm x 50mm x 1mm, Cat. No. 12-550-C).
- Scotch tape (3M Scotch® Transparent Tape 600).
- Stainless steel Scalpel or surgical blade with (Feather Safety Razor Co., LTD, Cat. No. 2976#11).
- Polystyrene Petri dish (Fisher Scientific, 100mm x 15mm, Cat. No. 08-757-12).
- Oven or hot plate (to work at 65°C).
- Tweezers.
- Gloves (do not use latex gloves).
- PDMS silicone elastomer base and curing agent (Sylgard 184, Dow Corning). Heptane H-350-1 (Fisher Scientific, Cat. No. 102258).
- Plasma oxidazer (Harrick Plasma PDC-001).
- Isoproppyl Alcohol (Isopropanol), (Fisher Scientific, Cat. No. 67-63-6, Lot #: 102109).
- 1.22 mm diameter biopsy puncher (Harris Uni-Core, Prod #15074).

4.3.2 Fabrication process

Once the device's layout is designed, a piece of Scotch tape has to be attached on the top of a glass slide. Usually this thickness is around 60μm which is perfectly useful for microchannels designing. The height can be increased by the adhesion of more layers of tape, achieving larger dimensions always multiples of 60μm.

Fig. 4.30 Attaching the film of Scotch tape on the glass slide

Once done it, the glass slide has to be placed on the printed layout (with the attached piece of tape facing up) and fix it to the printout in order to avoid any movement. Then using a scalpel the tape on the glass can be cut following the shape indicated by the printed layout.

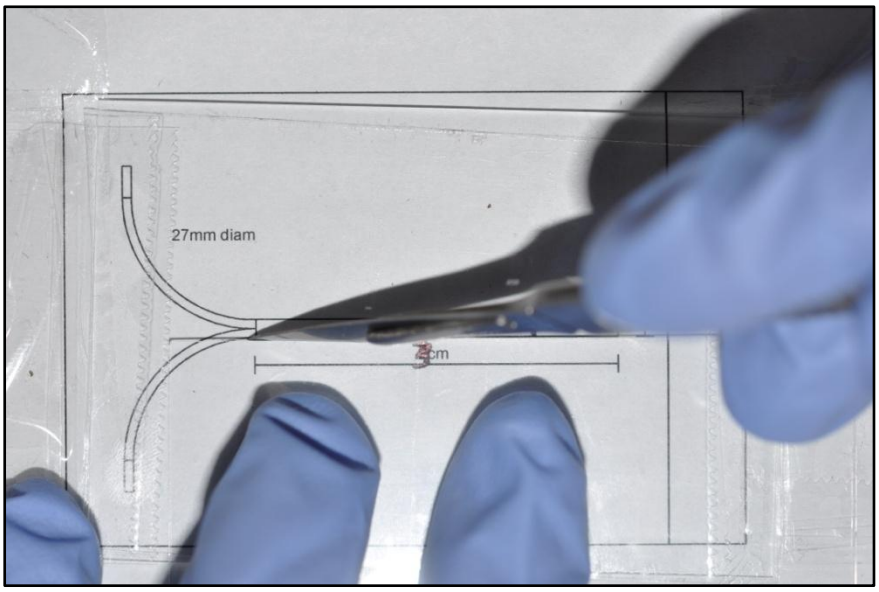

Fig. 4.31 Cutting the Scotch tape according with the layout

The next step is to take out the useless Scotch tape from the glass slide (all the tape except that in the layout of the microchannel) and clean the edges of the remained tape using isopropanol in order to remove the extra glue.

After that the glass slide with patterned Scotch tape has to be heated in oven at 65°C for 2 or 3 minutes that will provide a better adhesion of the Scotch tape to de glass

substrate. At this point the Scotch tape pattern fixed on the glass slide is ready to be used as a master for soft lithography uses.

Then mix the base and the curing PDMS components such as the manufacturer recommends (in this case 10 parts of base by 1 part of curing agent). Once the master is put in a petri dish the PDMS mixture is poured in the dish until it is totally covered.

PDMS has to be degassed in a vacuum chamber for at least 1 hour in order to remove all the air bubbles that can deform the device, and after that the petri dish can be placed in the oven at 65°C. After 1 hour the PDMS is totally cured and ready to be separated from the master.

Once the PDMS is cured, it should cut the slab containing the pattern using a scalpel. At this point the replica is ready to be peeled it off.

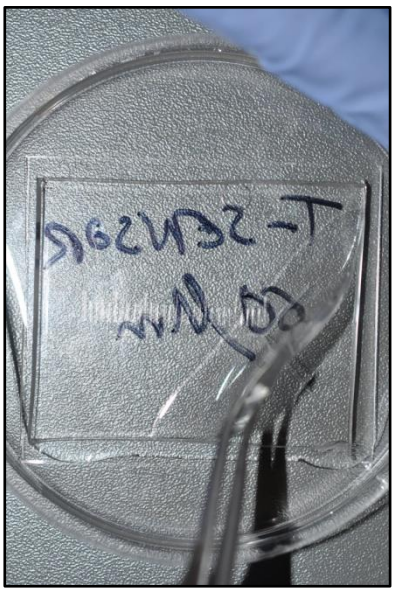

Fig. 4.32 Peeling of the PDMS from the master.

The next step is to punch holes in the replica for the inlets and the outlets of the device. Finally replica is sealed to a substrate (another clean glass slide) using an oxygen plasma oxidizer.

This sealing process is based in two steps, first the oxidation of the substrate by introducing the glass slide into the plasma oxidizer (with the surface that will be sealed to the replica facing up) at maximum power for 3 minutes. Then the PDMS replica has to be placed into the plasma oxidizer (with the surface that will be sealed to the glass substrate facing up) with the glass slide for 3 minutes more. At the end, the glass slide is exposed to the plasma for 6 minutes while the PDMS replica is exposed only for 3 minutes. After that putting the two faces in contact produce a chemical reaction that makes a covalent union between the glass and the PDMS yielding an irreversible bounding between them.

The last step is heating the device in the oven at 65°C for ten minutes to finalize the adhesion.

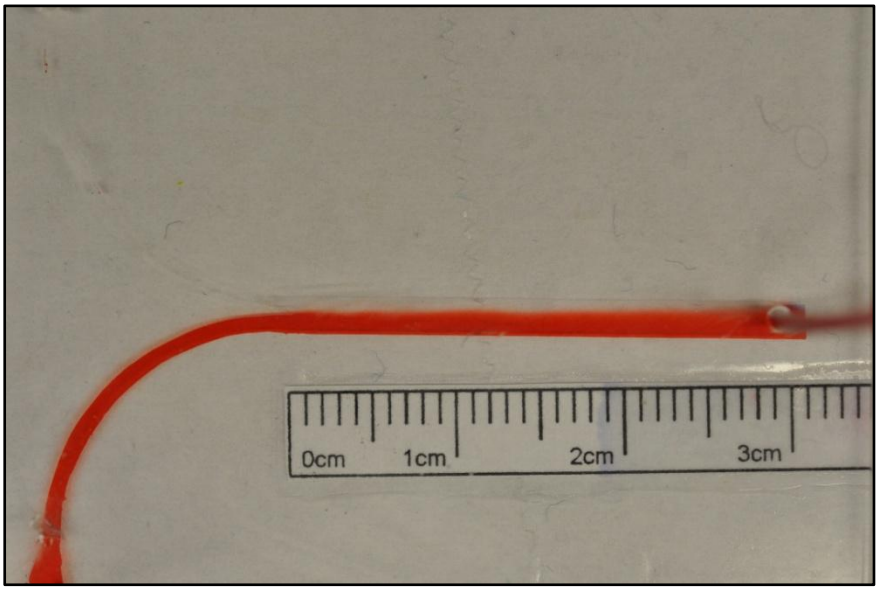

Fig. 4.33 T-Sensor filled with DI water and diluted red ink.

The figure Fig. 4.33 shows the behavior of a T-Sensor fabricated using the Scotch tape patterned method. It is possible to appreciate the laminar flow in the main channel and how the interdiffusion zone increases along the channel.

4.4 Experimental Characterization

The design and the fabrication of a T-SENSOR has been presented already, at this point is time to characterize the behavior of this microfluidic device. As it was said before the diffusion of molecules between streams may be observed through the downstream direction.

Two different devices will be fabricated with the same features except the thickness of the channels, and the same fluid will be infused with the same flow rate in each one. In one case the thickness will be 60 μm in the other case the thickness will be 120 μm. According to the theory more diffusion is expected for the system with lower fluid velocity, which is the device with higher thickness if the flow rate is the same for the two cases. This is because the mean velocity in the microchannel is:

$$\overline{V} = \frac{Q}{A} \qquad (4.31)$$

So, as soon as the cross section area increases the mean velocity decreases, and it means that the diffusion zone grows because the molecules have more time to diffuse.

Then if the fluids are colored, the interdiffusion zone is visible, and it can be determined.

The most important characteristics for the systems are presented in the next table:

	Device 1	***Device2***
w *(width)*	*2 mm*	*2 mm*
h *(height)*	*60 µm*	*120 µm*
L *(Longitude)*	*3 cm*	*3 cm*
Q *(Flow Rate)*	*20 nL/s*	*20 nL/s*
V *(Velocity)*	*166.66 µm/s*	*83.33 µm/s*

Table 4.3 T-Sensor features

Using a syringe pump, 2 fluids can be infused at the same time. In this experiment were used as fluids, a dissolution of red and blue ink in DI water, that produced and interdiffusion zone of black color clearly differentiated.

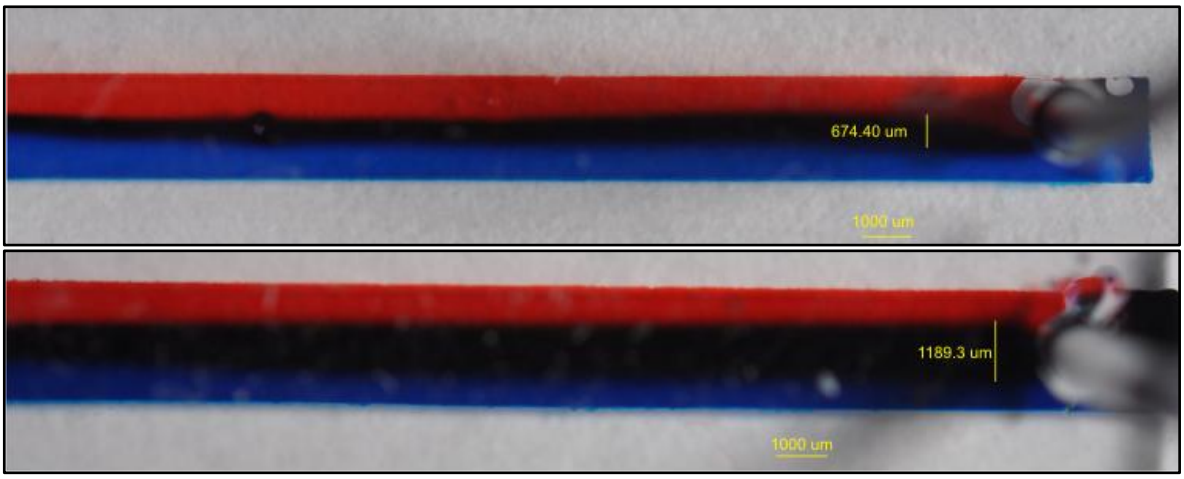

Fig. 4.34 On the top a T-Sensor with height of 60µm filled with red and blue ink. Its interdiffusion zone is 674.40µm. On the bottom a T-Sensor with height of 120µm filled with red and blue ink. Its interdiffusion zone is 1189.30µm.

The results in the figure Fig. 4.34 agree with the hypothetical results expected, the interdiffusion distance is almost double for the device with higher thickness. For low velocities the molecules can diffuse for more time, but the goal now is to know how the concentration of molecules is distributed along the main channel.

In a first approximation we suppose at the beginning (when the two fluids meet) there is maximum concentration of particles in one channel and minimum concentration in the other, yielding a gradient of concentration. Then, as soon as the particles flow downstream the two fluid mixes until a uniform concentration in the interdiffusion direction is achieved. It is possible to find out the concentration profile across the interdiffusion zone by optical monitorization along the main channel.

In order to characterize these concentration profiles, a simple inspection does not enough. The use of a microscope is needed to achieve more detailed images. The experiment consists in the observation of the interdiffusion zone in a T-Sensor introducing DI water in one inlet and a dissolution of fluorescein disodium 1Mm with DI

water in the other. Fluorescein is a molecule commonly used in microscopy that reacts to ultraviolet light making it visible. The molecules of fluorescein can be detected under the microscopy, and pictures at different points downstream can be taken at microscopic scale. Applying some image processes to these pictures it is possible to extract the concentration information of each one.

The proportion elected for this dissolution was made after the study of the fluorescence in eight different samples using different proportions. The final proportion elected was 16:1 (in 16 parts of dissolution 1 is fluorescein) according with the best results observed in the microscope.

The lent with minimum augment in the microscope was 4x. For this reason the width of the cannel cannot be bigger than 1mm if we can see the whole channel only in one picture. In order to solve this issue a device with 1mm width was fabricated.

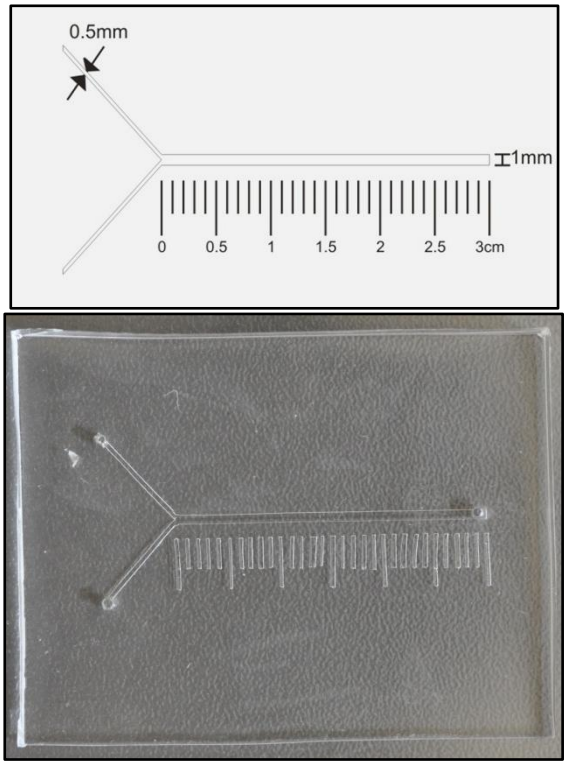

Fig. 4.35 On the top the layout for the T-Sensor. On the bottom the T-Sensor fabricated using the Scotch tape patterned method. The reason for which the inlets do not have a curved shape is for the complication in cutting this pattern of Scotch tape when the width is less than 1mm.

$$w = 1mm$$
$$h = 120\mu m$$
$$L = 3cm$$

The composition for the experiment was a syringe-pump with two 10mL syringe connected by 1.22 mm diameter polyethylene tubes to the T-Sensor. For observe the

interdiffusion zone the microscope Nikon Eclipse Ti was used. The lent used is Nikon Plan Flour 4x/0.13 and to be able to see the fluorescein flowing through the channel a fluorescent lamp was needed. The lamp was the Nikon Intensilight C-HGFIE. The images were acquired by the computer using de video camera CoolSnap HQ2.

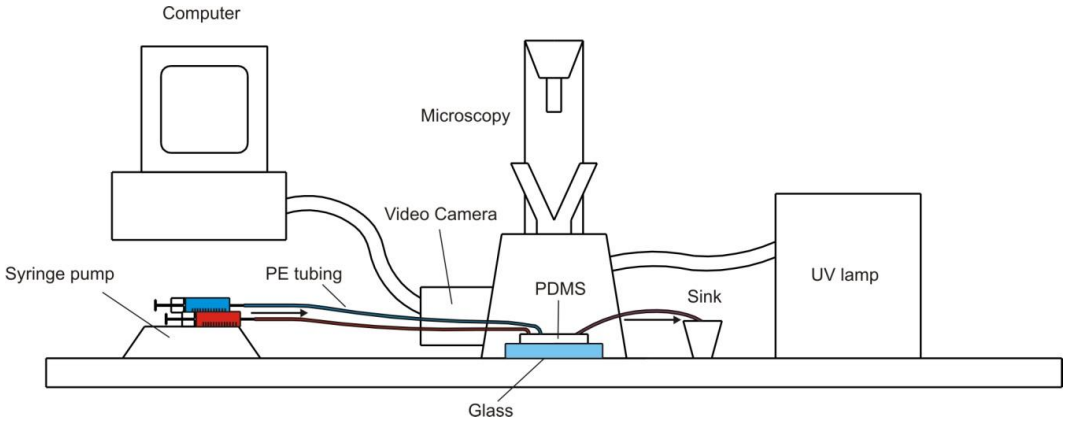

Fig. 4.36 Schematic (side view) of the experimental setup.

Under this conditions the fluid were infused into the T-Sensor for different flow rates in order to find which one gave a better images of the interdiffusion zone.

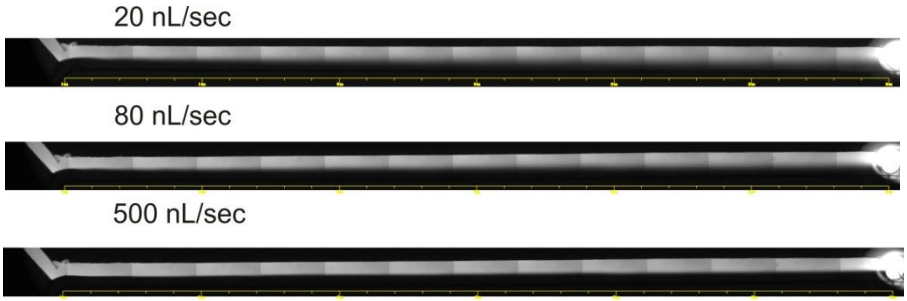

Fig. 4.37 T-Sensor infused with DI water and Fluorescein Disodium diluted in DI water with the proportion 16:1 for different flow rates. The images were taken using the microscope Nikon Eclipse Ti with the lent 4x, a fluorescent lamp with filter TRI. The images were taken with an exposure time of 60ms. The temperature in the room when the images were taken was 17°C

In the figure Fig. 4.37 are presented the pictures taken for three different flow rates. The white color shows the molecules of fluorescein, and it is easy to see how they diffuse along the interdiffusion direction. The image on the top (at 20 nL/s) provides the most clear interdiffusion zone, and it was selected to be processed for obtaining the concentration profiles at different points of the main channel.

4.4.1 Data acquisition and image processing

The image at 20nL/s was divided in 6 different JPEG images of 1mm width each at the positions 0, 5, 10, 15, 20, 25 and 30mm using Adobe Photoshop.

With MATLAB R2009b 10 randomly-distributed vertical lines [31] were chosen per each image and the pixel intensity light was extracted for each vertical line of pixels. The sum average of these lines provides the light intensity profile for each image which is proportional to the concentration profile.

In order to normalize the curve, we subtracted the minimum value of intensity and then we divided the intensity of each pixel by the maximum intensity value.

In the **Appendix C** the code written for doing this is shown.

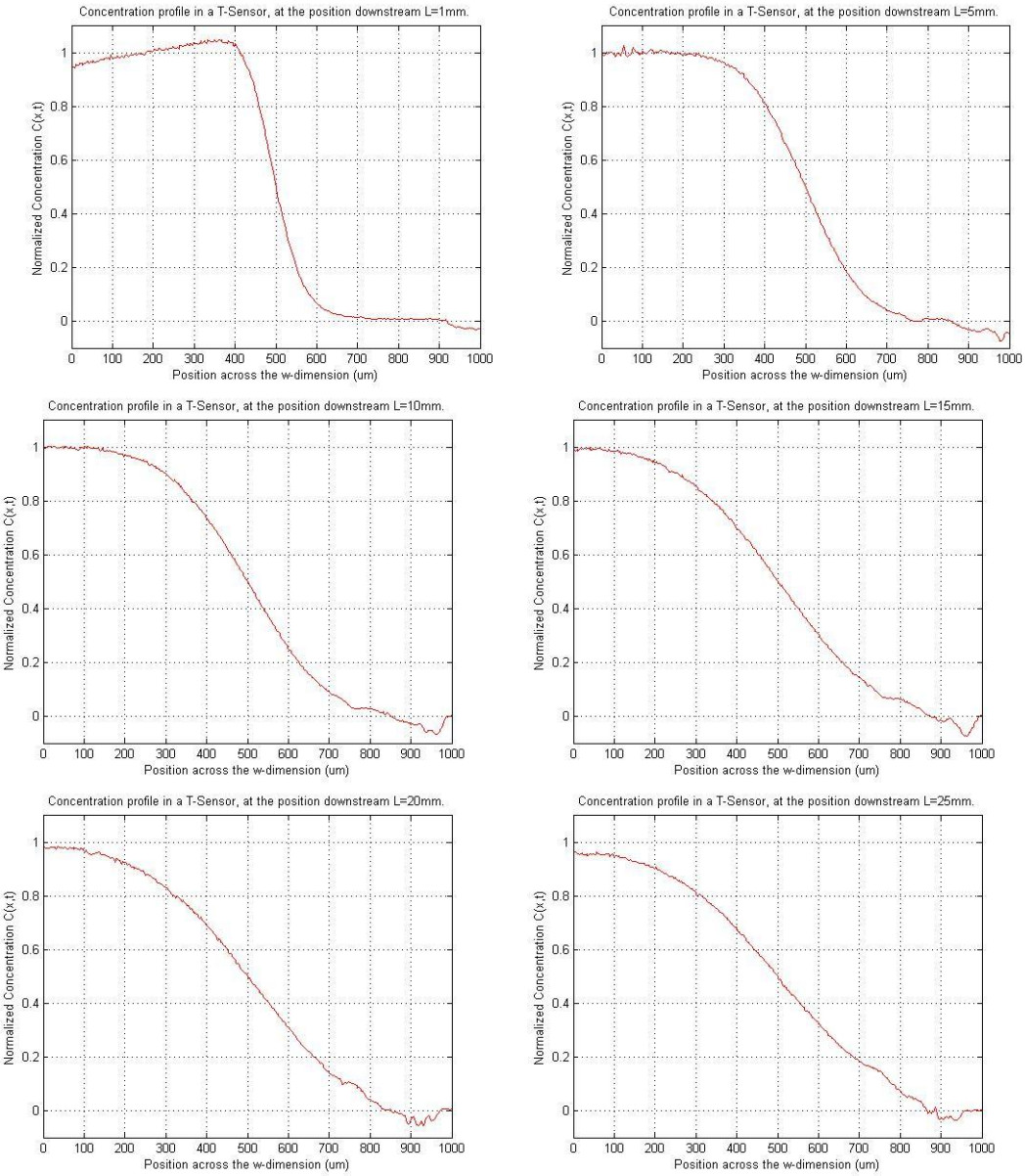

Fig. 4.38 Normalized concentration profiles in a T-Sensor of fluorescein disodium at different points downstream. Flow rate of 20 nL/s.

The image Fig. 4.38 shows a set of images that provide the concentration profile across the interdiffusion direction. We can see how as soon as the concentration is obtained in further positions downstream the tendency is to achieve a uniform concentration along the channel.

The persistent error at the end of the curve, when the position is around 900μm belongs from the shadows in the picture taken with the microscope.

4.5 Theoretical Characterization

Previously the T-Sensor has been presented as the perfect device to study the diffusion of particles in fluids.

A simulator that characterizes the theoretic behavior of this device may help in a better understanding of the diffusion process. As it has seen in previous chapters a closed analytical solution for the diffusion equation is hard to find and in the most cases is not possible to obtain. For this reason it is simpler to use a simulator based on numerical methods which provides an approximation as reliable as it is required of the real solution.

Two streams traveling in the main channel of a T-Sensor flow in a strictly laminar regime, yielding a gradient of concentration between fluids and starting the diffusion process of particles. The diffusion between two fluids which flow side by side with laminar flow is given by the equation of continuity for incompressible fluid (3.28):

$$\frac{\partial C\left(\bar{x},t\right)}{\partial t}+\bar{v}\cdot\nabla C\left(\bar{x},t\right)=D\cdot\nabla^2 C\left(\bar{x},t\right)+R\left(\bar{x},t\right)$$

Specifying this equation in a three dimensional space, the equation becomes:

$$\frac{\partial C}{\partial t}+\left(\bar{v}_x\frac{\partial C}{\partial x}+\bar{v}_y\frac{\partial C}{\partial y}+\bar{v}_z\frac{\partial C}{\partial z}\right)=D\left(\frac{\partial^2 C}{\partial x^2}+\frac{\partial^2 C}{\partial y^2}+\frac{\partial^2 C}{\partial z^2}\right)+R\left(\bar{x},t\right) \quad (4.32)$$

Where the coordinate axis are as in Fig. 4.28. The region where this equation is defined is:

$$0 \le x \le w$$
$$0 \le y \le L$$
$$0 \le z \le h$$

In a T-Sensor we can assume laminar flow because of the low Reynolds numbers complies, therefore there is only diffusion in the directions $\vec{x}$ and $\vec{z}$. All entry effects are ignored so it assumes that the fluids velocities in the directions $\vec{x}$ and $\vec{z}$ directions have to be zero, the fluid is only flowing downstream. Finally this simulation does not include any chemical reaction.

Application of these assumptions leads to [24, 38]:

$$\frac{\partial C}{\partial t} = V_y \frac{\partial C}{\partial y} = D\left(\frac{\partial^2 C}{\partial x^2} + \frac{\partial^2 C}{\partial z^2}\right) \qquad (4.33)$$

This equation is a three dimensional parabolic differential equation and it can be solved a numerical method known as "finite differences".

In mathematics, finite difference methods are numerical methods approximating the solutions to differential equations using finite differences equations to approximate derivatives. Approximations presented in Table 4.4 and Table 4.5 can substitute the derivatives in differential equations. That transforms these deferential equations into simple algebraic equations which are easily computed. Many mathematical models of real phenomenon based on partial differential equations such as the behavior of a steel sheet with a uniform charge q, the conductive heat transport, or the movement of particles by Brownian motion can be computed using finite differences.

	Approximation	***Error***
Forward approximation	$\left.\frac{\partial f}{\partial x}\right\|_i \approx \frac{f_{i+1} - f_i}{dx}$	$o(dx)$
Backward approximation	$\left.\frac{\partial f}{\partial x}\right\|_i \approx \frac{f_i - f_{i-1}}{dx}$	$o(dx)$
Central approximation	$\left.\frac{\partial f}{\partial x}\right\|_i \approx \frac{f_{i+1} - f_{i-1}}{2 \cdot dx}$	$o(dx^2)$
Second order Derivative	$\left.\frac{\partial^2 f}{\partial x^2}\right\|_i \approx \frac{f_{i+1} - 2 \cdot f_i + f_{i-1}}{dx^2}$	$o(dx^2)$

Table 4.4 Resume of finite difference approximations in the x-dimension

The same reasoning applies in order to obtain the approximations for the derivatives in the t-dimension.

	Approximation	***Error***
Forward approximation	$\left.\frac{\partial f}{\partial t}\right\|_j \approx \frac{f_{j+1}-f_j}{dt}$	$o(dt)$
Backward approximation	$\left.\frac{\partial f}{\partial t}\right\|_j \approx \frac{f_j-f_{j-1}}{dt}$	$o(dt)$
Central approximation	$\left.\frac{\partial f}{\partial t}\right\|_j \approx \frac{f_{j+1}-f_{j-1}}{2\cdot dt}$	$o(dt^2)$

Table 4.5 Resume of finite difference approximations in the t-dimension

4.5.1 1-Dimensional T-Sensor simulator

A one dimensional model of the T-Sensor would be:

$$\frac{\partial C}{\partial t} = D\frac{\partial^2 C}{\partial x^2} \qquad (4.34)$$

Hence, the equation (4.34) can be expressed using the finite differences method in a discrete environment. To do this, the derivatives are substituted by its approximations presented in Table 4.4 and Table 4.5 thus obtaining [39]:

$$\frac{C_i^{j+1}-C_i^j}{dt} = D\cdot\left(\frac{C_{i+1}^j-2\cdot C_i^j+C_{i-1}^j}{dx^2}\right) \qquad (4.35)$$

And arranging the equation (4.35) and isolating the term n+1:

$$C_i^{j+1} = \frac{D\cdot dt}{dx^2}\cdot\left(C_{i+1}^j-2\cdot C_i^j+C_{i-1}^j\right)+C_i^j \qquad (4.36)$$

The index i determines the position dependence and the index j determines the temporal point. The equation (4.36) shows that the value of the concentration in the instant $j+1$ is fixed by the value of the concentration in the instant before j and by its neighbor points. So it is possible to solve the diffusion equation by iteration using mathematical software as MATLAB.

The behavior of this device is easily described using the diffusion equation. The only point needed at this time is to define the boundary and the initial conditions in this system.

The no flux boundary condition applies in both walls. The T-Sensor is made using PDMS which is not permeable to liquids and as a result, the flux of fluids will always be zero at the walls. As initial condition the concentration at the beginning in one channel is

maximum and in the other channel minimum. The boundary conditions prohibit the flux at the walls:

- **Initial Condition:**

$$C(x,t=0)\big|_{x\in(0,\frac{w}{2})}=1$$
$$C(x,t=0)\big|_{x\in(\frac{w}{2},w)}=0 \qquad (4.37)$$

- **Boundary Conditions:**

$$\left.\frac{\partial C(x=0,t)}{\partial x}\right|_{t\geq 0}=0 \qquad (4.38)$$

$$\left.\frac{\partial C(x=w,t)}{\partial x}\right|_{t\geq 0}=0 \qquad (4.39)$$

Using the finite difference method these two equations become like:

$$\left.\frac{\partial C(x=0,t)}{\partial x}\right|_{t\geq 0}\approx\frac{C_2^j-C_1^j}{dx}=0\rightarrow C_2^j=C_1^j \qquad (4.40)$$

$$\left.\frac{\partial C(x=w,t)}{\partial x}\right|_{t\geq 0}\approx\frac{C_w^j-C_{w-1}^j}{dx}=0\rightarrow C_w^j=C_{w-1}^j \qquad (4.41)$$

With these equations it is possible to program a simulator which will be able to calculate a non closed solution as good as we want. The only limitation is the stability condition (4.42).

A T-Sensor simulator programmed by MATLAB R2009b is provided in the **Appendix A**.

The results obtained for a device with the following features is presented below.

***w** (width)*	*550 µm*
***L** (Longitude)*	*3 cm*
***D** (Diffusion Constant)*	*800 µm2/s*
***V** (Velocity)*	*333.33 µm/s*

Table 4.6 T-Sensor features

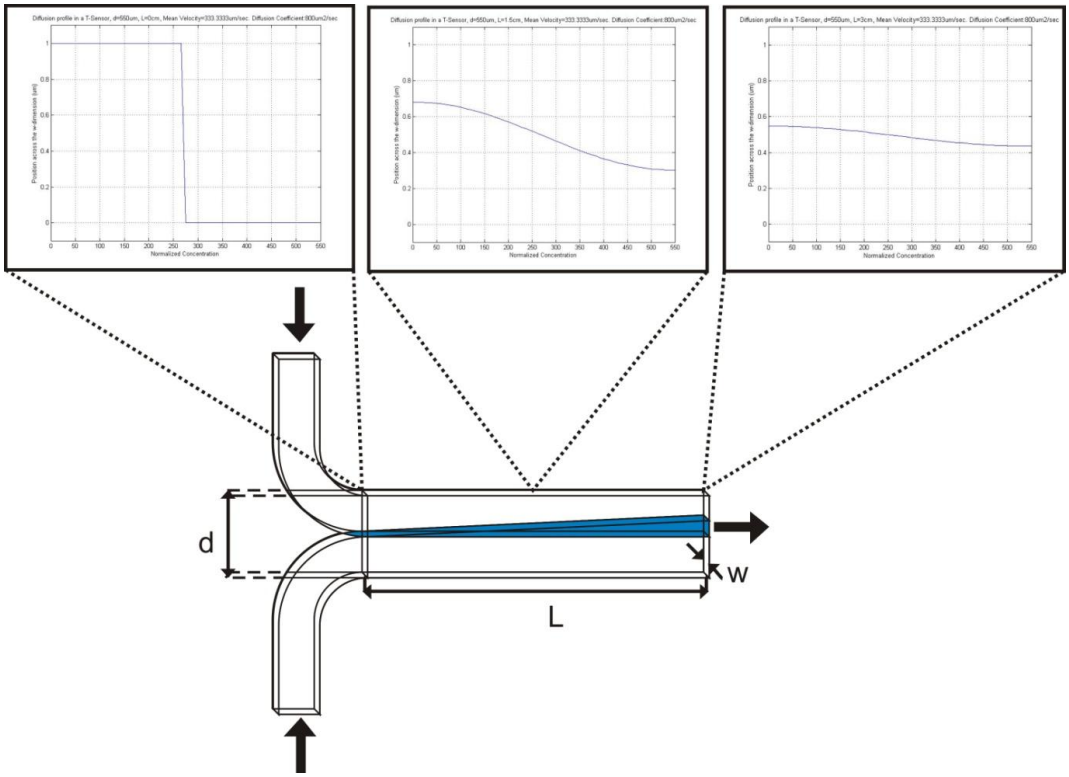

Fig. 4.39 Concentration across the w-dimension in a T-Sensor at distances 0cm, 1.5cm and 3cm downstream.

As it was expected at the beginning the concentration in the inlet 1 is maximum and the concentration in the inlet 2 is minimum. If we move downstream, the molecules start to diffuse across the w-dimension. This is reflected in the image because the concentration in the channel 1 decreases in the same way that it does the channel 2. This is the consequence of the boundary conditions, since the PDMS in not permeable, all the molecules must remain inside the device, so the global concentration of particles have to be constant.

At the end if the device was large enough the concentration would be 0.5 in every point across the w-dimension. This would mean that it would have been perfect mixing between the two fluids.

The diffusion of particles depends also on the velocity of the fluid where the molecules are suspended and of the diffusivity, parameter that provides an idea of how easy is for a molecule to move in a medium.

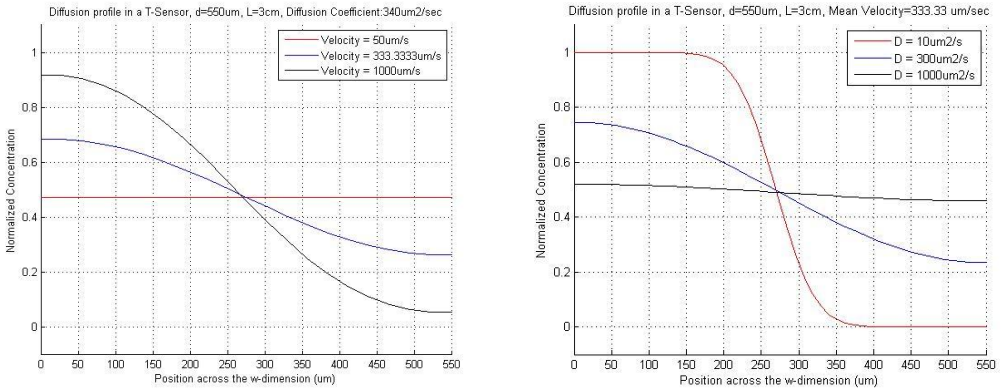

Fig. 4.40 On the left, concentration across the w-dimension in a T-Sensor at 3cm downstream for three different fluid velocities. w=550µm, L=3cm, D=340µm²/s. On the right, concentration across the w-dimension in a T-Sensor at 3cm downstream for three different diffusivities. w=550µm, L=3cm, V=333.33µm/s.

The simulator provides the theoretical behavior of the T-Sensor according to the velocity of the fluid and the diffusivity of the particles.

The stability of the solution is conditioned to the stability condition [39]:

$$\frac{D \cdot dt}{dx^2} \leq \frac{1}{2} \rightarrow dt \leq \frac{dx^2}{2 \cdot D} \qquad (4.42)$$

The practical explanation is that, given a spatial resolution and the velocity by which the molecules diffuse away, the temporal resolution has to be enough to "see" without mistake the evolution of all the particles.

4.5.2 2-Dimensional T-Sensor simulator

A two dimension model of the T-Sensor is presented in the equation (4.33). This system is defined by a three dimensional grid which comprehend the two spatial dimension $\vec{x}$ and $\vec{z}$, ant the temporal dimension t.

Using the finite differences approximations in this model we are able to find an approximation for the two-dimensional diffusion equation:

$$\frac{C_{i,j}^{n+1} - C_{i,j}^{n}}{dt} = D \cdot \left(\frac{C_{i+1,j}^{n} - 2 \cdot C_{i,j}^{n} + C_{i-1,j}^{n}}{dx^2} + \frac{C_{i,j+1}^{n} - 2 \cdot C_{i,j}^{n} + C_{i,j-1}^{n}}{dz^2} \right) \qquad (4.43)$$

Where the indexes i and j describe the spatial position in the mesh and the index n indicates the temporal position in the grid.

Arranging this equation and isolating the component $n+1$ we obtain:

$$C_{i,j}^{n+1} = \frac{D \cdot dt}{dx^2} \cdot \left(C_{i+1,j}^{n} + C_{i-1,j}^{n} \right) + \frac{D \cdot dt}{dz^2} \cdot \left(C_{i,j+1}^{n} + C_{i,j-1}^{n} \right) + C_{i,j}^{n} \cdot \left(1 - 2 \cdot \frac{D \cdot dt}{dx^2} - 2 \cdot \frac{D \cdot dt}{dz^2} \right) \qquad (4.44)$$

Once again it is possible to calculate the concentration in the next instant $n+1$ using the known values in the instant before n.

Since this model can be considered as an extension of the one dimensional situation, the boundary conditions and the initial condition must be the same. Maximum concentration in one channel and minimum in the other as initial condition; and no flux at the walls.

- **Initial Condition:**

$$\begin{aligned} C(x,z,t=0)\big|_{\substack{x\in(0,\frac{w}{2}) \\ z\in(0,h)}} &= 1 \\ C(x,z,t=0)\big|_{\substack{x\in(\frac{w}{2},w) \\ z\in(0,h)}} &= 0 \end{aligned} \qquad (4.45)$$

- **Boundary Conditions:**

$$\left.\frac{\partial C(x=0,\forall z,t)}{\partial x}\right|_{t\geq 0} = 0 \qquad (4.46)$$

$$\left.\frac{\partial C(x=w,\forall z,t)}{\partial x}\right|_{t\geq 0} = 0 \qquad (4.47)$$

$$\left.\frac{\partial C(\forall x,z=0,t)}{\partial z}\right|_{t\geq 0} = 0 \qquad (4.48)$$

$$\left.\frac{\partial C(\forall x,z=h,t)}{\partial z}\right|_{t\geq 0} = 0 \qquad (4.49)$$

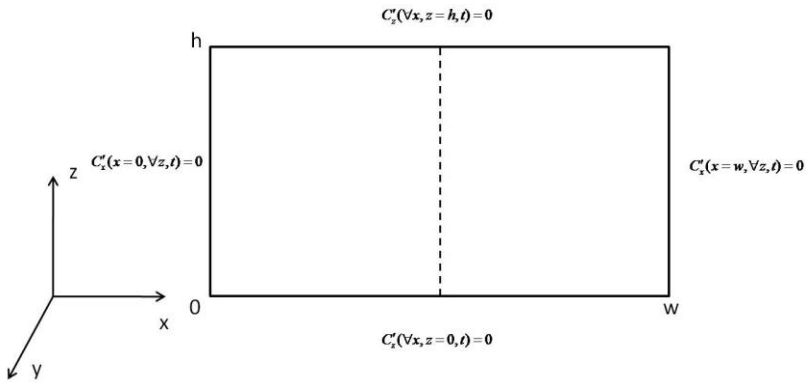

Fig. 4.41 Distribution of the boundary conditions in the device

Using finite difference the boundary conditions become:

$$\left.\frac{\partial C(x=0,\forall z,t)}{\partial x}\right|_{t\geq 0} = 0 \approx \frac{C_{2,j}^n - C_{1,j}^n}{dx} = 0 \rightarrow C_{2,j}^n = C_{1,j}^n \qquad (4.50)$$

$$\left.\frac{\partial C(x=w,\forall z,t)}{\partial x}\right|_{t\geq 0} = 0 \approx \frac{C_{w,j}^n - C_{w-1,j}^n}{dx} = 0 \rightarrow C_{w,j}^n = C_{w-1,j}^n \qquad (4.51)$$

$$\left.\frac{\partial C(\forall x, z=0,t)}{\partial y}\right|_{t\geq 0} = 0 \approx \frac{C_{i,2}^n - C_{i,1}^n}{dz} = 0 \rightarrow C_{i,2}^n = C_{i,1}^n \qquad (4.52)$$

$$\left.\frac{\partial C(\forall x, z=h,t)}{\partial y}\right|_{t\geq 0} = 0 \approx \frac{C_{i,h}^n - C_{i,h-1}^n}{dz} = 0 \rightarrow C_{i,h}^n = C_{i,h-1}^n \qquad (4.53)$$

A T-Sensor simulator programmed by MATLAB R2009b is provided in the **Appendix B**. The results obtained for a device characterized in the following table will be presented below.

w *(width)*	*550 μm*
h *(height)*	*60 μm*
L *(Longitude)*	*3 mm*
D *(Diffusion Constant)*	*320 μm2/s*
Q *(Flow Rate)*	*11 nL/s*
V *(Velocity)*	*333.33 μm/s*

Table 4.7 T-Sensor features

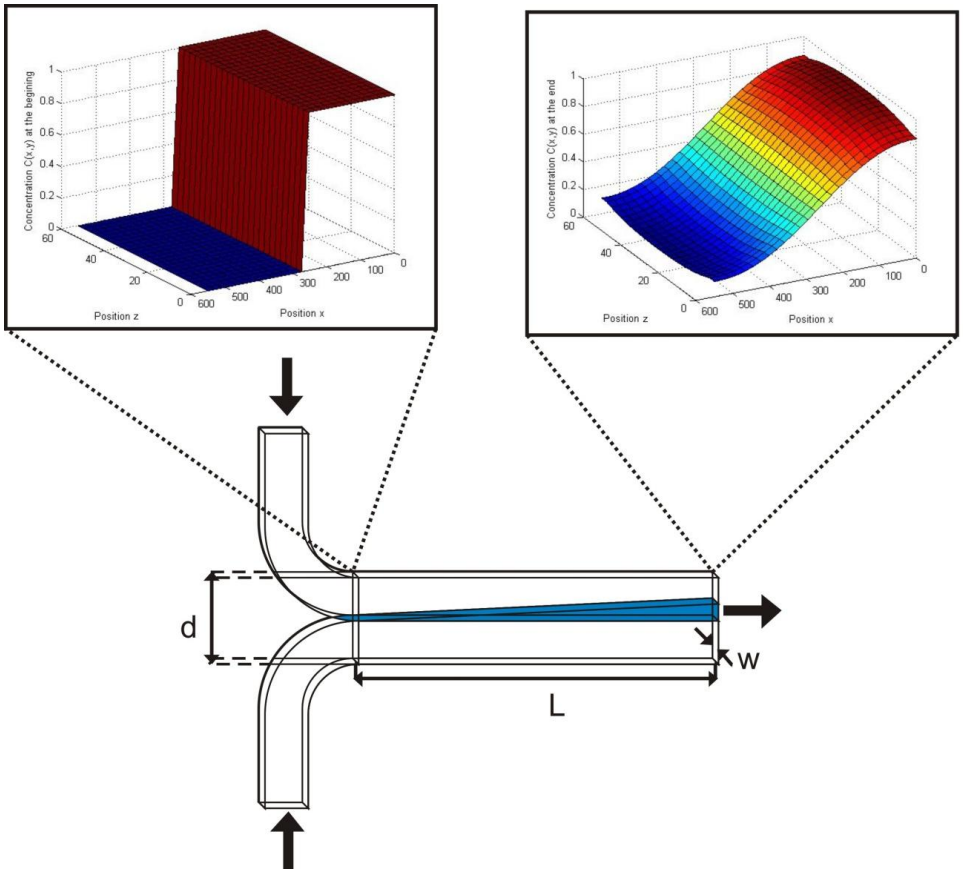

Fig. 4.42 Concentration profile across the w-dimension in a T-Sensor at distances 0cm and 3cm downstream.

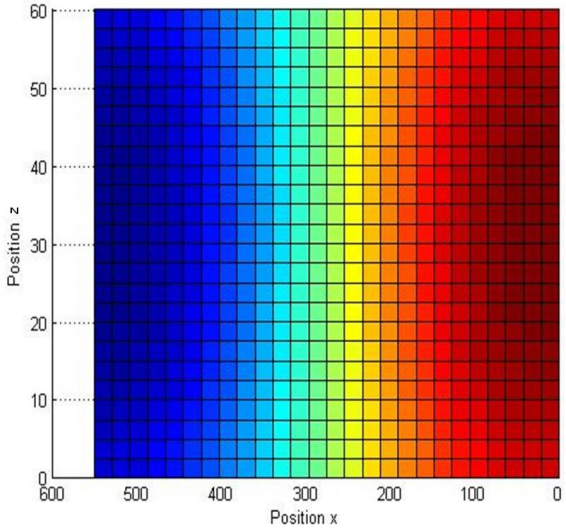

Fig. 4.43 X-Z view of the concentration in a T-Sensor at distance 3mm downstream. Using a parabolic velocity profile appears the "Butterfly Effect".

Such as we can see in Fig. 4.43 the concentration across the z-dimension (the height) presents a curve shape. In this model has been considered the fluid's velocity as a constant in every point. The velocity profile for a pressure-driven flow in a rectangular

duct device is parabolic such as it has been demonstrated before. It means that the velocity at the walls is almost 0 and maximum in the duct center. The profile follows a function as (3.13).

For channels with an aspect ratio, w/h, greater than 20, the velocity profile across w is unchanging for at least 90% of its length.

This velocity profile has an important effect in the diffusion inside the T-Sensor. Because the velocity is lower at the walls in the points closed to them the molecules move slower. It results that there is more time to diffuse in the w-direction. That means a molecule near to the top or bottom walls will diffuse more distance to the w-direction than another molecule situated in the center of the device. This effect is called "Butterfly Effect".

The stability condition in this case if $dx = dt$ is:

$$dt \leq \frac{dx^2}{4D} \qquad (4.54)$$

4.6 Results and Discussions

The fabrication of microfluidic devices using a very simple and inexpensive technique has been presented. As we have demonstrated this technique is completely useful for the fabrication of micro-devices with width up to 300μm. For devices below 1mm it is possible to use magnificent glasses in the fabrication process, but when the features are smaller than 300μm this technique is not suitable.

By the realization of two different experiments using three different devices we have demonstrate that this method is completely useful, and it is much easier, faster and inexpensive that all those methods that need the use of a clean room for the fabrication of the master.

One of the most important applications of the T-SENSOR is the calculus of the diffusivity of molecules. In these cases what it is done is the extraction of the concentration profiles of these molecules such as it has been done before. After that a simulator can be used to find out which is the diffusion coefficient that fits better with the experimental results.

In the following chapters a simulator of the diffusion will be programmed, and the results that we have got before will be use to verify the reliability of that simulator.

The T-SENSOR is a microfluidic device that allows the study of the diffusion of particles. It may provide us a better understanding of this phenomenon, and utilize this knowledge in the study of molecular communication based on diffusion processes.

However theoretical simulator has presented results that fix with the experience shown in the experiments with the real device, it is still necessary a validation for the simulator. In order to ensure that the behavior of the device is the same than the simulated, we will validate either with theoretical results and experimental results the veracity of this simulator.

4.6.1 1-Dimensional simulator validation with theoretical results

In order to determinate if this simulator works properly it will compare the results obtained in the simulations with some other simulations already published.

The first paper used is: "*E.Kamholz, P. Yager; Theoretical Analysis of Molecular Diffusion in Pressure-Driven Laminar Flow in Microfluidic Channels*".

The device used in this paper has the following features:

***w** (width)*	*2405 µm*
***h** (height)*	*10 µm*
***L** (Longitude)*	*5500 µm*
***D** (Diffusion Constant)*	*65 µm2/s*
***Q1** (Flow Rate)*	*1000 nL/s*
***Q2** (Flow Rate)*	*500 nL/s*
***Q3** (Flow Rate)*	*250 nL/s*

Table 4.8 T-Sensor features

In this simulation the authors wanted to see the concentration profile across the diffusion dimension at the end of the channel for three different flow rates.

In this situation is expected more diffusion for the minimum flow rate because of its slower velocity downstream. This is because the molecules move slower downstream and then they have more time to diffuse in the w-dimension. A simulation of this device was made using the 1-D T-Sensor simulator and the difference are shown below:

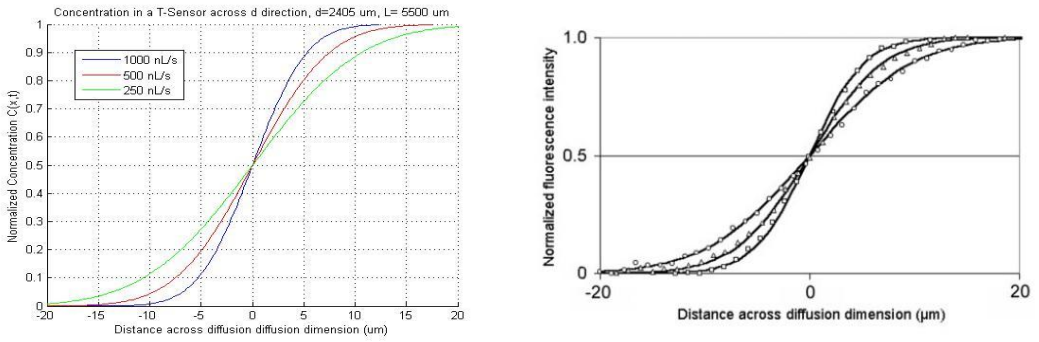

Fig. 4.44 On the left simulation using the 1-D T-Sensor simulator. On the right the results observed in the E. Kamholz, P. Yager paper [38].

And doing an overlap of these two images:

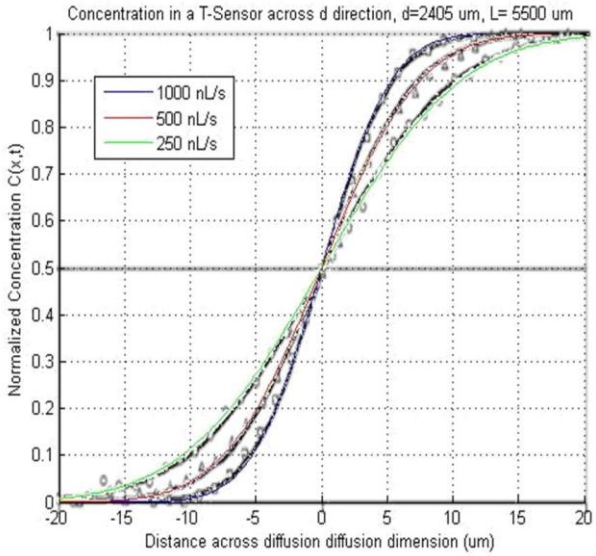

Fig. 4.45 Overlap of the obtained results using the 1-D simulator and the observed results in the paper E. Kamholz, P. Yager [38].

The results are very similar. The differences may be due because of the number of points used in the mesh.

The second paper used is: "*E. Kamholz, P. Yager: Molecular diffusive laws in pressure-driven microfluidic channels: deviation from one-dimensional Einstein approximations*".

In this case the device used is:

***w** (width)*	*2405 μm*
***h** (height)*	*10 μm*
***L** (Longitude)*	*2000 μm*
***D** (Diffusion Constant)*	*340 μm²/s*
***Q** (Flow Rate)*	*42 nL/s*
***V** (Velocity)*	*1700 μm/s*

Table 4.9 T-Sensor features

In this simulation the objective was to see the distance traveled by the molecules across the w-dimension at different points downstream in the device. For do that the authors considered the fluid had diffused until one point if the concentration was 30% of the initial bulk concentration.

The results using the 1-D T-Sensor simulator for this device and the comparison with the previous paper are shown below:

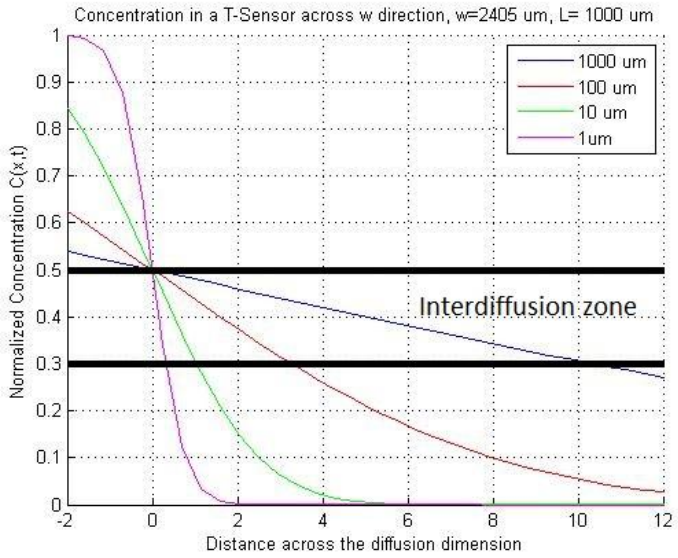

Fig. 4.46 Simulation using the 1-D T-Sensor simulator for the device presented in Table 4.9.

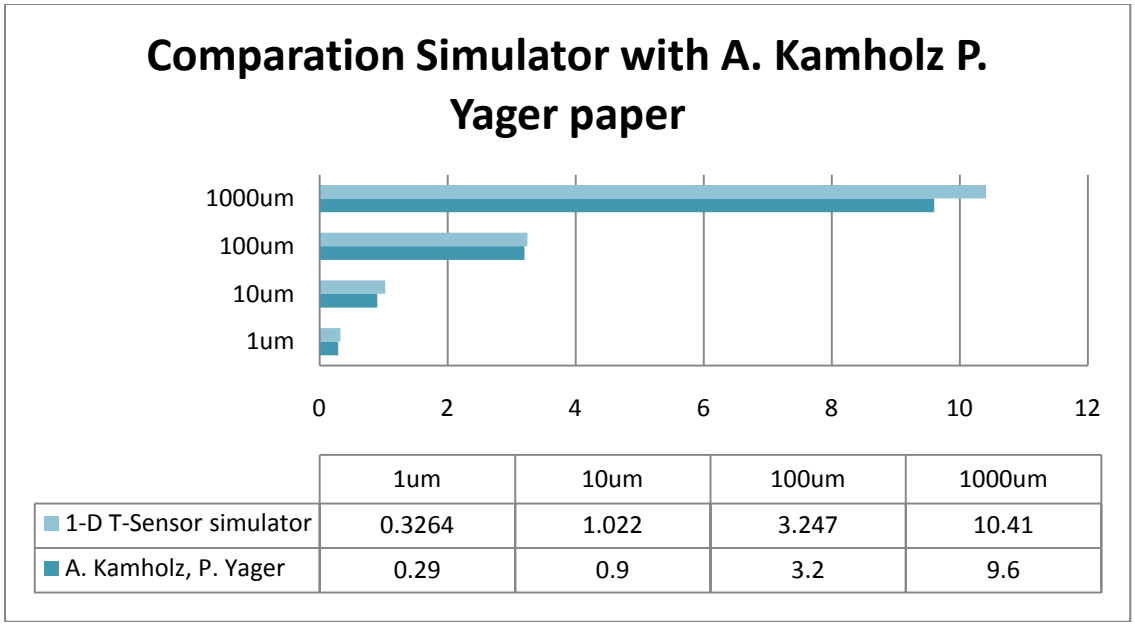

	1um	10um	100um	1000um
1-D T-Sensor simulator	0.3264	1.022	3.247	10.41
A. Kamholz, P. Yager	0.29	0.9	3.2	9.6

Fig. 4.47 Comparison between the E.Kamholz, P. Yager paper end the simulation using the 1-D T-Sensor simulator [40].

Again the results are very similar to each other. The error between them is probably because the number of points used to build the mesh is not the same.

The results here presented shows that the one dimensional simulator agrees with simulations realized by other scientists. Their results have been published in important journals that give credibility to their work. Is for this reason that we can state our simulations are reliable.

However, an experimental validation would provide even more reliability to this simulator.

4.6.2 1-Dimensional simulator validation with experimental results

Using the results of the characterization of the T-Sensor presented in Fig. 4.38, is possible to simulate the theoretic behavior for the same system and figure out which is the diffusion coefficient that fits better to the experimental profiles.

The value of diffusivity for the molecule fluorescein is well known, and many documents report it. If this parameter coincides with the one find by simulation, we will be able to state that the simulator predicts faithfully the diffusion of particles in a T-Sensor.

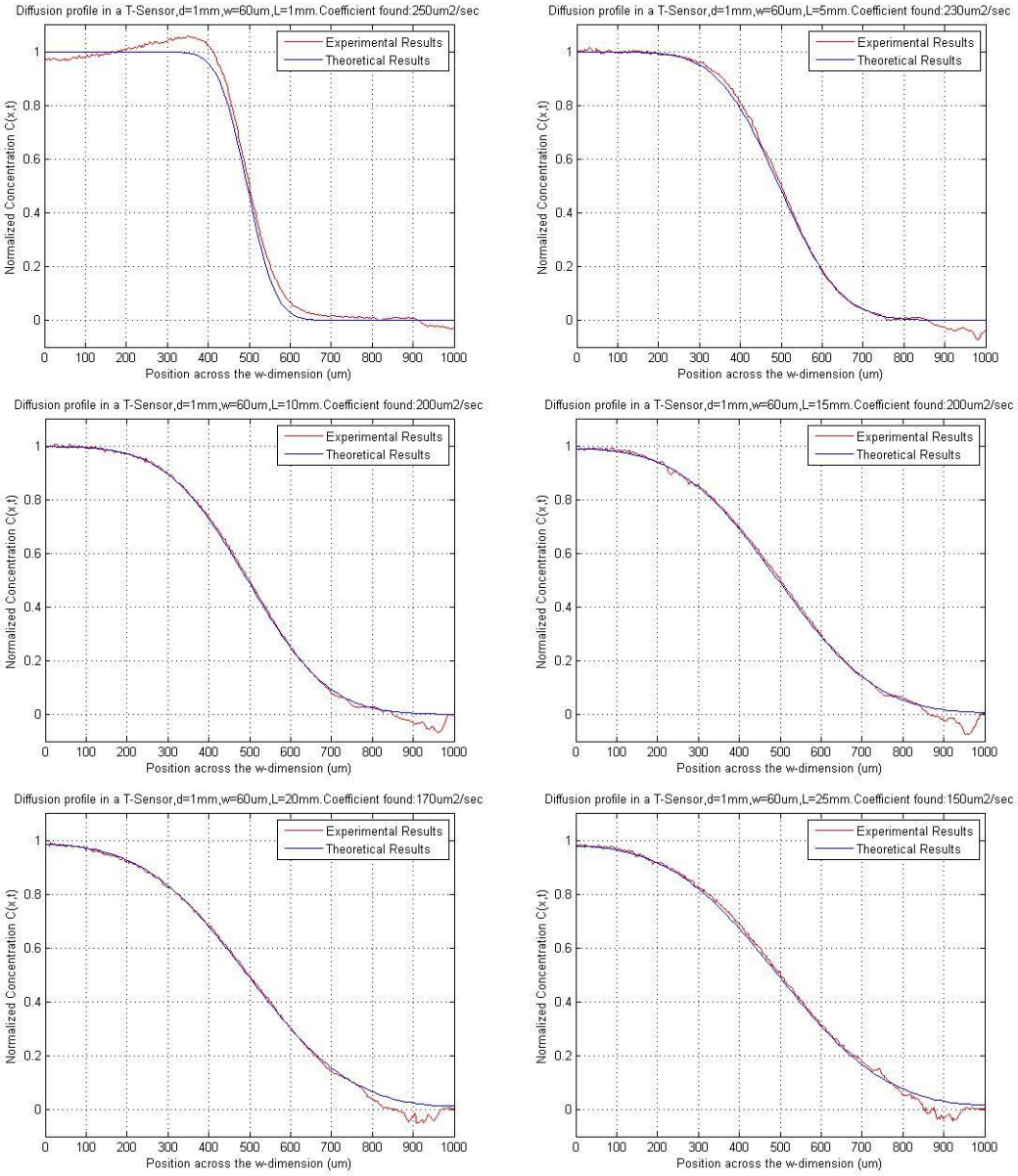

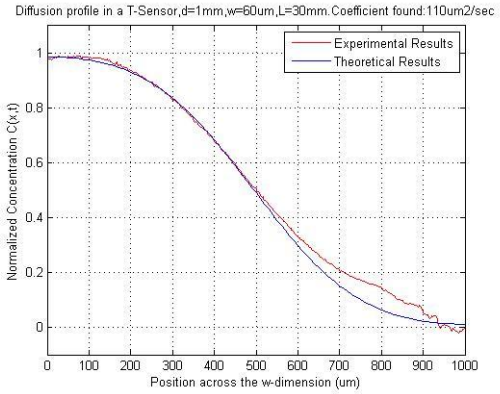

Fig. 4.48 Comparison between the theoretic concentration profile and the profile found experimentally. In each image we have found the diffusion coefficient which best approximates to the theoretical curve.

A simulation for the device studied in the characterization of the T-Sensor was made at different points downstream according to the data got from the pictures. For each image the diffusivity whose value fit better to the concentration profile was stored, and at the end the mean average of those values was calculated in order to fin the mean value of the diffusion coefficient.

The results for the best diffusion coefficients in each image are the following:

Distance downstream (mm)	***Diffusion Coefficient (μ2/s)***
1	*250*
5	*230*
10	*200*
15	*200*
20	*170*
25	*150*
30	*110*

Table 4.10 Diffusion Coefficient at different points downstream for the Fluorescein Disodium. Flow rate 20nL/s, width 1 mm, height 120 μm and longitude 3 cm.

The mean value for the Diffusion coefficient is:

$$\overline{D} = 187 \mu m^2 / s$$

The next table shows the common values found for other publications of the diffusion coefficient for the molecule Fluorescein:

Paper	***Temperature***	***Diffusion Coefficient (μm²/s)***
Rapid Diffusion of Fluorescent Tracers into Staphylococcus epidermidis Biofilms Visualized by Time Lapse Microscopy [41]	*21.5°C*	*490 μm²/s*
Measurements of local diffusion coefficients in biofilms by microinjection and confocal microscopy. Biotechnol [42]	*21.5°C*	*From 500 to 600 μm²/s*
Introduction to microfluidics by Patrick Tabeling [18]	*20°C*	*300 μm²/s*

Table 4.11 Values of the diffusion coefficient found in other publications for the molecule Fluorescein.

According with the Table 4.11, the value that we have found is significantly low.

Probably this difference is because of the temperature. The diffusion coefficient changes very quickly with the temperature. At 21.5°C the diffusion coefficient is very similar, around 500μm²/s, but when the temperature is to 20°C the diffusivity decreases to 300μm²/s. Our experiment was done in a room whose temperature was 17°C. Temperature may be a reasonable explanation for the value of diffusivity found with the experiment.

Following the comparison for the experimental results with the theoretic results using the mean value of the diffusion coefficient are presented:

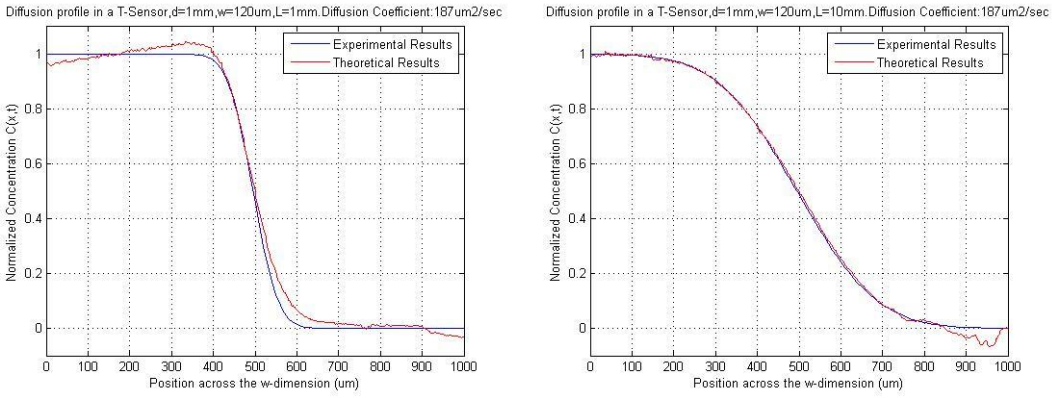

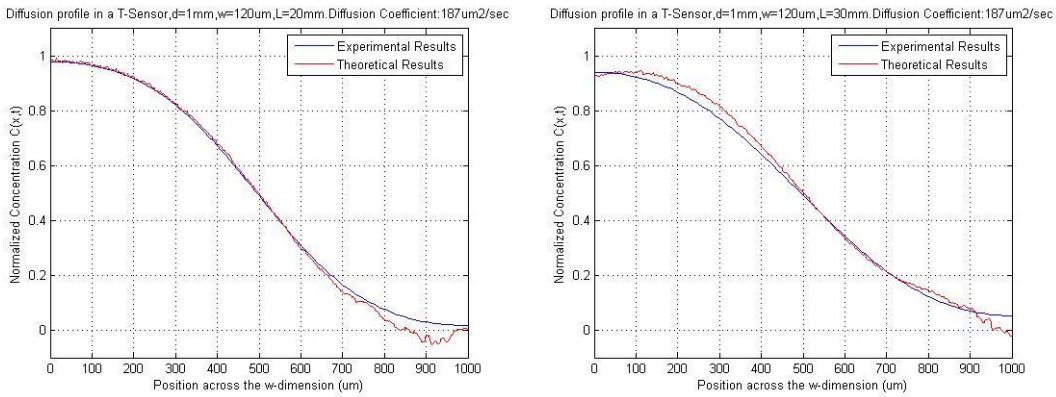

Fig. 4.49 Comparison between the theoretic concentration profile and the profile found experimentally. The diffusion coefficient is 187μm²/s for all the simulations.

The simulations using the mean value of the diffusivity fit perfectly to the experimental results.

Finally after theoretical validations (by comparison of previous reported results in papers) and experimental validations (comparing the simulations with experimental results) we are able to state the reliability of this programmed simulator.

The programming of this simulator have provides a strong background in processes based on diffusion of particles. Following the same procedure we are able to find new simulators that adapted to specific situations are able to describe real phenomena mathematically.

5 FABRICATION AND CHARACTERIZATION OF A MICROFLUIDIC DEVICE: PLANAR DIFFUSION CHAMBER (PDC)

Chapter five is the main part of this work. In this section a device capable to release different chemical signals at the same time avoiding shear stress is presented. The section is divided in two parts: in the first one the device is fabricated using a technique based on a thin layer known as mortar layer and in the second one the device is fabricated using regular soft-lithography techniques.

5.1 Microfluidic Diffusion Chamber

The generation of chemical gradients by the release and diffusion of particles controls many complex processes in biology. For example, chemotaxis (the migration of cells along a chemical gradient) plays a key role in cancer spreading.

Models of biochemical gradients have been used to validate by looking at cellular response to specific soluble signal. Due to the simplicity of the approach, devices that generate gradients by using laminar flow (such as the T-Sensor) have been used extensible to study chemotaxis of adherent cells [43]. However, this method implies the introduction of convective flow that cells may not experience normally. As we saw in previous chapters, convective flow provokes shear stress on the cell surfaces, which sometime may yield unexpected and unwanted results.

Here is presented a device that allows the generation of multiple chemical gradients using different chemical signals (soluble molecules), avoiding the issues that devices based on convective flow present.

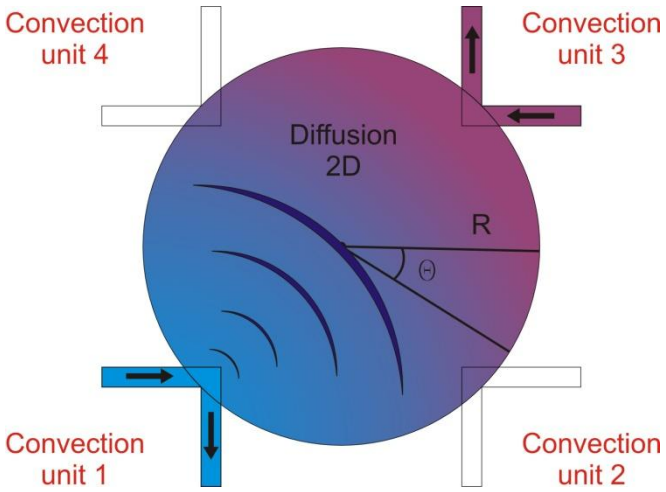

Fig. 5.50 Schematic representation of the PDC shape. The fluids flow in the convection unit channels, but there is no convective flux inside the circular micro-chamber.

The fluid flows in the convection units only. Some of the molecules present in the fluid are able to go in the micro-chamber by diffusion process, which means that all the particles placed in the micro-chamber move only by Brownian motion.

This device is able to generate up to four different gradients at the same time, just infusing the required molecule dissolved in a solvent in the convenient convection unit.

5.2 Design

In order to achieve the goal of multiple chemical signaling at the same time avoiding convective flow (shear stress), the convective units and the micro-chamber cannot be placed in the same layer. Otherwise the flux would get in the chamber producing shear stress.

What we suggest is a device with three different layers, each one on the other. The aim of this work is to achieve four different signals reaching a cell culture, so obviously, there have to be a space where grow those cells. That space is called cell culture chamber or diffusion layer, because in this chamber the motion of particles has to be only by diffusion. Cells are usually grown on petri dishes or on glass slides, so this layer must be just on these surfaces, which means that this layer must be placed below the others. The microfluidic layer that contains the microchannels (convection units), will be placed on the top of the device (over the cell culture chamber). In order to avoid the infusion of convective flux into the cell chamber, these two layers have to be physically separated, but at the same time the passage of molecules from the microchannels into the chamber by diffusion must be guaranteed. Using a polycarbonate nano-porous membrane, we can achieve this behavior.

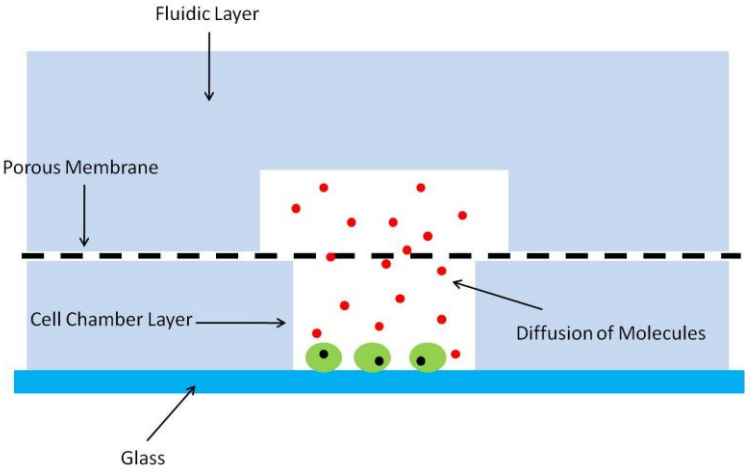

Fig. 5.51 Schematic representation of the main PDC behavior. Molecules dissolved in a solvent flow in the fluidic layer. When these molecules pass over the membrane, they are able to diffuse across the porous into the diffusion layer.

Such as we did in the chapter before, we will study the laminarity of the microfluidic layer:

The basic features for the fluidic layer are:

$$w = 0.7mm$$
$$h = 60\mu m$$
$$L = 15mm$$

Since the results of the T-Sensor made by hand were definitely good, we have decided to apply the same technique for this device. It is for that reason the dimensions of the microchannels are that big.

According to the expression (4.30), using this features the minimum mean velocity that would not ensure laminar flow is:

$$\mathrm{Re} < 2300 \Leftrightarrow \bar{v} < \frac{2300 \cdot \upsilon}{2h} = 21.7\, {}^{m}\!/_{s} = 78.12\, {}^{km}\!/_{h} \qquad (5.55)$$

This is a huge velocity in terms of microfluidics, so we can state that the system's dimensions ensure laminar flow inside the device. Before starting the fabrication process, a layout of the device, specifying all dimensions and the position of each part in the device is needed. Using Corel DrawX drawing software, we designed the scheme of PDC at real scale:

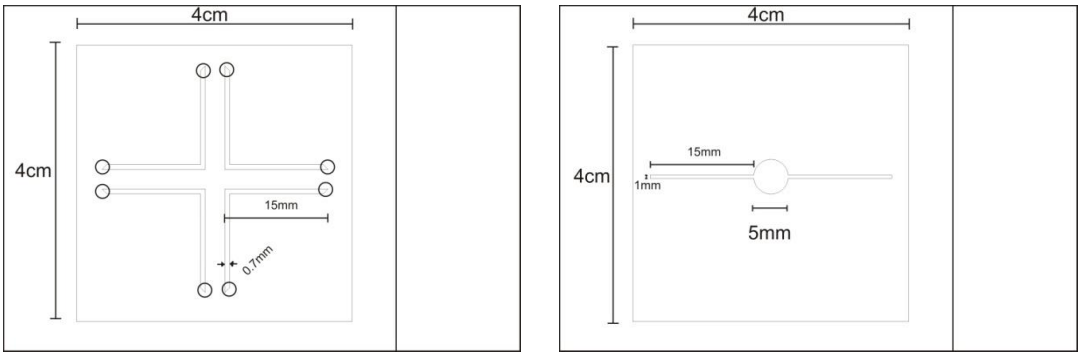

Fig. 5.52PDC layout fluidic layer (on the left) and diffusion layer (on the right).

5.3 Fabrication

Because of the features of this device are large enough we can use the Scotch Tape Patterned Method instead of common photolithography techniques that are much more expensive and slow. As we have seen in **Chapter 4** this technique provides quality master to be used in replication of devices by PDMS stamping.

5.3.1 Required materials

The required materials to fabricate the master are those used in the fabrication in the master of the T-SENSOR. In order to fabricate PDC we need the same tools and some others. Below is presented the whole list of materials that were used in the fabrication of PDC:

- Glass slides, pre-cleaned from Manufacturer (Fisher Scientific, 75mm x 50mm x 1mm, Cat. No. 12-550-C).
- Scotch tape (3M Scotch® Transparent Tape 600).
- Stainless steel Scalpel or surgical blade with (Feather Safety Razor Co., LTD, Cat. No. 2976#11).
- Polystyrene Petri dish (Fisher Scientific, 100mm x 15mm, Cat. No. 08-757-12).
- Tweezers.
- Oven or hot plate (to work at 65°C).

- Gloves (do not use latex gloves).
- PDMS silicone elastomer base and curing agent (Sylgard 184, Dow Corning).
- Heptane H-350-1 (Fisher Scientific, Cat. No. 102258).
- 200 nm pore-size polycarbonate membrane (Cat. #29559, Whatman, Piscatway, NJ).
- 1.22 mm diameter biopsy puncher (Harris Uni-Core, Prod #15074).
- Spinner WS-400 Lite Series Spin Processor (Laurell Technologies Corporation).
- Circular shape pattern.

5.3.2 Fabrication process: chemical bonding

The most important issue fabricating PDMS devices and incorporating synthetic membranes is how sealing the membrane to the PDMS. As first approach we decided to use a technique called "chemical bonding".

This method consists in the fabrication of two layers using a mixture of base and curing agent of PDMS different to the regular 10:1. With excess of base in one layer and excess of curing agent in the other, when we put in contact the two layers only semi-cured, there is a chemical bonding on the contact surface. If the two mixtures were able to cross the membrane, this union would be made linking the two layers across the membrane, what would mean an irreversible bonding of the membrane to the PDMS.

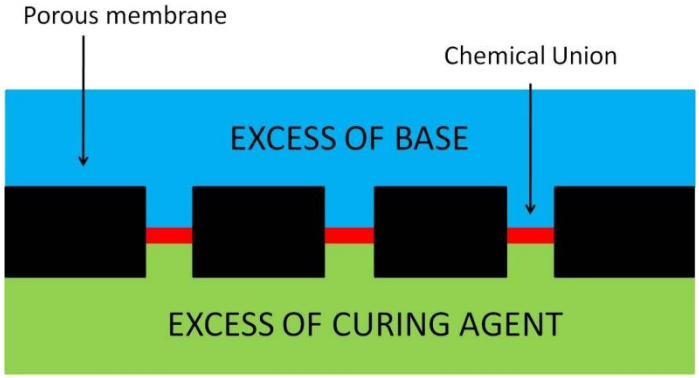

Fig. 5.53 Schematic of chemical bonding. The excess of base presented in the layer on the top uses the excess of curing agent presented in the layer on the bottom. After curing this union in the two surfaces gets completely cured providing an irreversible chemical bonding.

The proportions used are [44]:

- 3:1 Microfluidic layer.
- 30:1 Diffusion layer.

The layer with excess of curing agent (fluidic layer) once is cured becomes more rigid than a piece of regular PDMS. On the other hand, the layer with excess of base (diffusion) once is cured becomes stickier than the regular PDMS. The selection of what layer would be fabricated using each proportion was made according to this behavior, minimizing the difficulty of the fabrication process.

Once the master is fabricated using the Scotch Tape Patterned Method, we mix the base and the cuing agent according to the proportions presented below. When the two masters are put in petri dishes the PDMS mixtures are poured into the dishes until the masters are totally covered.

PDMS has to be degassed in a vacuum chamber for at least 1 hour in order to remove all the air bubbles that can deform the device, and after that the petri dish can be placed in the oven at 65°C.

The microfluidic layer replica has to be in the oven for 10 minutes, just to semi-cure the PDMS. That means PDMS is cured enough to be manipulated with tools but still needs more time in the oven in order to be completely cured.

Then, we cut the replica and peel the replica off gently because since the PDMS is not totally cured it becomes very fragile, so this step must be done carefully.

After that, using a biopsy puncher we make holes at the beginning and at the end of each microchannel, and also placing the replica on the diffusion layer layout, we make holes where channels connected to the chamber will be placed.

The diffusion layer replica has to be in the oven for 31 minutes, just to semi-cure the PDMS. That means PDMS is cured enough to be manipulated with tools but still needs more time in the oven in order to be completely cured.

Then, we cut the replica and peel the replica off gently. Again, this step has to be done carefully because the PDMS is not completely cured yet and it is susceptible to be broken.

Once the two layers are ready, we put the porous membrane on the diffusion layer surface, trying to ensure that the whole chamber is covered. After that we place the microfluidic layer on the top of the duo diffusion layer-membrane, making sure that the corners of the four channels are positioned over the cell culture chamber.

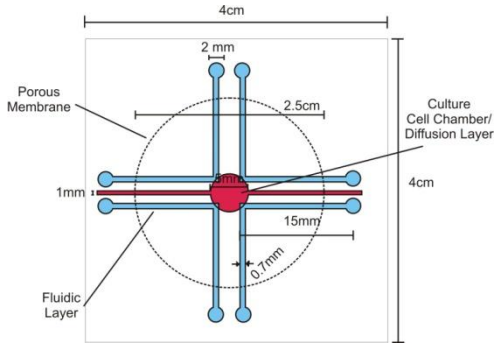

Fig. 5.54 Schematic of PDC.

Finally, the complete system is kept in the oven for at least two more hours in order to cure the PDMS.

The results demonstrated that this was not a good system because the PDMS was not able to penetrate into the membrane and cure inside. Then, even achieving perfectly adhesion in zones PDMS-PDMS, the membrane was not sealed to the system, inducing to leakage issues. Also, the diffusing layer (with excess of base/monomer) never achieved complete curing, which means that many of the monomers had not reacted with the curing agent (that yielded in that stickiness). Those free monomers are extremely toxic for the cells, which makes this technique inappropriate.

5.3.3 Fabrication process: mortar layer

In **Chapter 3** the concept of the PDMS-PDMS bonding using a "*mortar layer*" of uncured PDMS was presented. The main idea is use a thin film of uncured PDMS as glue. This uncured PDMS has the same molecular structure as the layers of cured PDMS that we want to seal. That provokes the molecular chain of this polymer presented in one layer can continue across of the mortar layer and reach the second layer. Doing this, and after curing the mortar layer we achieve a strong bonding between the two pieces of PDMS.

After the first try using chemical bonding as sealing method we decided to use this second method that is easier and does not waste the large amount of PDMS the chemical bonding does. We can divide the fabrication protocol in four parts: microfluidic layer fabrication, diffusion layer fabrication, the mortar layer spinning and three layers bonding.

- **Microfluidic layer:**

First of all, the masters of the microfluidic layer and the diffusion layer are fabricated using the Scotch Tape Patterned Method [3], and once it is done we replicate only the microfluidic master using a PDMS stamps.

When the replica is ready, cured and peeled off the petri dish, we punch holes in the PDMS replica for the inlets and outlets for each microchannel.

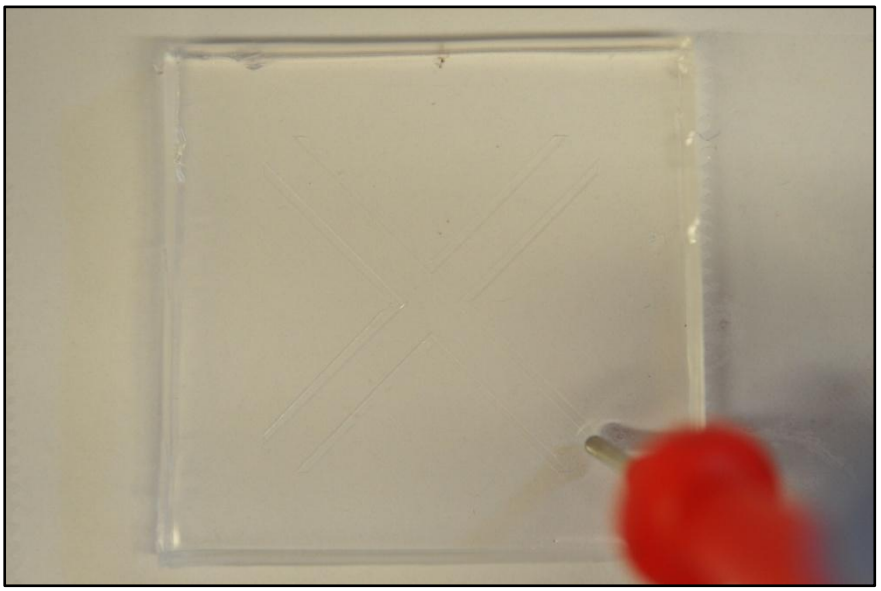

Fig. 5.55 Punching inlet and outlet holes in each microchannel in the fluidic layer.

In this layer we also have to make the holes that will connect the tubing to the inlet and outlet of the channels presented in the cell chamber. In order to do that, firstly we put the PDMS stamp on the culture cell layout with the channels facing down and ensuring that the four corners of the channels are inside the chamber. Then we punch holes in the PDMS replica for the inlets and outlets channels in the culture cell layer

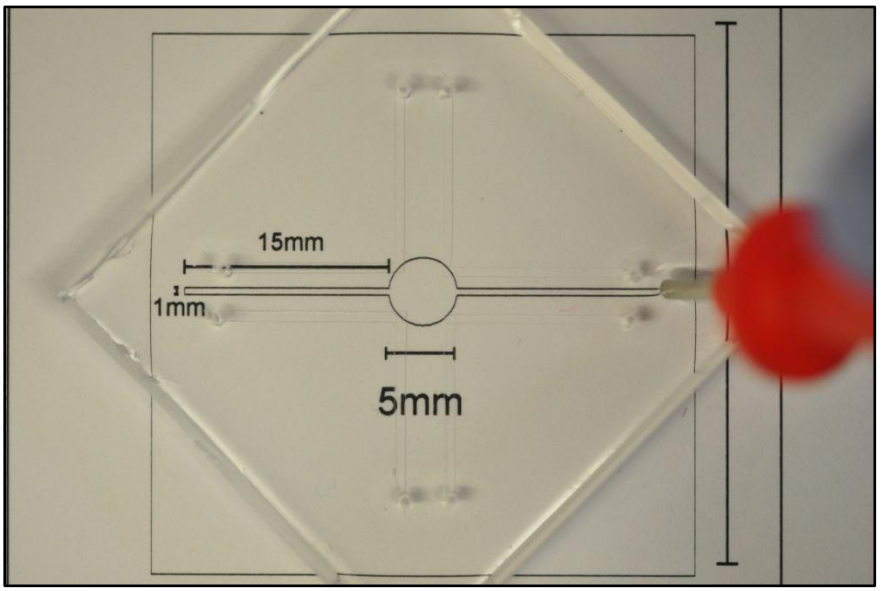

Fig. 5.56 Punching inlet and outlet holes in the diffusion layer microchannel.

Finally we clean the surface marked with the microchannels with Scotch Tape.

- **Diffusion layer:**

We want the cell culture chamber placed on a piece of glass, because is better when we grow cells. For this reason we fabricate this layer using a different method. Firstly we

mix the base and curing components of PDMS following the proportion 10:1 base:curing agent and we spin a layer of PDMS on a glass slide with a thickness of 200 µm. In order to do that use the spinner WS-400 Lite programming the next steps:

	Time (s)	***Rate (rpm)***	***Acceleration (rpm/s)***
Step 1	*5*	*550*	*544*
Step 2	*20*	*550*	*544*

Table 5.12 Steps configuration for achieve a 200 µm thickness layer of PDM.

Once the uncured PDMS is spreaded on the glass slide, it is time to cure it in an oven at 65°C for 30 minutes. After that we will cut the shape of the diffusion layer from the layout, and for doing this it is necessary to place the glass slide on the printout with the coated spin PDMS facing up. Align the glass slide to the cell culture chamber layout and fix it to the printout with a piece of Scotch tape on the corner of the slide. Then, using a scalpel, we cut the PDMS on the glass slide according to the layout (for cutting we used another glass slide as a ruler and a circular shape pattern).

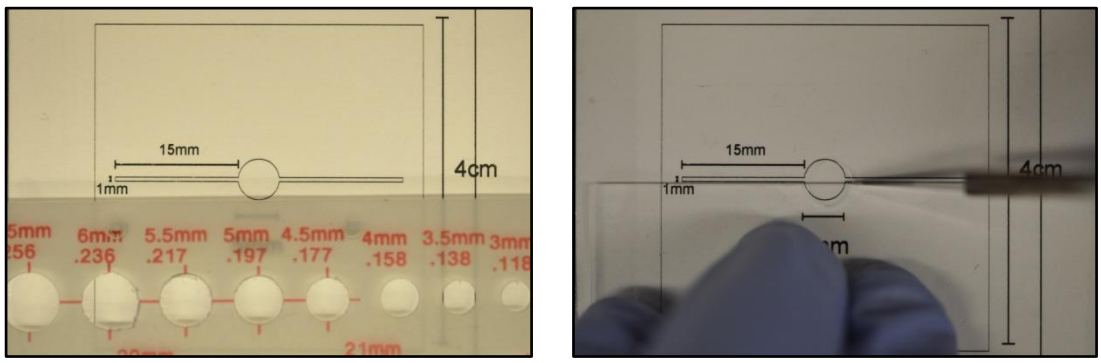

Fig. 5.57 Cutting the cell culture chamber.

Now, the cell culture chamber and the microchannels connected to it are exposed to everything. What we have to do is protect this channels and the chamber with Scotch Tape. In order to get that, we attach a strip of Scotch tape to another glass slide, and we cut the shape of the chamber and the channels just using the same technique as we used before. Covering the chamber and the channels with this tape we will protect the device in the next steps.

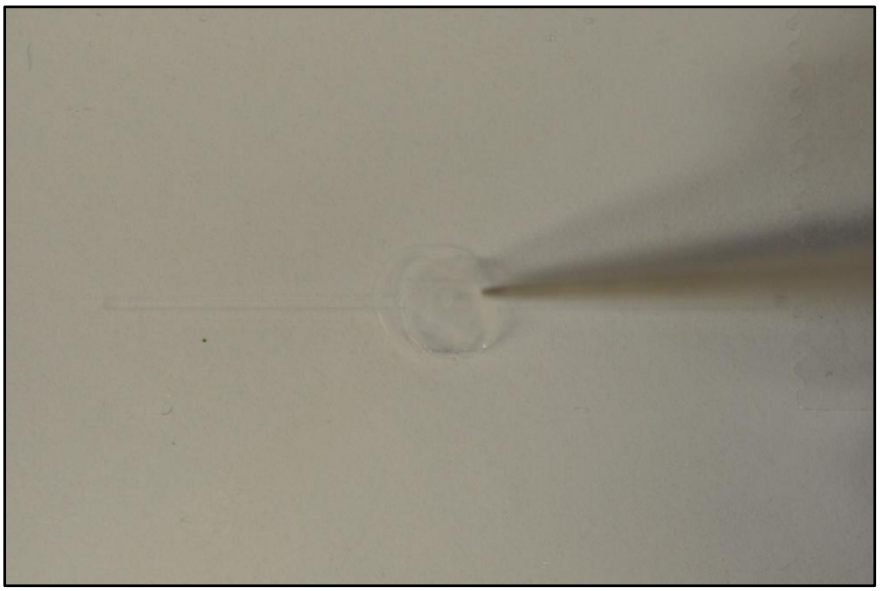

Fig. 5.58 Peeling off the tape with the shape of the chamber that will protect the real chamber of future processes.

- **Mortar layer spinning:**

The mortar layer will act as glue attaching the two layers of PDMS, and making a sandwich with the membrane. This mortar layer has to be thick enough in order to achieve good levels of adhesion, but a layer too much thick will produce overflow in the microchannels. A mortar layer of 15 μm guarantees enough adhesion avoid the overflow. The main problem is with PDMS 10:1 we can only can get layers of 30 μm as minimum using a spinner. It is necessary to dissolve the PDMS making it more liquid, achieving lower values of thickness.

We mix PDMS with the regular proportion (10:1) with the dissolvent heptane following the proportion 1:1 PDMS:heptane [37]. We dissolve the PDMS with heptane in order to achieve a layer of PDMS lower than 30 μm.

The it is possible to spin a layer of PDMS on a glass slide with a thickness of 15 μm. In order to do this use the spinner WS-400 Lite programming the next steps:

	Time (s)	***Rate (rpm)***	***Acceleration (rpm/)s***
Step 1	*5*	*500*	*544*
Step 2	*29*	*4800*	*1088*

Table 5.13 Steps configuration for achieve a 15 μm thickness layer of PDMS.

We do not cure this layer in the oven yet.

- **Three layers bonding:**

Finally it is time to seal the whole system. First of all we cut piece of PDMS with a thickness of 5 mm approximately and make a circular hole of 20 mm diameter. From now will call this piece as membrane holder.

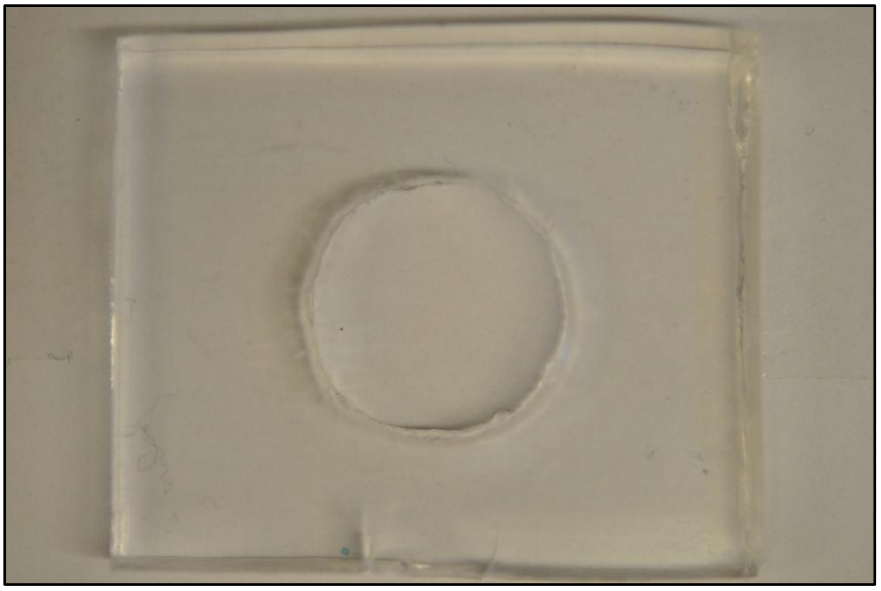

Fig. 5.59 Porous membrane holder.

The transference of the mortar layer from the glass slide to the layers of PDC is made by surface contact. So now we put in contact the channel structure and the membrane holder with a glass slide spin-coated with a heptane-diluted PDMS for 30 seconds.

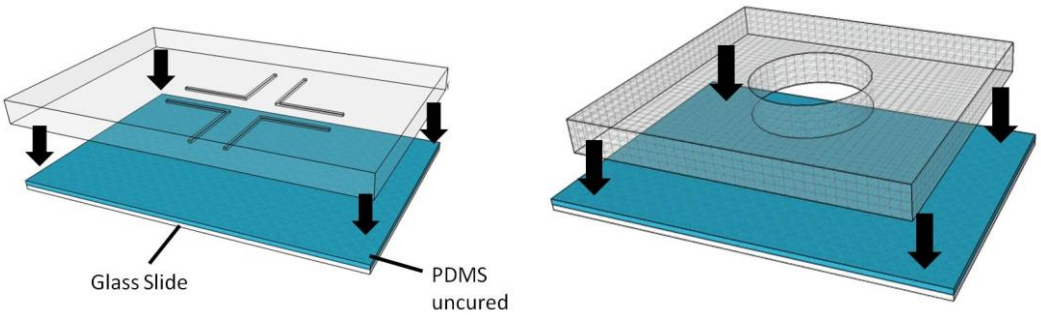

Fig. 5.60 PDMS mortar layer transfer to the microfluidic layer (on the left) and to the membrane holder (on the right).

When we make a sandwich with the membrane in the middle of the two layers, around the membrane always is formed an air gap. The liquid flowing in the microchannels can leak into this gap of air arriving to the other microchannels. In order to solve this problem we can fill this gap with mortar before, thus, blocking the access to possible leakages. What we have to do is stamping the edges of the membrane with uncured PDMS.

Achieving this is easy putting the porous membrane on the holder with the surface with PDMS facing up.

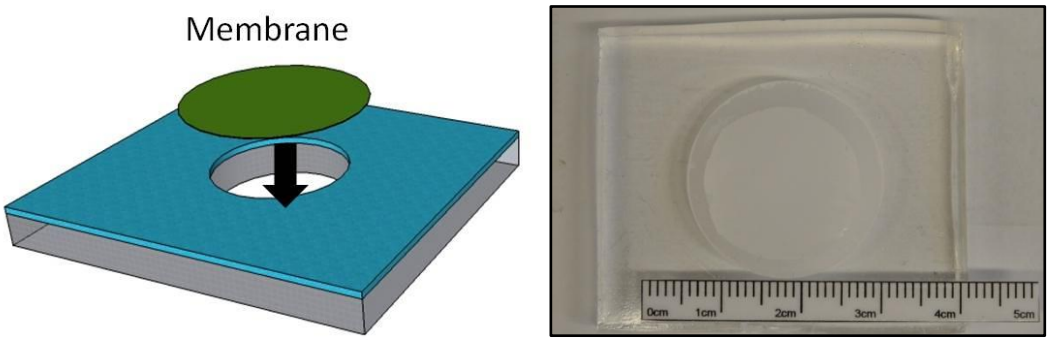

Fig. 5.61 PDMS mortar layer transfer to the membrane (on the left) and to the membrane holder with the membrane (on the right).

At this point we have transferred mortar to the microfluidic layer and to the membrane. Now is time to transfer it to the diffusion layer. We will do it spinning a thin layer of mortar on the surface of this piece. Spin a layer of 15 µm on the cell culture chamber layer. (The cell chamber and the inlet and outlet were covered with tape in order to avoid the filling of them with PDMS in this step).

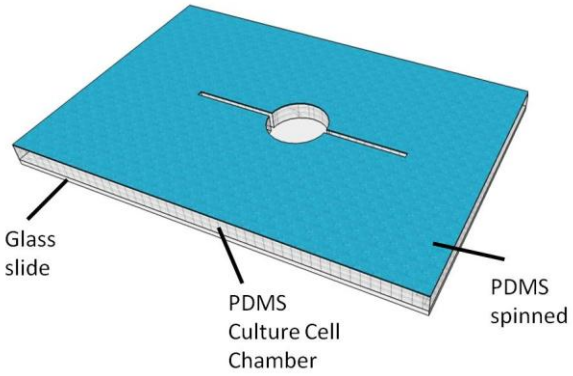

Fig. 5.62 Scheme of mortar layer spinned on the surface of the diffusion layer.

Since we cover the chamber and the channels with tape before, now they are not filled with uncured PDMS. we peel the unwanted tape in the culture cell layer off.

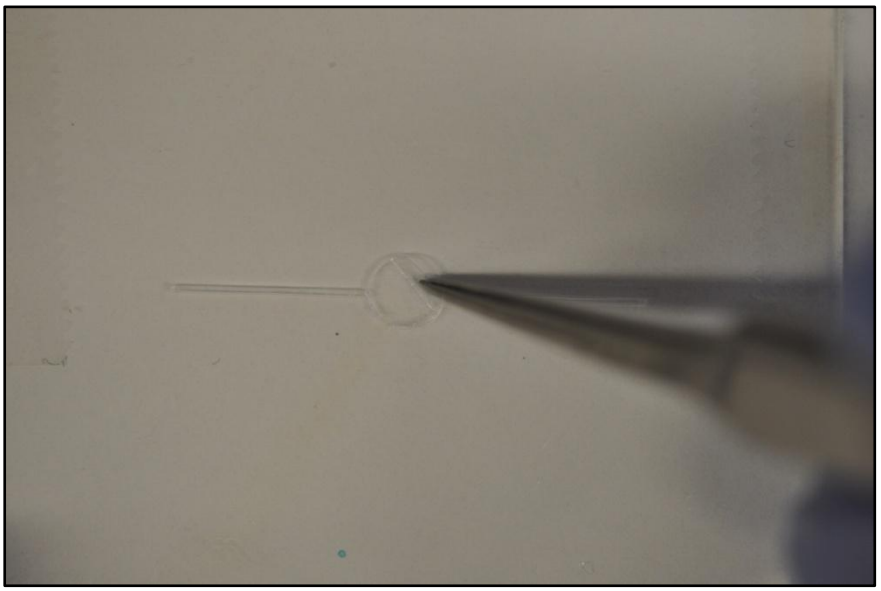

Fig. 5.63 Peeling off the tape that is covering the chamber and the channels.

All the pieces have been impregnated with a thin layer of uncured PDMS that will act as glue, sealing the whole system together. Now we must put the three parts together and we start by putting the membrane on the cell culture chamber layer ensuring that the chamber gets completely covered by the membrane.

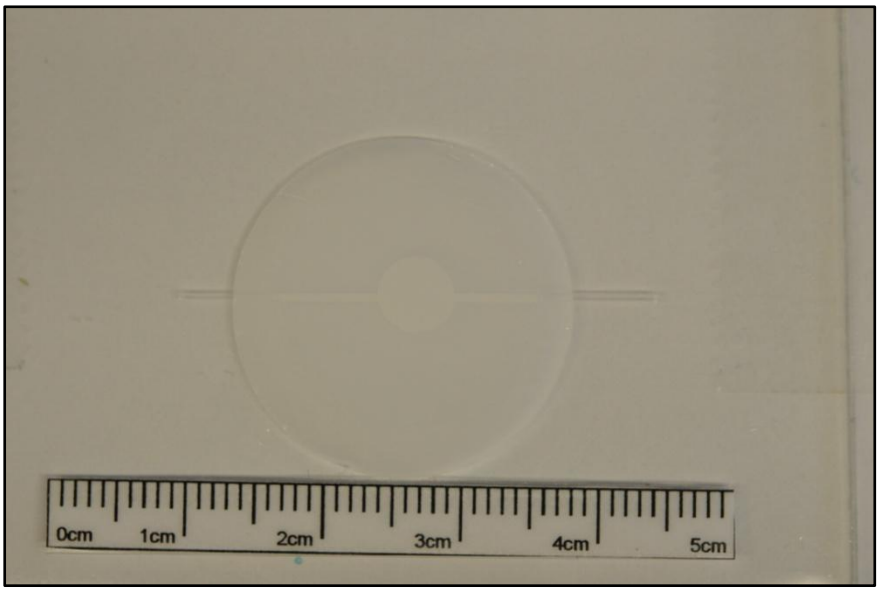

Fig. 5.64 Adhesion of the membrane with the diffusion layer.

This process is delicate; we have to make sure that there are no air bubbles between the membrane and the PDMS layer. After that we put the microchannel layer on the cell culture chamber layer ensuring that the 4 corners in the channels get over the chamber.

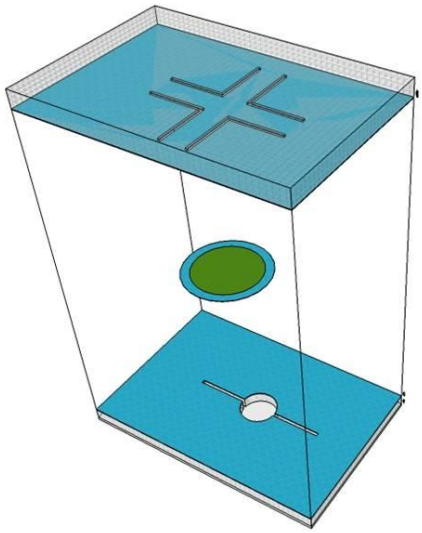

Fig. 5.65 Scheme of three impregnated layers giving form to PDC.

Finally the device is completed and only rest to cure the mortar layer that will provide irreversible bonding to the three pieces. Before to keep the system in the oven we leave the combined system at ambient conditions for 30 minutes in order to eliminate air bubbles trapped along the edge of the membrane. The last step is curing the combined system at 65°C in an oven for at least 60 minutes.

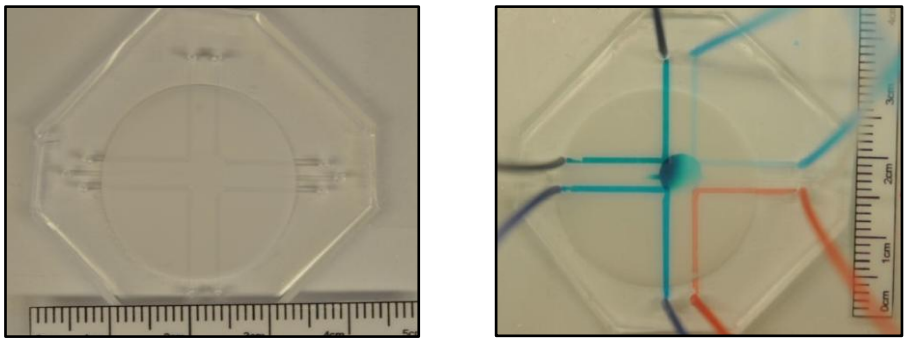

Fig. 5.66 PDC after complete the whole fabrication protocol (on the left), PDC behavior (on the right).

The figure Fig. 5.66 shows the device resulting of this process. We can appreciate how, again, using the simple technique of the "Scotch Tape Patterned Method" we can fabricate complicated microfluidic devices.

5.4 Experimental Characterization

Once the device has been fabricated it is time to characterize its behavior experimentally. In order to do that a PDC was fabricated using the same features and the same processes presented before. For simplicity, just one convection unit was working with constant flow (20nL/sec) of DI water and red ink. In addition cell culture chamber was filled only with DI water, producing a differential gradient of ink particles between the diffusion and the fluidic layers. We expected that when the flow in the microfluidic

layer passed over the cell culture chamber, some molecules would be able to cross the nano-porous membrane, and once they were in the diffusion layer would diffuse everywhere in the chamber.

The most important characteristics for the systems are presented in the next table:

w *(width microchannel)*	*700 µm*
h *(height microchannel)*	*60 µm*
L *(Longitude microchannel)*	*15+15 mm*
h' *(height chamber)*	*200 µm*
R *(Radius chamber)*	*2.5 mm*
Q *(Flow Rate in convection unit)*	*20 nL/s*
V *(Velocity in convection unit)*	*476.19 µm/s*

Table 5.14 PDC principal features.

The evolution of this process was recorded at 24 frames per second in a MJPG format video during more than 6 minutes. Using MATLAB we load the video in memory and we could get captures of the frames of interest. Below are showed captures every two minutes with which we can understand the behavior of this device. This experiment was made four different times achieving always the same results.

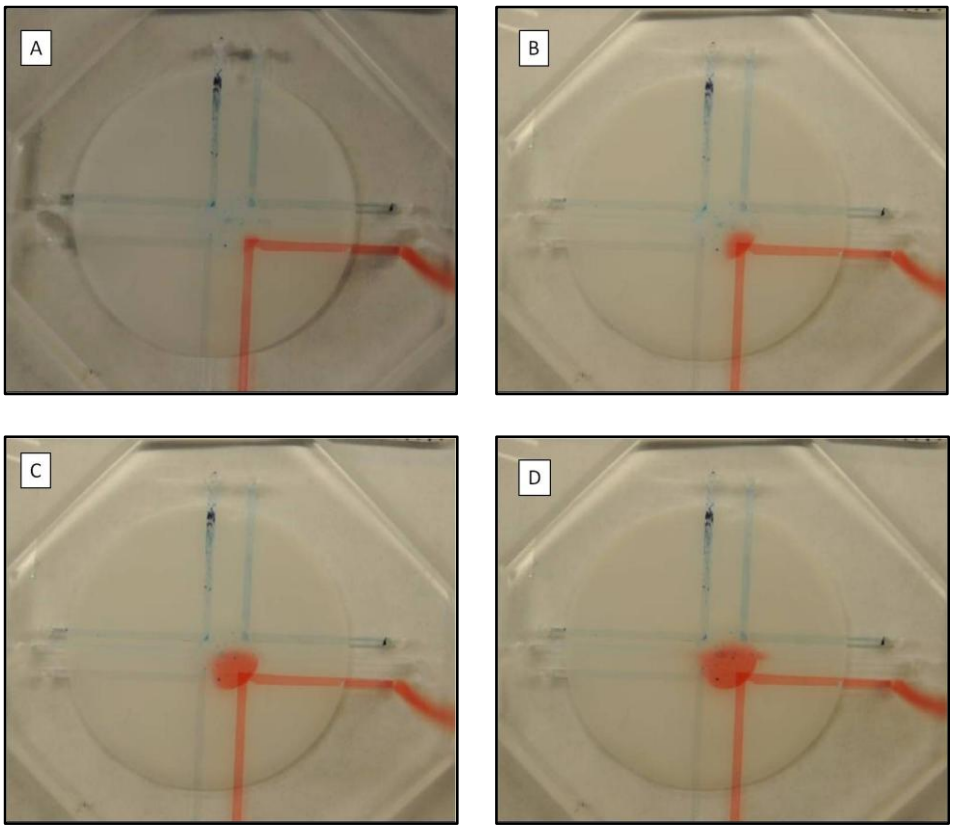

Fig. 5.67 Diffusion of red ink in the cell culture chamber. Captures were taken at instants 0 (image A), 2 (image B), 4 (image C) and 6 (image D) minutes.

Figure Fig. 5.67 describes the behavior of PDC. During the time more molecules coming from the microchannels placed at the fluidic layer, goes into the chamber, and they diffuse following a circular distribution. These results agree with our first hypothesis very well.

5.4.1 Data acquisition and image processing

The frames extracted from the video were processed in order to get the pixel intensity information that is proportional to the real concentration of molecules. The frames of interest were taken from 0 to 4 minutes every 30 seconds, so the required captures from the 8952 frames that the video had got were:

$$FrameNumber = 24\,fps \cdot 30\,\text{sec} \cdot i$$
$$i = 0,1,2,\ldots,8$$

The concentration profiles must be taken along lines inside the chamber. Thereby we defined three different segments; AB, AC and AD, over which we will extract the intensity of each pixel per each frame.

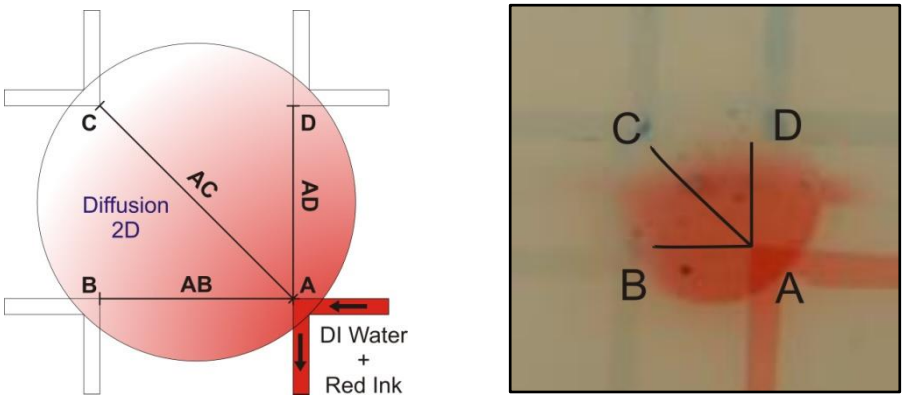

Fig. 5.68 Distribution of segments where the concentration profile will be calculated. On the left schematic, on the right real picture.

Ink molecules diffuse from the section of channel in contact with the chamber across the membrane; this is a circular sector area. We could think that the first point A should be placed in the center of this area instead of just in the corner of the microchannel. In the figure Fig. 5.68 (right) we can see how the light intensity of this sector area is higher than the intensity at any other place in the chamber. This is because red ink molecules in the microchannel are just above of those red molecules in the cell chamber, producing the addition of their light intensity in that zone.

Because the concentration under this area have to be very similar to the concentration of just in the corner of the channel, we took that point as the beginning of the segment, choosing the intensity in that point as the maximum concentration of molecules in the chamber. This concentration is taken a value used to normalize the concentration profiles during the image processing.

Once the data has been acquired (getting the frames) it has to be processed, and we do it with MATLAB R2009. Every color image in MATLAB is treated as three dimensional matrix ***Height x Width x RGB*** where RGB is 3, and correspond to the three different planes Red, Green, Bleu in which the code RGB is based on. The intensity information that is required in this case depends on these three different planes at the same time. Therefore, we have to transform this three dimensional matrix into a two dimensional one with a specific average of their planes. A lineal transformation called *"grayscale" [45]*:

$$Intensity_{GrayScale} = 0.3 \cdot Intensity_{Red} + 0.59 \cdot Intensity_{Green} + 0.11 \cdot Intensity_{Blue} \qquad (5.56)$$

With this transformation the image becomes a two dimensional matrix ***Height x Width***, where each element is encoded with 8 bits, taking a value between 0 and 255. In this kind of codification 0 corresponds to color black and 255 corresponds to color white and this number is tightly related with the concentration of molecules in its position.

We could take the information of a single line of pixels according to the segment of interest and obtain the intensity information from them. That would provide an intensity profile over that segment, and after some processing we would get the normalized concentration profiles. This method presents a disadvantage; if along this line of pixels in the matrix (row, column...) appears some unwanted value, coming from a shadow for example, it would be represented in the final concentration profile. In order to reduce this type of errors we should average the line of pixels with some other lines around it.

For the segment AB we took the pixels from the row of interest and the pixels from the two rows above and two rows below. These five rows were averaged reducing the errors of possible shadows. The same process was followed for the segment AD, the five columns averaged were; the column of interest, two on the left and two more on the right.

The MATLAB code necessary to process the images coming from the video is shown in the **Appendix D.**

The results obtained in this image processing are presented below:

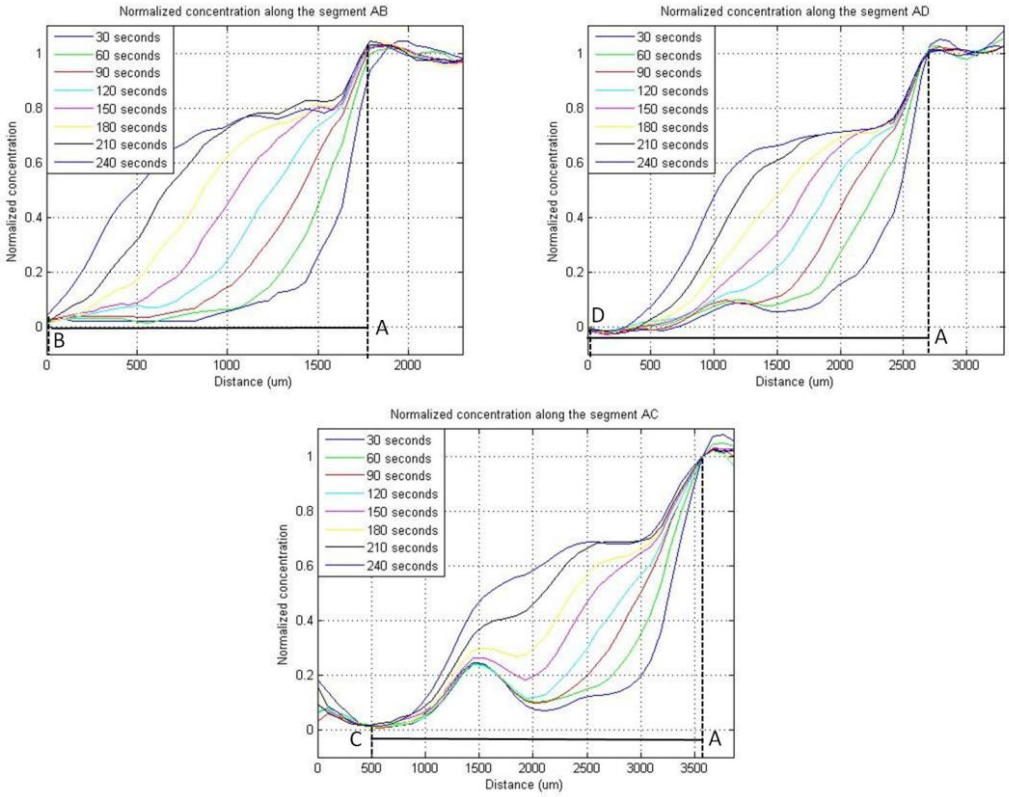

Fig. 5.69 Normalized concentration profiles in PDC of red ink for the three different segments. In each image are plotted the profiles in the segment at every 30 seconds for 4 minutes.

Fig. 5.69 shows the concentration profiles during the time for each segment. Such as it was expected, the concentration of particles inside the chamber increases as soon as the time goes on. In Fig. 5.68 (right), we can appreciate that just in the corner, over the cell culture chamber, the red intensity is larger than the rest of the parts. This is represented in the concentration profiles in the flat area around 1000 μm. The corner of the microchannel, in other words, the beginning of the segment only in the chamber is placed in the position where all profiles intersect. We can consider that point as the beginning of the real segment, normalizing the concentration taking the value of maximum intensity there (for this reason the flat area is over 1).

We can detect that around -400 μm in the segment AC there is an unexpected behavior. Suddenly the concentration increases in that point. Checking the frames from which these profiles belong we can appreciate that, unfortunately, there is a spot in the center of the chamber, and the segment AC crosses that spot.

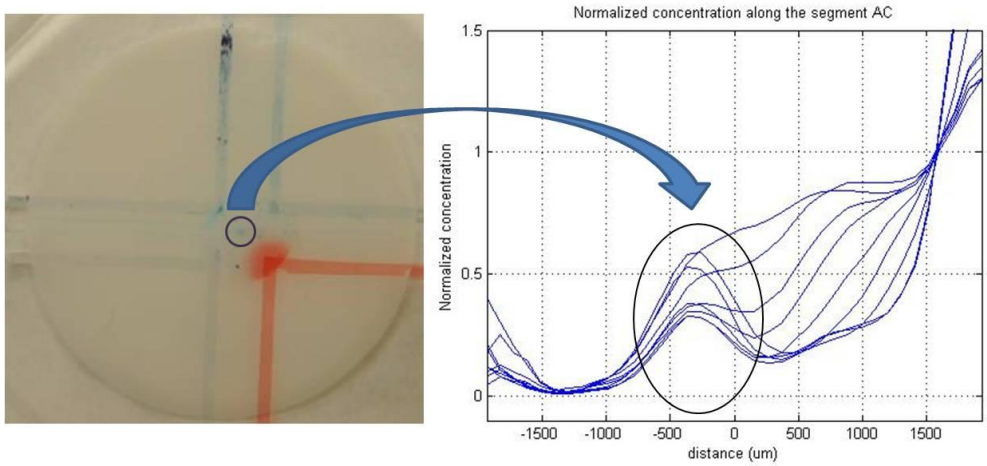

Fig. 5.70 Error due to an unexpected spot in the original image.

In order to remove this error the original image is modified changing the values of the pixels with the spot by some other pixels that are near to them. We apply the hypothesis that nearby pixels have similar intensity. The results changing the image are:

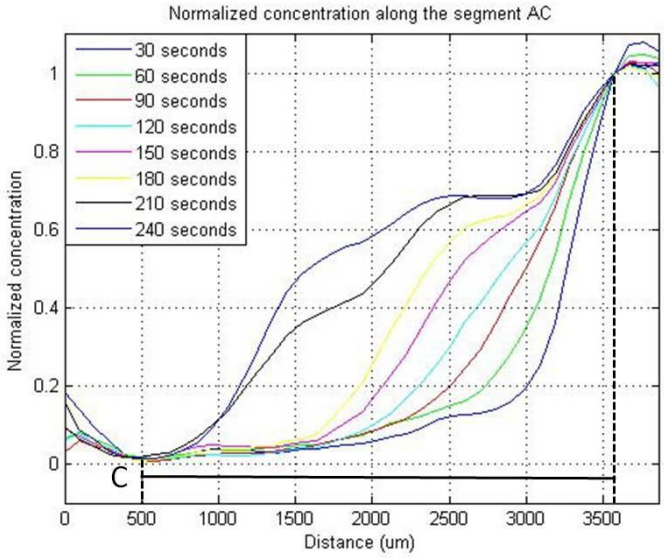

Fig. 5.71 Normalized concentration profile along the segment AC erasing the errors.

In Fig. 5.71 around -400 μm we can see how the concentration it is similar to the concentration around -600 μm. This is due to the modification of the image copying the pixels in closed positions.

5.5 Theoretical Characterization

Once an experimental characterization has been done, compare these results with a theoretical explanation will provide a better understanding of the PDC behavior as well as a way to predict how the system will respond without having to repeat the experiment every time.

In **Chapter 4** a simulator able to predict the behavior of a T-Sensor is explained. PDC is also a microfluidic device based on the process of diffusion of particles, so it can be modeled in the same way, by using the diffusion equation (4.33).

The 2-D T-SENSOR simulator can be taken as example in this case because we want to simulate the concentration in a two dimensional area during the time. But some considerations have to be taken.

In this case the area has a circular shape, instead of the case presented with the T-SENSOR, where the area had a rectangular shape. Then the easiest way to proceed is to solve the system in polar coordinates, and thus, the first step is to find a new definition of the grid used in finite differences.

In polar coordinates the mesh is defined by radius and angles. The circle is divided in a finite number of angles N, and in a finite number of longitudes M.

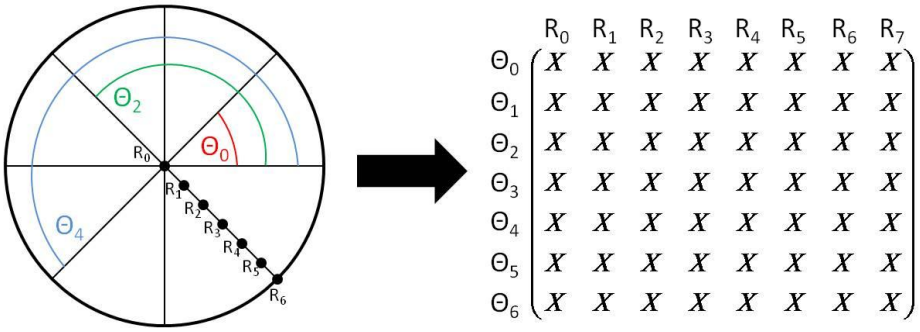

Fig. 5.72 Grid of points in polar coordinates used by finite differences.

The second step is to recalculate the diffusion equation in polar coordinates. In the equation (4.33) the terms related to the positions $\bar{x}$ and $\bar{y}$ must be changed by the new direction terms $\bar{r}$ and $\bar{\theta}$:

The relation between polar and rectangular coordinates is:

$$\begin{aligned} x &= r\cos(\theta) \\ y &= r\sin(\theta) \end{aligned} \qquad (5.57)$$

We shall now find the diffusion equation in polar coordinates. First of all it is needed the concentration partial derivative in terms of r.

$$\frac{\partial C}{\partial r} = \frac{\partial C}{\partial x}\cdot\frac{\partial x}{\partial r} + \frac{\partial C}{\partial y}\cdot\frac{\partial y}{\partial r} = \cos(\theta)\frac{\partial C}{\partial x} + \sin(\theta)\frac{\partial C}{\partial y} \qquad (5.58)$$

And the second derivative is:

$$\frac{\partial^2 C}{\partial r^2} = \frac{\partial}{\partial r}\left\{\frac{\partial C}{\partial r}\right\} = \frac{\partial}{\partial r}\left\{\frac{\partial C}{\partial x}\cdot\frac{\partial x}{\partial r} + \frac{\partial C}{\partial y}\cdot\frac{\partial y}{\partial r}\right\} = \frac{\partial A}{\partial r} + \frac{\partial B}{\partial r}$$

$$A = \frac{\partial C}{\partial x}\cdot\frac{\partial x}{\partial r} \qquad (5.59)$$

$$B = \frac{\partial C}{\partial y}\cdot\frac{\partial y}{\partial r}$$

Following the chain rule we will finally obtain:

$$\frac{\partial^2 C}{\partial r^2} = \frac{\partial^2 C}{\partial x^2}\cos^2(\theta) + 2\cdot\frac{\partial^2 C}{\partial x \partial y}\sin(\theta)\cos(\theta) + \frac{\partial^2 C}{\partial y^2}\sin^2(\theta) \qquad (5.60)$$

Now the derivative in terms of θ:

$$\frac{\partial C}{\partial \theta} = \frac{\partial C}{\partial x}\cdot\frac{\partial x}{\partial r} + \frac{\partial C}{\partial y}\cdot\frac{\partial y}{\partial r} = -r\cdot\cos(\theta)\frac{\partial C}{\partial x} + r\cdot\sin(\theta)\frac{\partial C}{\partial y} \qquad (5.61)$$

And the second derivative is:

$$\frac{\partial^2 C}{\partial \theta^2} = \frac{\partial}{\partial \theta}\left\{\frac{\partial C}{\partial \theta}\right\} = \frac{\partial}{\partial \theta}\left\{\frac{\partial C}{\partial x}\cdot\frac{\partial x}{\partial \theta} + \frac{\partial C}{\partial y}\cdot\frac{\partial y}{\partial \theta}\right\} = \frac{\partial A'}{\partial \theta} + \frac{\partial B'}{\partial \theta}$$

$$A' = \frac{\partial C}{\partial x}\cdot\frac{\partial x}{\partial \theta} \qquad (5.62)$$

$$B' = \frac{\partial C}{\partial y}\cdot\frac{\partial y}{\partial \theta}$$

And finally:

$$\frac{\partial^2 C}{\partial \theta^2} = \frac{\partial^2 C}{\partial x^2}r^2\sin^2(\theta) + \frac{\partial^2 C}{\partial y^2}r^2\cos^2(\theta) - 2\cdot\frac{\partial^2 C}{\partial x \partial y}r^2\sin(\theta)\cos(\theta) - \frac{\partial C}{\partial x}r\cos(\theta) - \frac{\partial C}{\partial y}r\sin(\theta) \qquad (5.63)$$

Thereby, we can conclude that the diffusion equation in polar coordinates is:

$$\frac{\partial C}{\partial t} = D\cdot\left(\frac{\partial^2 C}{\partial r^2} + \frac{1}{r^2}\frac{\partial^2 C}{\partial \theta^2} + \frac{1}{r}\frac{\partial C}{\partial r}\right) \qquad (5.64)$$

When the differential equation is clear, it is necessary to define the initial and the boundary conditions. In this scenario we will only solve the equation inside the cell culture chamber avoiding the process of diffusion from the fluidic layer to the diffusion layer for simplicity. Thus the boundary condition is no flux in the circular wall of the

chamber, and the initial condition is maximum concentration in all those points which are just below of the convection unit.

5.5.1 2-Dimensional PDC simulator

A code able to solve this differential problem was written in MATLAB, but using finite differences in problems of partial differential equations, the time of calculus increases quickly as soon as the numbers of dimensions do it. For this reason this code was not useful for our proposals and we decided to use commercial finite element solver software: COMSOL Multiphysics 4.0. This software is very useful in situations where we need to solve the equation over rare two dimensional or three dimensional surfaces.

The geometry of the cell culture chamber was defined in two dimensions (top view) and both initial and boundary conditions were established; no flux boundary condition and maximum concentration under the microchannel placed in the fluidic layer. Properties about materials were also provided and after all definitions, a transient simulation for four minutes was realized.

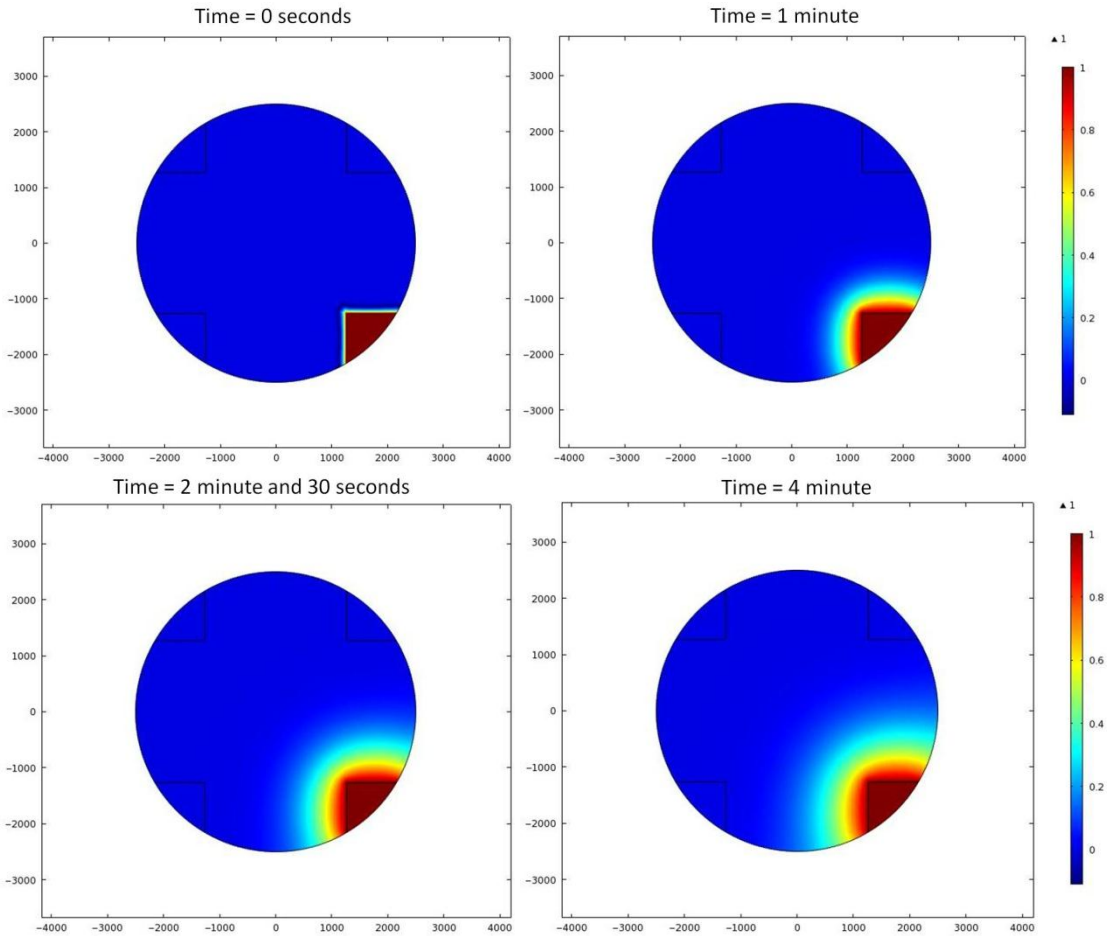

Fig. 5.73 Two dimensional concentration simulation in the cell culture chamber for 0 minutes, 1 min, 2 min and 30 sec and 4 minutes respectively.

Such as it is shown in Fig. 5.73 the theoretical behavior of PDC corresponds to the experimental results observed in Fig. 5.67.

Since the value of the red ink diffusion coefficient is unknown we tried with different simulations until finding diffusivity that fitted with the experimental results. The value was:

$$D = 200\mu m^2 / s$$

This value had the same order of magnitude as the one found for molecules of fluorescein.

5.5.2 1-Dimensional PDC simulator

Although two dimension simulations are interesting to understand the behavior of PDC, to point out the concentration profiles along the segments AB, AC and AD would provide us the information required to compare with the experimental results. These three segments were defined in COMSOL, and simulations were made over them in order to get those one dimensional profiles.

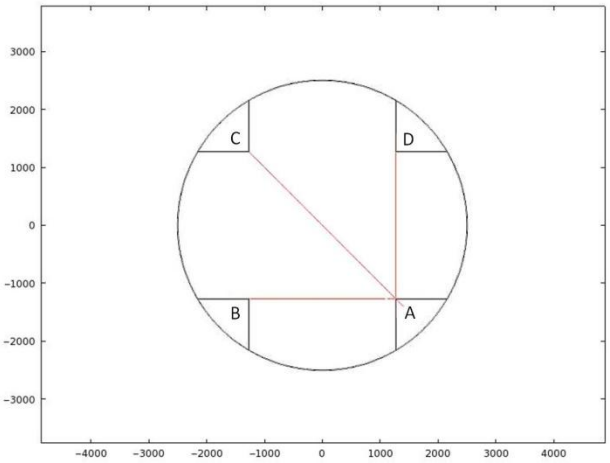

Fig. 5.74 Definition of the segments in COMSOLMultiphysics 4.0.

The results of these simulations were exported to MATLAB and processed there achieving the profiles in each segment.

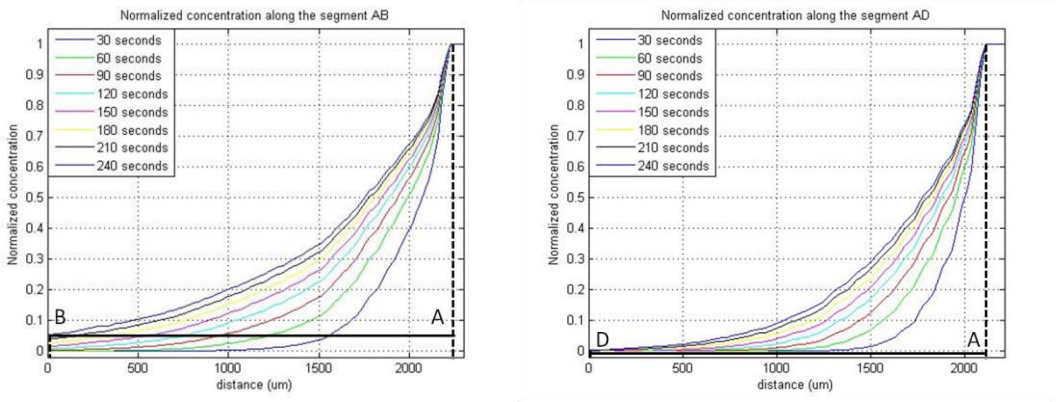

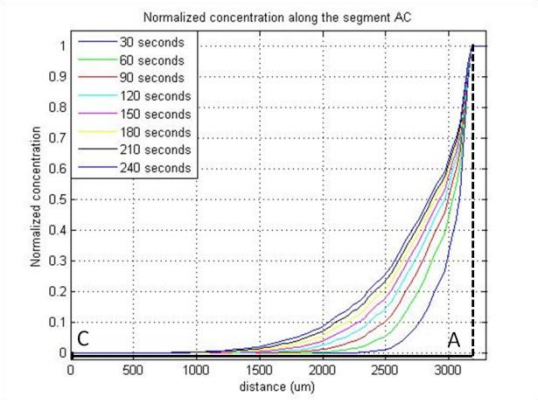

Fig. 5.75 Simulated concentration profiles in PDC of red ink for the three different segments. In each image are plotted the profiles in the segment at every 30 seconds for 4 minutes.

The image above shows the concentration profiles along the segments AB, AD and AC.

5.6 Improving Device: PDC v2.0

The fabrication process of PDC is hard and sometimes non-viable with the final application. All steps which the mortar layer requires may be impossible to execute in small microchannels or in more complex structures. For this reason it was decided to redesign PDC in order to change the fabrication protocol.

The main problem in the fabrication of PDC is the air gap that appears around the membrane when this is sandwiched between the microfluidic and the diffusion layers. This gap interconnects all convection units causing cross-talk interferences between them. To solve this problem we stamped the edges of the membrane with uncured PDMS that once it was placed between the two layers it filled the air gap. As it has been said, this is hard and useless many times. We can change this technique redesigning the device, forcing that all elements in the fluidic layer are kept in a circumference smaller than the membrane.

5.6.1 Design

Reducing the size of the microfluidic layer, we can make possible to keep all channels in the membrane. Doing this, the air gap around the membrane it is not a problem, because the microchannels never pass on the gap, so the fluid cannot reach the gap causing any leakage.

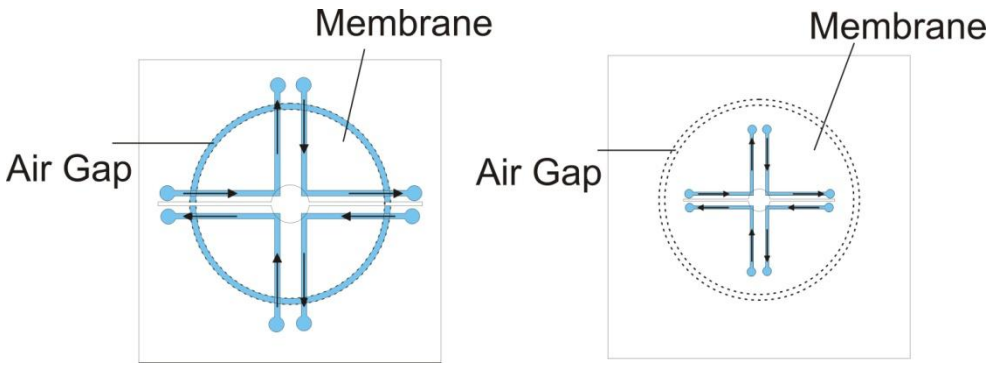

Fig. 5.76 On the left, leakage of fluid through the air gap around the membrane. On the right, non leakage through the gap around the membrane because the whole device is now smaller than the membrane.

In microfluidics corners may produce some micro-turbulences, which affect in the diffusion of particles. In order to ensure that this problem will never occur, these corners may be rounded.

The basic features for the fluidic layer are:

$$w = 400\mu m$$
$$h = 50\mu m$$
$$L = 4.6mm$$

The basic features for the diffusion layer are:

$$Radius = 250\mu m$$
$$w = 150\mu m$$
$$h = 50\mu m$$
$$L = 16.5mm$$

According to the expression (4.30), using this features the minimum mean velocity that would not ensure laminar flow is:

$$\mathrm{Re} < 2300 \Leftrightarrow \bar{v} < \frac{2300 \cdot \upsilon}{2h} = 25.99\, {}^{m}\!/_{s} = 93.56\, {}^{km}\!/_{h} \qquad (5.65)$$

This is a huge velocity in terms of microfluidics, so we can state that the system's dimensions ensure laminar flow inside the microchannels places the fluidic layer.

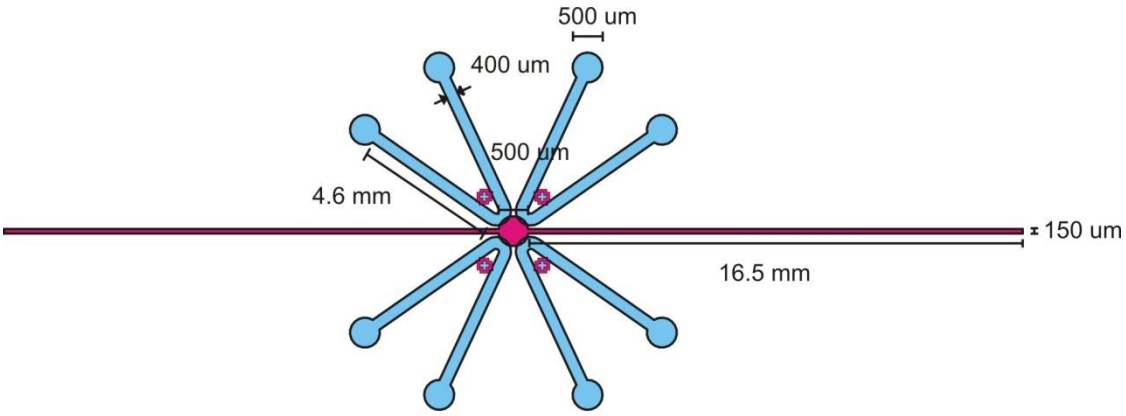

Fig. 5.77 Schematic of PDC v2.0.

Since the dimensions of this device are very small and the alignment of the two layers is critical, some alignment markers are required. For this work it was decided to use cross-shaped markers.

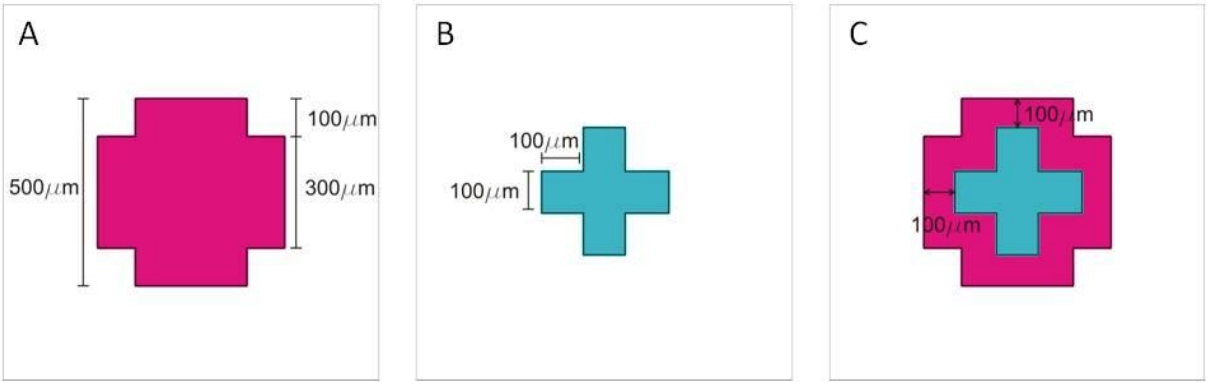

Fig. 5.78 Alignment cross-shaped markers. Alignment marker in the diffusion layer (A). Alignment marker in the microfluidic layer (B). Superposition of the two markers (C).

Because of the small dimensions and the complexity of the shape of each layer, we decided to fabricate the master using photolithography instead of the "Scotch Tape Patterned Method". For this reason in the device design process it was necessary to draw the required masks. Using AutoCAD 2010 drawing software, we designed the masks at real scale.

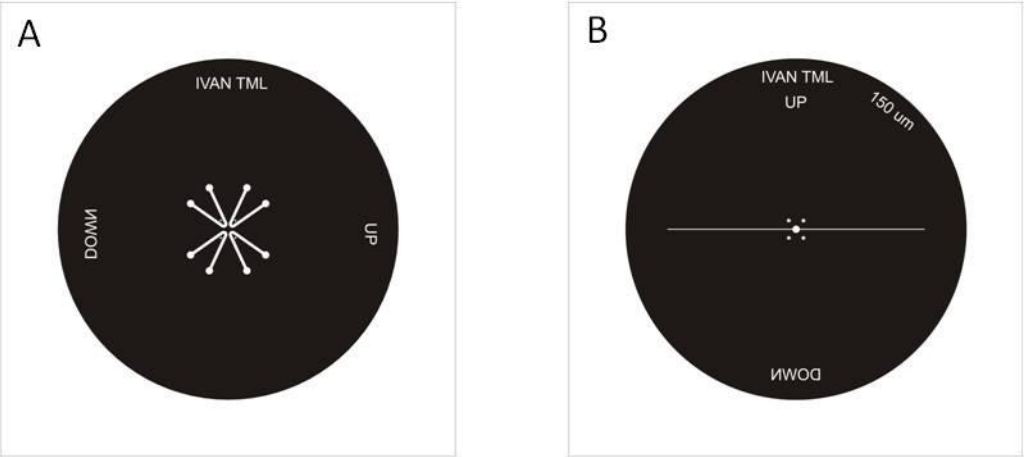

Fig. 5.79 Photolithographic masks at real scale for the microfluidic layer (A) and the diffusion layer (B).

5.6.2 Fabrication: photolithography and surface oxidation by oxygen plasma

As is has been said before, PDC v2.0 master is made by photolithography techniques. This is definitely needed when the dimensions of microchannels and culture cell are very small and also when the shape of the system is complex and hard to replicate by hand. Once the replicas of master are made, the sealing protocol of the two layers to the membrane is made using only oxygen plasma, which is much easier than the mortar layer protocol.

5.6.2.1 Tools, materials and equipments

Masters will be fabricated on 2 inch wafers due to the size of the device using SU-8 as a photocurable resin.

Tools requirement:

- Stainless steel Scalpel or surgical blade with (Feather Safety Razor Co., LTD, Cat. No. 2976#11).
- Polystyrene Petri dish (Fisher Scientific, 100mm x 15mm, Cat. No. 08-757-12).
- 1.22 mm diameter biopsy puncher (Harris Uni-Core, Prod #15074).
- Tweezers.
- Glass slides, pre-cleaned from Manufacturer (Fisher Scientific, 75mm x 50mm x 1mm, Cat. No. 12-550-C).
- 200 nm pore-size polycarbonate membrane (Cat. #29559, Whatman, Piscatway, NJ).
- PDMS silicone elastomer base and curing agent (Sylgard 184, Dow Corning).

Material requirement:

- Silicon wafer, Crystal Technology Inc. (LN: 76.2(Φ) x 1.0mm, Zpol./Pol, W.O.50229, Boule #2008061902, Sequence no. 28-31).

- Negative photoresists SU-8 50, MicroChem Corporation. (Product item #: Y1312690500L1GL, Bt#: 794, Lot #: 08090669).
- Propylene glycol monomethyl ether acetate ≥99.5% (PGMEA as SU-8 developer), Aldrich Chemicals. (CAS 108-65-6, Batch#: 06421TH).
- Isoproppyl Alcohol (Isopropanol), (Fisher Scientific, Cat. No. 67-63-6, Lot #: 102109).
- Acetone, ACE hardware corporation, Newark NJ, USA.
- Ethyl Alcohol (Ethanol), (Fisher Scientific, Cat. No. A962F-1GAL).
- DI water (DI water tap in a lab).

Equipments:

- Plasma oxidizer (Harrick Plasma PDC-001).
- Photoresists spinner WS-400 Lite Series Spin Processor (Laurell Technologies Corporation).
- Hot plate, Corning Incorporated. (Model No. PC-620D, Catalog No. 6795-620D).
- Oven (to work at 65°C).
- UVA Lamp, Uvitron International, Inc. (Model: PORTA-RAY 400R, Part N0. UV1197).
- Lithography exposure facility. (Constructed in Lab using PORTA-RAY 400R UV lamp, UV exposure intensity 7.4mW/cm^2 in full power mode).
- Clear and Dry Air (CDA) supply available in laboratory.
- Glass petri dishes and trays, Corning Incorporated. (Pyrex® 3160).
- Wafer tweezers/forceps. (Reserved for SU-8 fabrication).
- Microscope (Nikon Eclipse Ti).

Personal protective equipments:

- Nitrile gloves (Microflex corporation, catalog no. FFS-700-M).
- UV protection goggles, Sperian Protection. (wip#: 843001P-02-107).
- Eye protection goggles (Fisher scientific, model 19-130-2088).

5.6.2.2 Fabrication process: SU-8 master

Fabrication of microfluidic masters using SU-8 as a photosensitive resin is a very well known field [46]. Its basic protocol is based on 7 different steps:

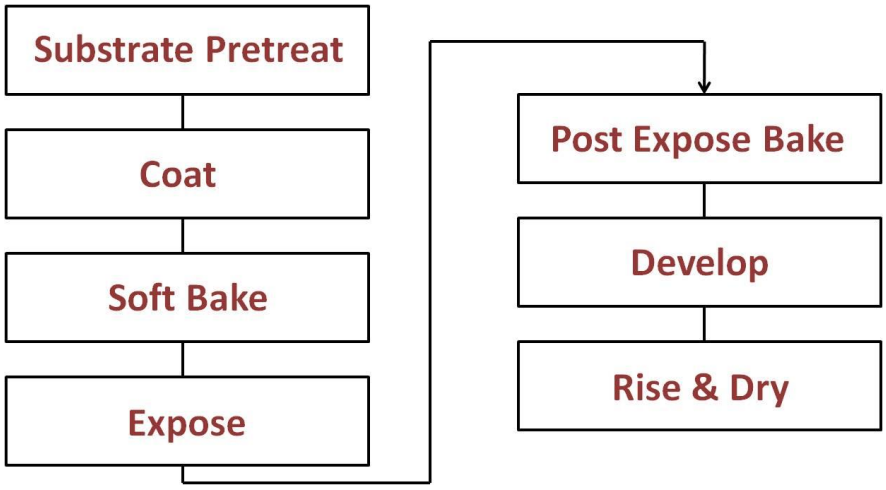

Fig. 5.80 Fabrication protocol for SU-8 masters.

- **Substrate Pretreat:**

To obtain maximum process reliability, substrates should be clean and dry prior to applying the SU-8 resist. A plasma treatment in the plasma cleaner cleans the wafer from any possible dirt incrusted in its surface.

- **Coat:**

SU-8 is a resin designed to produce low defect coatings in a large rage of film thickness using a variety of spin coat conditions.

The wafer spin coating is based on three different steps. First of all **deposition** of resist on the wafer. Then a spread cycle that spreads all resist over the wafer uniformly. Finally a spin cycle that defines the thickness of SU-8 on the wafer. Relation between the film thickness and the spin speed is provided in Table 5.15.

Thickness (µm)	***Spin speed (rpm)***
40	*3000*
50	*2000*
100	*1000*

Table 5.15 Thickness vs. spin speed for SU-8 50.

With SU-8 50 we can only achieve thickness up to 100 µm. For thicker designs it would be needed SU-8 100.

The recommended spin coat conditions are:

- Spread cycle:

Ramp to 500 rpm at 100 rpm/sec acceleration and hold for a total of 10 sec. This is necessary since the viscosity of SU-8 50 is so high.

- Spin cycle:

Ramp to final spin speed (defined in Table 5.15) at an acceleration of 300 rpm/sec and hold for a total of 30 sec.

- **Soft Bake:**

Soft baking is a process used to evaporate the solvent and densify the film after applying the resist to the substrate. SU-8 may be baked either on hot plate or in a convection oven. Better results are achieved stepping the soft baking process, the solvent evaporates out of the film in a more controlled way, the edge beads are reduced and the adhesion of the resist to the substrate is improved. The next table presents the recommendations for two steps contact hot plate baking:

Thickness (µm)	***Soft Baking Time (minutes)***	
	Step 1 65°C	*Step 1 95°C*
40	*5*	*15*
50	*6*	*20*
100	*10*	*30*

Table 5.16 Recommended soft bake process.

- **Expose:**

SU-8 is optimized near UV (350-400 nm) exposure. It is virtually transparent insensitive above 400 nm and is highly absorbent and reactive below 350 nm. Excessive exposure below 350 nm may result in over exposure of the top portion of the resist film. The optimal exposure dose depends on film thickness such as it is shown in Table 5.17.

Thickness (µm)	***Expose Dose (mJ/cm²)***
40	*250-300*
50	*400-500*
100	*500-650*

Table 5.17 Recommended expose dose processes.

The expose dose and the exposition time are related by the intensity of the UV light. The next equation describes this behavior:

$$ExposureTime = \frac{\text{UV exposure dose (mJ/cm}^2\text{)}}{\text{Intensity of UV light (mW/cm}^2\text{)}} \qquad (5.66)$$

- **Post Expose Bake (PEB):**

Post exposure bake must be performed to selectively cross-link exposed portions of the film and also to improve the adhesion to the substrate. SU-8 can be post baking either on a hot plate or in a convection oven.

SU-8 is readily cross-linked and can result in a highly stressed film. This stress may cause cracking and in order to avoid this phenomenon we should apply a slow ramp of temperature or a two steps contact hot plate.

Thickness (µm)	***Post Exposure Baking Time (minutes)***	
	Step 1 65°C	*Step 1 95°C*
40	*2*	*4*
50	*2*	*5*
100	*3*	*10*

Table 5.18 Recommended PEB process.

As we can see in Table 5.18 the post baking time is much lower than the soft baking time.

- **Develop:**

Develop process is responsible to remove the remains of resist that have not been exposed to the UV light. The SU-8 spin coated wafer is immersed in a container filled with PGMEA (or some other dissolvent able to remove SU-8) for a specific time (defined in Table 5.19) while agitation movements are applied to the wafer.

Thickness (µm)	***Development (minutes)***
40	*6*
50	*6*
100	*10*

Table 5.19 Recommended develop processes.

- **Rinse and Dry:**

Rinse and dry processes clean the substrate of remains of PGMEA. The substrate is rinsed briefly with isopropanol and then dried with a gentle stream of dry air (CDA). If a white film is produced during rinse, this is an indication that the substrate has been under developed. Simply immerse the substrate with SU-8 developer to remove the film and complete the development process.

Following these steps a SU-8 master over a silicon wafer was fabricated. For more information on the SU8 negative photoresists and its datasheet [47].

5.6.2.3 Fabrication process: oxygen plasma sealing

Once the masters are done, they are replicated in PDMS (10:1) by pouring the polymer on the master and curing everything in an oven for 1 hour at 65°C.

The sealing process is made by oxidation of the surface by oxygen plasma this time. This process will produce an air gap around the membrane such as it has been explained before, but in this case this is not a problem, because microchannels in the fluidic layer are placed totally on the membrane. Thus there is no possibility to leak thorough the gap.

First of all the cell culture chamber is sealed to a clean glass slide using the plasma cleaner exposing to the plasma for 6 minutes and the replica of the diffusion layer (with the surface with the channels and the chamber facing down) for 3 minutes. Once they have been exposed, we put in contact the two exposed surfaces causing a condensation reaction. We keep the union in the oven at 65°C for 10 minutes and then the covalent union that appears after the reaction is irreversible.

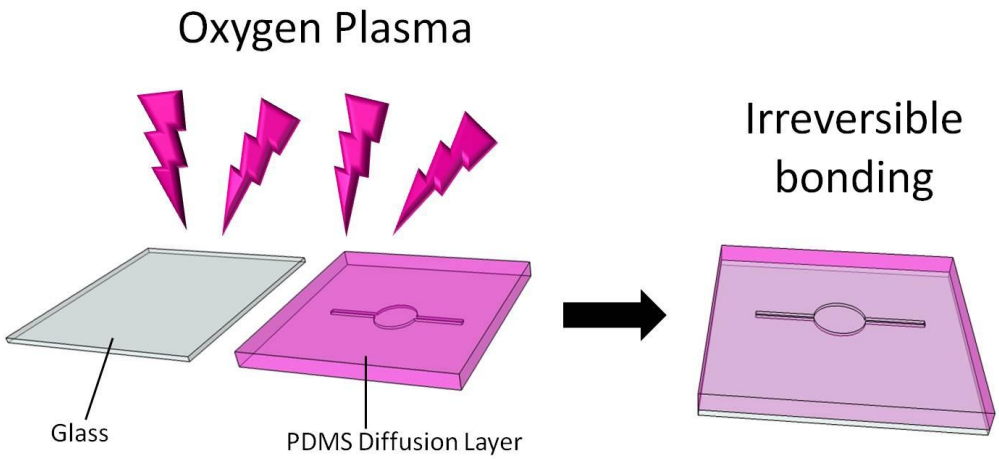

Fig. 5.81 Schematic of surface oxidation of glass and diffusion layer with oxygen plasma and bonding between them.

After that, we want to make holes on the microfluidic layer inlets and outlets. In order to do that we wet the surface with channels of the fluidic layer with some drops of ethanol. We align the diffusion layer and the microfluidic layer putting a transparency in the middle using the microscope. Because the fluidic layer has been wetted with ethanol we can move this layer without problem under the microscope, achieving the perfect alignment easily. After alignment we let the evaporation of the ethanol for 25 minutes.

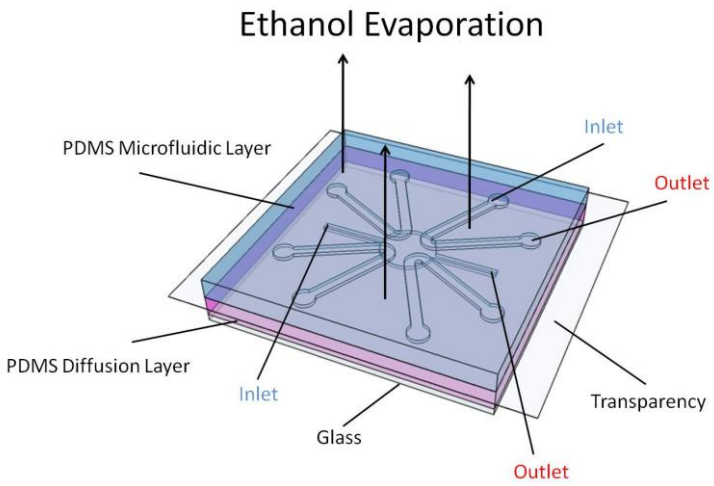

Fig. 5.82 Schematic of holing process. After the ethanol evaporation we make holes in the inlets and outlets of the fluidic and the diffusion layers.

Once this is done, we can make the holes (8 holes inlets/outlets for the channels in the microfluidic layer, and 2 more holes inlet/outlet for the connection to the chamber in the diffusion layer) without damaging the diffusion layer surface because the transparency is protecting this surface.

When the holes are made we separate the fluidic layer from the transparency, and we apply plasma treatment to this layer (channels surface facing up) and to one surface of the polycarbonate membrane for 3 minutes. We have to align the membrane to the fluidic layer, taking care of keep all microchannels under the membrane. Doing that is easier if we wet the membrane with some drops of ethanol, because the ethanol inhibits the sealing for a while and we can move easily the membrane over the layer.

Once the membrane is placed in its right position, we leave the group membrane-fluidic layer for 25 minutes until the ethanol has evaporated. After heat the union in an oven at 65°C for 10 minutes the bonding between PDMS and membrane is not irreversible but is very strong.

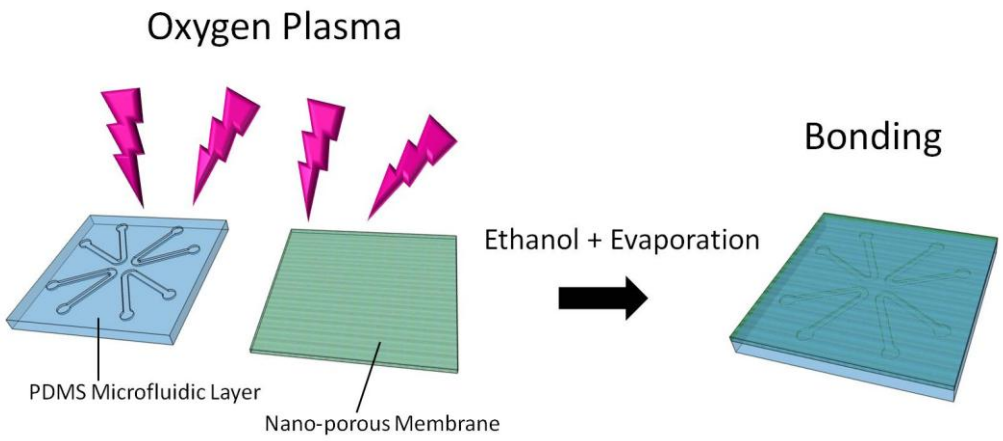

Fig. 5.83 Schematic of surface oxidation of membrane and microfluidic layer with oxygen plasma and bonding between them.

The last step is to fabricate the whole system. We apply plasma treatment to the group glass-diffusion layer and membrane-microfluidic layer for 3 minutes. We need to wet both surfaces with ethanol if we want to align properly, otherwise in the moment that we put the surfaces in contact they would bind directly. We move the layers under the microscope until we align the four cross-shaped markers. Now we only need to wait 25 minutes until complete evaporation of the remaining ethanol and keep the device in the oven at 65°C for 30 minutes. After this time the system is ready to be used.

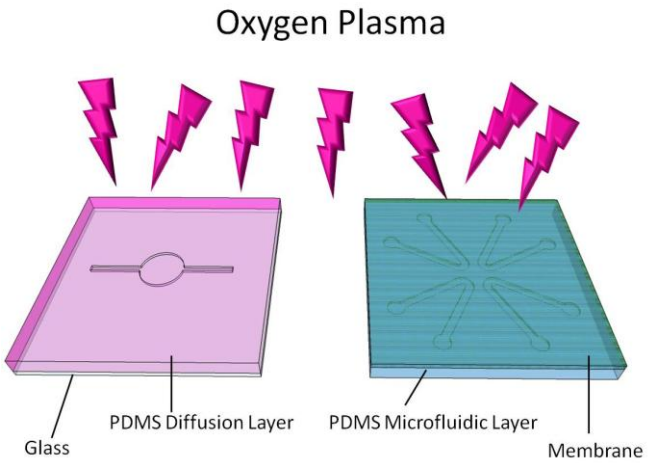

Fig. 5.84 Schematic of surface oxidation of membrane-microfluidic layer and glass-diffusion layer with oxygen plasma.

We keep in the oven the whole system only as a method to be sure of all ethanol has evaporated.

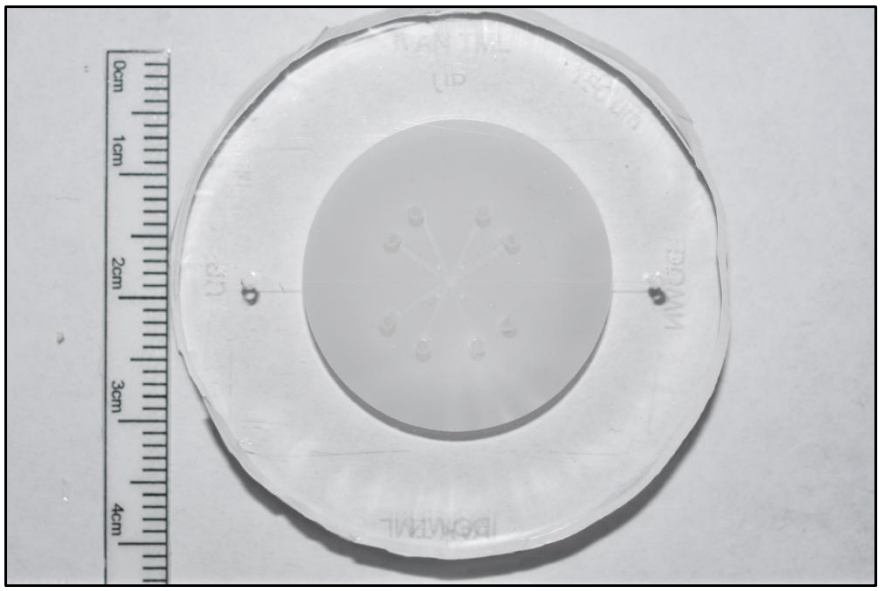

Fig. 5.85 PDC v2.0 after complete the whole fabrication protocol.

Fig. 5.85 shows PDC v2.0 after the execution of all the steps explained in the previous fabrication protocol. Such as we can see in the image the four microchannels

placed in the microfluidic layer remain in the circle formed by the membrane, avoiding in this way any possible leakage through the air gap. We can see that the inlet and outlet channels of the chamber remain out the circle described by the membrane, but this is not a problem because once the chamber is filled with water, there is any flux in these channels. That minimizes a lot the possibility of leaking because there is no pressure difference, but even if some leaking appeared that would not be a problem because in this layer there are no problems with cross-talk interferences.

5.7 Results and Discussions

For simple PDC once again a microfluidic device has been fabricated using the Scotch Tape Patterned Method achieving very good results. Laminar flux inside the convective channels is ensured, enabling the diffusion of particles from the microfluidic layer to the cell chamber across of the nano-porous membrane.

The adhesion of the polycarbonate membrane to the PDMS has succeeded using the mortar layer technique. The air gap that usually appears when some material is forced to be placed in the middle of two others as a sandwich was filled with uncured PDMS achieving no leakage at any convective unit. Otherwise these units might have interconnected appearing cross-talk interferences.

At the same time, it is also true that this mortar layer technique is very tedious and with a low index of reproducibility. Because of that, new techniques for the sealing of polycarbonate membranes to PDMS should be found out.

Experimental and theoretical results presented in images Fig. 5.69 and Fig. 5.75 describe the behavior of PDC as it was expected. With PDC we are able to release a constant concentration of molecules into the cell culture chamber avoiding any convective flux in this layer, and thus avoiding any shear stress issue caused by this convection. Besides in Fig. 5.66 (right) the possibility of reaching a culture cell with more than one chemical indicator at the same time is shown. We can conclude that PDC is a device able to release multiple chemical signals at the same time avoiding shear stress issues yielded by convective flows.

Concentration profiles shown in Fig. 5.69 and Fig. 5.75 have similarities and differences. In these images we can observed how in both cases the diffusion of particles arrive to further positions along the segment AB. In the same way, both experimental and theoretical results revels that the segment with lower diffusion is AD.

Finally some differences are between simulations and experimental profiles. Especially these differences appear in the shape of these profiles where in the theoretical case profiles shown an exponential form, instead of the experimental profiles where the form is similar to an "*S*" shapes.

As we said before new methods to seal the polycarbonate membrane to PDMS were necessary to improve the fabrication protocol of PDC. The mortar layer technique is

useful but too hard and sometimes unviable. For this reason we decided to redesign the system in order to reduce its dimensions and fit all microchannels inside the membrane. Doing this the air gap around the membrane is not a problem anymore, and we do not have to use mortar layer to fill that gap. Instead we can seal PDMS easily using oxygen plasma and sandwich the membrane between two layers.

Photolithography as method of fabricating masters allows us to design more complex structures than those that we are able to achieve by hand, which is always a very good point. On the other hand it is slower and more expensive, and some products such as SU-8 or PGMEA are carcinogenic. Many times lithography techniques are exclusively restricted to clean rooms because of the sophisticated instruments and equipment that they need (UV lamps, spinner, chemical hoods, CDA supply...). For this work all of these instruments were available in the laboratory so that was not an important inconvenient.

Lithography masks were printed in a regular inkjet printer using special transparencies because that made the global cost of the device much more inexpensive. We studied the possibilities of these masks and we concluded that they were useful for devices a critical characteristic up to 100 μm, never below this threshold. At the same time we detected that those masters fabricated using these masks had small remains of SU-8.

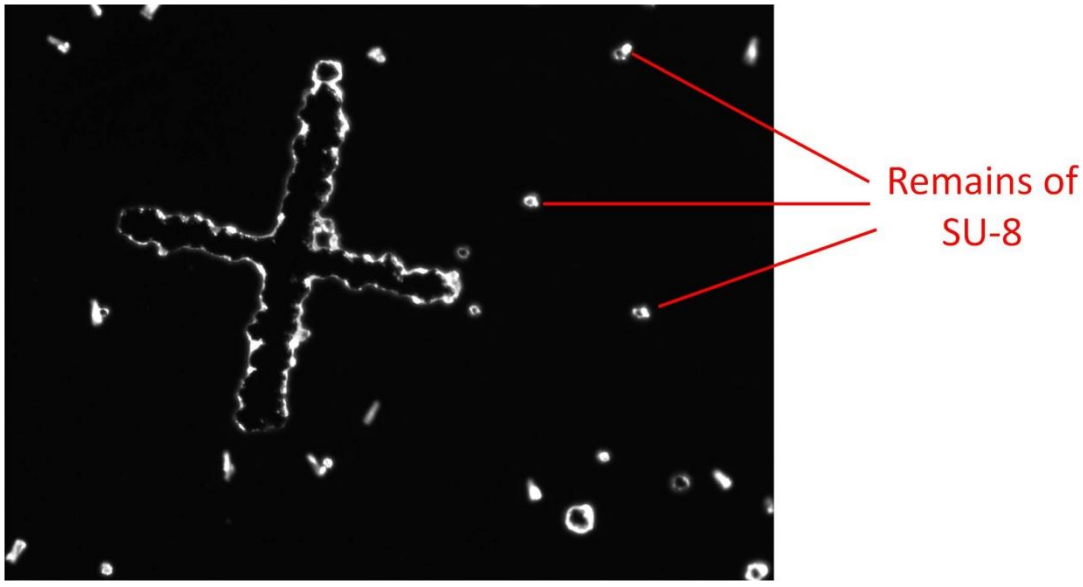

Fig. 5.86 Detail of cross-shaped marker of the silicon wafer. All white dots that appear in the image are remains of SU-8.

These remains of SU-8 only appeared on the surface of the PDMS so never affect to the microchannels or to the cell chamber. We also detected that as soon as the same master was used to replicate more devices, these remains were disappearing. The cause of these remains was the non complete opacity of the mask due to be printed in a regular inkjet printer.

In the fabrication of PDC v2.0 we conclude that using plasma treatment the fabrication of the device is much easier and faster. The amount of PDMS used is much lower and we do not need to use any dissolvent such as heptane that we wasted with the previous protocol.

The adhesion of the microfluidic layer to the polycarbonate membrane was studied by using fluorescent molecules.

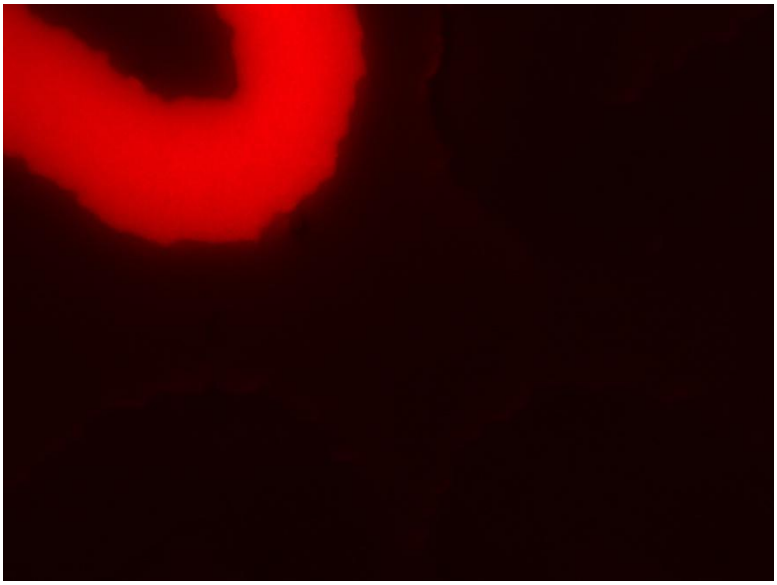

Fig. 5.87 Convection unit filled with fluorescein disodium.

In Fig. 5.87 we can see a convection unit where dissolution 16:1 of DI water and fluorescein disodium is infused at 20 nL/s on the polycarbonate membrane. No leakage appears demonstrating that the adhesion between PDMS and polycarbonate membrane is perfectly useful for our proposals.

In a future work PDC v2.0 would have to characterize using fluorescein and applying the required image post-processing in order to determine the diffusion of molecules in the chamber and compare them with the theoretical results that we already have.

6 CONCLUSIONS AND FUTURE WORK

Molecular communications are the key in the near future for many of the current battles in medicine as well as to make a significant step in the use of nanotechnology at global scale.

In this work we have tried to design a system which permits the study of this type of communications experimentally. A microfluidic device capable to provide a cell culture up to four different chemical signals at the same time avoiding shear stress issues has been fabricated.

It was very important to supply these chemical signals only by means of diffusion processes, because convective flows flowing over cells could cause unwanted reactions. For this reason the understanding of this process was of extreme importance.

In order to achieve this goal it started with the fabrication of a simpler microfluidic device also based on the same phenomenon, diffusion of particles, called T-SENSOR. The device was fabricated using a new process known as "Scotch Tape Patterned Method" that presents the same features as the methods based on lithography being much more inexpensive and simple. It was found that this method is useful until sizes that can be treated with bench top tools, around 300 μm.

This device was experimentally characterized by process of fluorescence. By means of a syringe pump fluorescent molecules were infused into the microchannels and the fluorescent information was captured using a microscope. These results were processed by image techniques until reach the concentration profiles at different positions downstream. This type of characterization is very useful in microfluidic devices and in biological experiments. This experimental characterization provided important qualitative information of the behavior of systems based on diffusion processes.

Theoretical characterization was made by programming a finite differences simulator using MATLAB R2009. With this tool quantitative information could be extracted about T-SENSOR and a more rigorous understanding about the diffusion was acquired. Simulations were done either in 1 or 2 dimensions providing more information about the diffusion the second one. But the longer computation time made us to decide that the 1-dimensional simulator was more useful for our purposes.

In order to determine whether or not numerical methods based on finite differences achieved a reliable approximation of particles diffusion processes, the 1-dimensional simulator was validated using the experimental and theoretical data. Firstly the results of the simulator were compared with those profiles obtained in the experimental characterization, achieving the value of the fluorescein diffusivity by inspection. After that, a theoretical validation of the simulator was done by comparing the results of the simulator with some other results published in scientific journals. In both cases the validation was a complete success achieving the real value of diffusivity in the first one and observing an impressive concordance of results in the second one. Thereby, after experimental and theoretical validations we conclude that the T-SENSOR simulator

based on finites differences provides us a faithful prediction of the behavior of the device.

The experiments with T-SENSOR gave us a strong knowledge about microfluidic devices based on diffusion processes. With this knowledge we designed PDC (Planar Diffusion Chamber) as a microfluidic device capable to "transmit" 4 different signals to a cell culture, "sending" the information only by diffusion. The main idea was to separate the device in three layers where all convective flows would be contained in one layer and all process of diffusion would occur in a different layer. That was possible thanks to the third layer, a nano-porous membrane that allows diffusion across it, but never convective flow.

Because of the sizes of this device were larger than 300 μm the technique used to fabricate the masters was the same used in Chapter 4, using tape as material to pattern a relief structure.

The main problem in the fabrication of this device was how to seal the polycarbonate membrane to a PDMS structure. This problem was solved using a thin layer of uncured PDMS as glue of the three layers. Using this technique we got perfect adhesion between the PDMS and the membrane avoiding any leakage and ensuring that only diffusive flow appear in the cell culture chamber.

Experimental characterization of PDC was done in a similar way to that of Chapter 4. However in this case we did not use fluorescence methods but we only used ink molecules to describe the behavior of PDC. The practical experiment was recorded and then processed frame to frame until obtaining the concentration profiles inside the chamber for different times. This experimental characterization agreed with our first hypothesis.

Theoretical characterization was done in order to get some qualitative data about the system. Firstly a simulator similar to the T-Sensor simulator was programmed, but because it needed an impracticable processing time we decided to use the commercial finite element solver COMSOL Multiphysics 4.0. Using this simulator we got theoretical data about the behavior of PDC.

Comparing the experimental data with the theoretical data we observed that they did not agree very much at the first look. Especially the shape of the profiles was significantly different. After a second look we detected that there were some important similarities between experimental and theoretical results. First of all they agree in which segment appeared more diffusion (AB) they also agreed in which segment there was the lowest diffusion (AC). Although the shapes were different in both cases the behavior was the same, the chamber was filling of molecules as time progressed. In both cases for a very long time we may have seen maximum concentration of molecules at everywhere.

Although the results for this device were promising, the fabrication protocol was hard and sometimes unavailable. The mortar layer technique had to be changed in order

to get a better device with a higher index of reproducibility; that was done by reducing the sizes of the device. The microfluidic layer was designed to make fit all channels on the membrane, and thus avoid any possible leakage through the air gap around the membrane. With these new features this air gap was not a problem anymore, so we could change the sealing protocol.

A new device called PDC v2.0 was fabricated using soft-lithography to fabricate the masters and oxygen plasma to seal the three layers. During the fabrication process we detected that in the masters some unexpected remains of SU-8 appeared after the development because they had been cured during the exposition time. The only explanation was that the mask was not completely opaque and some UV light was able to cross the mask even in the black zones curing the photoresist. That was not a real problem because it did not affect to the channels and also those remains disappeared as soon as the master was replicated.

The adhesion between PDMS and the polycarbonate membrane was observed infusing fluorescein in one microchannel after the sealing process. No leakage was observed with the microscope, demonstrating that the bonding was strong enough for our proposals.

We can conclude that the fabrication of PDC using oxygen plasma instead mortar layer is much easier and faster and the amount of PDMS required in the process is lower. On the other hand the global cost per device is higher for PDC v2.0 and equipment required to fabricate SU-8 masters over silicon substrates is not available to everybody. In addition the second device uses during its fabrication toxic components such as PGMEA or SU-8. For this work PDC v2.0 is the better option because the simplification in the fabrication process worth all of possible disadvantages that it presents.

In the future work PDC v2.0 should be experimentally characterized using fluorescent techniques in order to observe the diffusion of molecules from the fluidic channel the cell chamber. During this characterization more than one convective unit should be working at the same time, and the concentration profiles should be got from these results. In further experiment the device could be used with Belousov-Zhabotinsky reactions which would provide very interesting information. Finally some experiments with real cell cultures should be done sending different chemical signals to these cells and observing how they react.

APPENDIX A

1-D T-Sensor Simulator

This code simulates the behavior of a T-Sensor of 550um width and 3cm longitude for a diffusion coefficient of 340u2/s.

Constants Definition

```
numx=61;%number of grid points in x

numt=2000;%number of iterations and t points in the grid

t(1)=0;

Dn=340;%Diffusion Coefficient


C=zeros(numx,numt);%we inicialize de matrix to 0

% The device width is 550um

dx=550/(numx-1);

dt1=0.045;

% The time simalated is T=numt*dt, so in this case is T=90sec. Because an

% steady state system the knoledge of the time is exactily de the same thant the
knlowledge of the position: V=x/T

x=0:dx:550;


stability1=(Dn*dt1)/(dx^2)
```

```
stability1 =


    0.1821
```

Initial Conditions

The initial condition force maximum concentration at the beginning in one channel and minimum in the other. We are going to browse the matrix through the first column, putting the values of the uniform distribution.

```
for i=1:fix(numx/2)

    C(i,1)=1;

end
```

Main loop

Now we can calculate the coefficients of the matrix C in the time t(j+1), using the results in the time t(j).

```
for j=1:numt

    t(j+1)=t(j)+dt1;

    for i=2:numx-1

        C(i,j+1)=C(i,j)+(C(i+1,j)-2*C(i,j)+C(i-1,j))*(Dn)*(dt1/(dx)^2);

    end

    % Boundary Conditions, no flux at the walls

    C(1,j+1)=C(2,j+1);

    C(numx,j+1)=C(numx-1,j+1);


end


L=3; %The device's longitude is 3cm

Velocity=(L*10000)/(numt*dt1);
```

Plotting results

We are going to plot the concentration profile at 3 different points downstream, for L=0cm, L=0.5cm and L=3cm.

```
figure(1)

plot(x,C(:,1));

title(['Diffusion profile in a T-Sensor, d=550um, L=0cm, Mean
Velocity=',num2str(Velocity),'um/sec. Diffusion Coefficient:',num2str(Dn),'um2/sec']);

xlabel('Normalized Concentration');

ylabel('Position across the w-dimension (um)');

grid;

axis([0 550 -0.1 1.1]);

figure(2)

plot(x,C(:,250));

title(['Diffusion profile in a T-Sensor, d=550um, L=0.5cm, Mean
Velocity=',num2str(Velocity),'um/sec. Diffusion Coefficient:',num2str(Dn),'um2/sec']);

xlabel('Normalized Concentration');

ylabel('Position across the w-dimension (um)');

grid;

axis([0 550 -0.1 1.1]);

figure(3)
```

```
plot(x,C(:,2000));

title(['Diffusion profile in a T-Sensor, d=550um, L=3cm, Mean
Velocity=',num2str(Velocity),'um/sec. Diffusion Coefficient:',num2str(Dn),'um2/sec']);

xlabel('Normalized Concentration');

ylabel('Position across the w-dimension (um)');

grid;

axis([0 550 -0.1 1.1]);
```

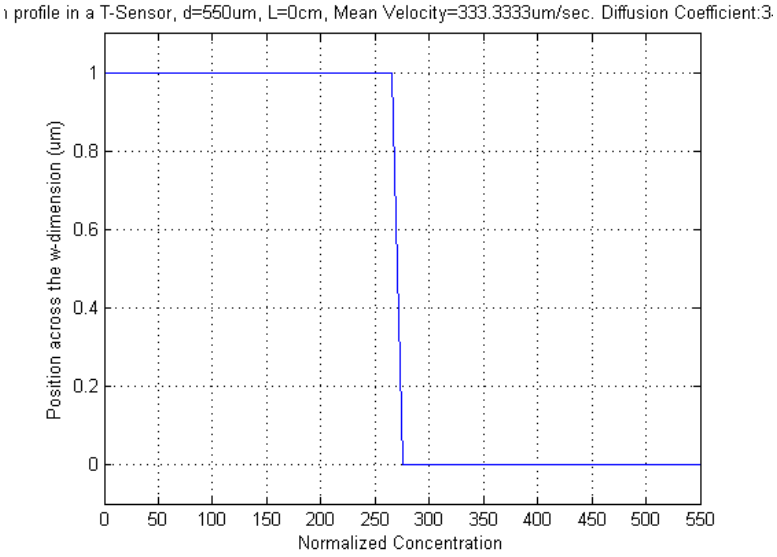

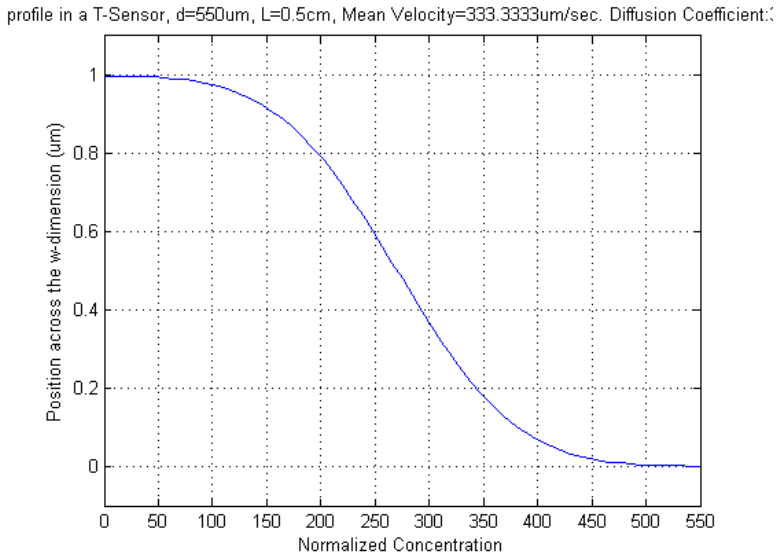

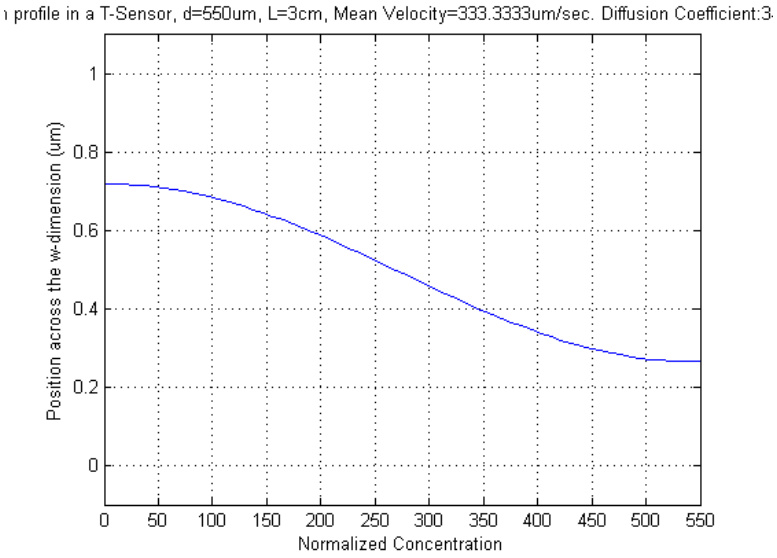
ı profile in a T-Sensor, d=550um, L=3cm, Mean Velocity=333.3333um/sec. Diffusion Coefficient:3
Position across the w-dimension (um)
Normalized Concentration
0
0.2
0.4
0.6
0.8
1
0
50
100
150
200
250
300
350
400
450
500
550

APPENDIX B

2-D T-Sensor Simulator

This code simulates the behavior of a T-Sensor device of any size. This is the function which is called from the user interface. In that interface introduces the information of width, height, and longitude and also the diffusion coefficient. Because the number of points to calculate, the system's memory may not be big enough, so this code have to storage the information in the hard disk in order to avoid this problem.

```
function out = funcion_tsensor(d,w,L,Dn,Vmax,numx,numy,dz)

tic

% d  length in the x-dimension

% w length in the y-dimension

% L length in the z-dimension

% Dn micrometer per second

% Vmax micrometer/sec

% dz distance between z points

% numx number of x points in the grid

% numy number of y points in the grid
```

Constants declaration

```
numiter=7000; %number of iterations

dx=d/(numx-1); %distance between x points

dy=w/(numy-1); %distance between y points

b=dy/dx; %proportionality constant


Vz=zeros(numy);


numz=fix(L/dz); %number of z points in the grid


a=numz/numiter;

num_matrix=fix(a);%number of matrix of size (numx x numy x numiter) we have to
calculate

r=numz-(num_matrix*numiter);%number of residual points to calculate


x=0:dx:d; %vector with x positions
```

```
y=0:dy:w; %vector whit y position


C=zeros(numx,numy,numiter);% Inizialize concentration matrix to 0
Cinitial=zeros(numx,numy);%initial concentration matrix
counter=0;
```

```
Input argument "d" is undefined.


Error in ==> funcion_tsensor at 25
dx=d/(numx-1); %distance between x points
```

Initial Conditions

The initial condition forces maximum concentration in one channel and minimum concentration in the other channel.

```
for i=1:fix(numx/2)%Inicial condition: Concentration max. in all analite microchannel
    for j=1:numy
        for k=1:numz
            C(i,j,1)=1;
        end
    end
end


Cinitial=C(:,:,1);%in the first iteration C and Cinitial are equal


for j=1:numy+1 %parabolic profile velocity in a laminar flow
    Vz(j)=400+Vmax*(1-(((j-1)*dy-w/2)^2/(w/2)^2));%el perfil parabolic sobre pedestal
es una patillada perque no es faci inestable el sistema!!!!
end;
```

Main Loop

This part calculates the concentration in each point of the grid. Is an extension for the 2 dimensional case. The intention is to calculate the points for a grid numx x numy x numz in a matrix, and if the system is bigger, keep this information in the hard disk and reuse the same matrix for save the memory of the system.

```
for q=1:num_matrix+1
```

```
    if q ~= num_matrix+1


        C(:,:,1)=Cinitial; % the initial condition for each matrix depends on the state
in the previous matrix.


        % we can calculate the concentration in the point k+1 using the information

        % in the k point

        for k=1:numiter

            for i=2:numx-1

                for j=2:numy-1

                    C(i,j,k+1)=C(i,j,k)+((C(i+1,j,k)+C(i-1,j,k))+C(i,j+1,k)*b^2+C(i,j-
1,k)*b^2-(2+2*b^2)*C(i,j,k))*(dz/dy^2)*(Dn/Vz(j));

                end


            % Boundary conditions, no flux in the walls. We have to be

            % careful, because in this case we have four walls, top, bottom

            %, left and right walls.

                C(i,1,k+1)=C(i,2,k+1);

                C(i,numy,k+1)=C(i,numy-1,k+1);

            end

            % no flux in the walls boundary condition

            for j=1:numy

                C(1,j,k+1)=C(2,j,k+1);

                C(numx,j,k+1)=C(numx-1,j,k+1);

            end


        Cinitial=C(:,:,numiter); % we use the last iteraton as the initial value in the
next iteration


        counter=counter+1;

        l_distance(counter,C,k,numz);% function which save the matrix with the results
each 10% of the L size

        end


    else % the residual r points, less than numiter

       if r~=0

        C(:,:,1)=Cinitial;


        % we can calculate the concentration in the point k+1 using the information
```

```
            % in the k
            for k=1:r
                for i=2:numx-1
                    for j=2:numy-1
                        C(i,j,k+1)=C(i,j,k)+((C(i+1,j,k)+C(i-1,j,k))+C(i,j+1,k)*b^2+C(i,j-
1,k)*b^2-(2+2*b^2)*C(i,j,k))*(dz/dy^2)*(Dn/Vz(j));
                    end
                    % no flux in the walls boundary condition
                    C(i,1,k+1)=C(i,2,k+1);
                    C(i,numy,k+1)=C(i,numy-1,k+1);
                end
                % no flux in the walls boundary condition
                for j=1:numy
                    C(1,j,k+1)=C(2,j,k+1);
                    C(numx,j,k+1)=C(numx-1,j,k+1);
                end

            counter=counter+1;
            l_distance(counter,C,k,numz);

            end
           else
           end
        end
end
```

Plotting Results

```
mean_distance=fix((3*numx)/4);
width=(numy-1)/2;
plot_results(x,y,mean_distance,width);% we plot the found results

out=1;

toc
```

l_distance Function

This function save a matrix with the concentration points in 10 regions of the L size

```
function correct_distance = l_distance(counter,C,k,numz)


if counter == 1
    A=C(:,:,k);
    save concentration0.txt A -ascii;
elseif counter == fix(0.1*numz)
    A=C(:,:,k);
    save concentration10.txt A -ascii;
elseif counter == fix(0.2*numz)
    A=C(:,:,k);
    save concentration20.txt A -ascii;
elseif counter == fix(0.3*numz)
    A=C(:,:,k);
    save concentration30.txt A -ascii;
elseif counter == fix(0.4*numz)
    A=C(:,:,k);
    save concentration40.txt A -ascii;
elseif counter == fix(0.5*numz)
    A=C(:,:,k);
    save concentration50.txt A -ascii;
elseif counter == fix(0.6*numz)
    A=C(:,:,k);
    save concentration60.txt A -ascii;
elseif counter == fix(0.7*numz)
    A=C(:,:,k);
    save concentration70.txt A -ascii;
elseif counter == fix(0.8*numz)
    A=C(:,:,k);
    save concentration80.txt A -ascii;
elseif counter == fix(0.9*numz)
    A=C(:,:,k);
```

```
        save concentration90.txt A -ascii;
    elseif counter == numz
        A=C(:,:,k);
        save concentration100.txt A -ascii;

    end
    correct_distance=1;
```

```
Input argument "counter" is undefined.

Error in ==> l_distance at 6
if counter == 1
```

Plot function

This function plot the results stored in the hard disk.

```
function correct_plot = plot_results(x,y,distance,width)
aa=load('concentration0.txt');
a=load('concentration10.txt');
b=load('concentration20.txt');
c=load('concentration30.txt');
d=load('concentration40.txt');
e=load('concentration50.txt');
f=load('concentration60.txt');
g=load('concentration70.txt');
h=load('concentration80.txt');
i=load('concentration90.txt');
j=load('concentration100.txt');

figure(2)
surf(y,x,aa);
xlabel('Position y');
ylabel('Position x');
zlabel('Concentration C(x,y) at the begining');

figure(1)
surf(y,x,a);
```

```
xlabel('Position y');
ylabel('Position x');
zlabel('Concentration C(x,y) at the end');


% figure(3)
% surf(y,x,b);
% xlabel('Position y');
% ylabel('Position x');
% zlabel('Concentration C(x,y) in 20% of L');
%
% figure(4)
% surf(y,x,e);
% xlabel('Position y');
% ylabel('Position x');
% zlabel('Concentration C(x,y) in 50% of L');
%
% figure(5)
% surf(y,x,h);
% xlabel('Position y');
% ylabel('Position x');
% zlabel('Concentration C(x,y) in 80% of L');
%
% figure(6)
% surf(y,x,j);
% xlabel('Position y');
% ylabel('Position x');
% zlabel('Concentration C(x,y) in 100% of L');
%
% figure(7)
% title('Diffusion in d dimension');
% hold on
% plot(x,a(:,width),'b');
% plot(x,b(:,width),'r');
% plot(x,c(:,width),'r');
% plot(x,d(:,width),'r');
% plot(x,e(:,width),'r');
% plot(x,f(:,width),'r');
```

```
  % plot(x,g(:,width),'r');
  % plot(x,h(:,width),'r');
  % plot(x,i(:,width),'r');
  % plot(x,j(:,width),'b');
  % xlabel('Position x');
  % ylabel('Concentration C(x)');
```

correct_plot=1;

APPENDIX C

Image processing

This code pretends to extract the concentration profile from a .jpg image and compare this profile with the theoretical in order to find what the best diffusion coefficient is

Get image

```
[name,path]=uigetfile('*.jpg','Select the input JPG file');
fullname=strcat(path,name)
image2=imread(fullname);
image=rgb2gray(image2);
image=double(image);
[row,col]=size(image);
```

```
fullname =

D:\Lab\Probes imatges\Tratamiento de las imagenes del microscopio\20nlsec\15mm.jpg
```

Diffusion coefficient

```
%The key is to change this value until find the theretical caoncentration
%which most agree with the experimental results
Dn=200;
```

Obtaining the concentration information from the image

I take 10 random columns from the image and I extract the light intensity from each pixel. Then I average the 10 different curves.

```
pixel=1:1:row;
pixel=pixel';
for i=1:10
    x1(i)=random('unid',col);
```

```
end
X=zeros(row,10);
for i=1:10
    X(:,i)=image(:,x1(i));
end

A=zeros(row,1);
for j=1:row
    for i=1:10
        A(j)=A(j)+X(j,i);
    end
end
A=A/10;
```

Calculus of the max and min average for normalize the curve

In order to normalize the concentration profile, the maximum and the minimum values are obtained averaging the first points, where the curve has a maximum value and the lasts points where the concentration is minimum.

```
%Firstly a manual way to do that for any imatge it is shown.

% plot(pixel,A);
%
% msgbox('Insert in the prompt in the pixels at max concetration','Max
concentration','help');
% start1=input('First Pixel: ');
% start2=input('Second Pixel: ');
% msgbox('Insert in the prompt in the pixels at min concetration','Min
Concentration','help');
% eend1=input('First pixel: ');
% eend2=input('Second pixel: ');

% But for the images used in this work all of those point have been found
% and they are the following

% 1mm
```

```
% start1=240;
% start2=300;
% eend1=685;
% eend2=1040;
% position=1;
% limit=236;

% %5mm
% start1=193;
% start2=313;
% eend1=701;
% eend2=1040;
% position=5;
% limit=260;

% %10mm
% start1=208;
% start2=252;
% eend1=712;
% eend2=1040;
% position=10;
% limit=268;

%15mm
start1=215;
start2=261;
eend1=721;
eend2=1040;
position=15;
limit=266;

% %20mm
% start1=197;
% start2=256;
% eend1=729;
% eend2=1040;
% position=20;
```

```
% limit=271;


%25mm
% start1=241;
% start2=248;
% eend1=741;
% eend2=1040;
% position=25;
% limit=262;

% %30mm
% start1=280;
% start2=310;
% eend1=745;
% eend2=1040;
% position=30;
% limit=247;

% minavg=mean(A(eend1:eend2));
% B=A-(minavg);
% maxavg=mean(B(start1:start2));
% B=B/maxavg;
% plot(pixel,B);
```

Theoretical profile

"tensor" is the function which calculates the theoretical concentration curve. It returns the maximum and the minimum concentration value because they are needed to normalize the concentration profile coming from the image.

```
[inipoint endpoint]=tsensor(Dn,position);


% This is true only in the cases when the concentration at the walls are 1
% or 0. As the boundary conditions permit this no happen always, sometime a
% correction in the normalization is required. The values at the walls can
% be found using the simulator.
```

```
minavg=mean(A(eend1:eend2));
B=A-(minavg)+endpoint;
maxavg=mean(B(start1:start2));
B=(B/maxavg)*inipoint;
```

```
stability1 =

    0.0900

Warning: Ignoring extra legend entries.
```

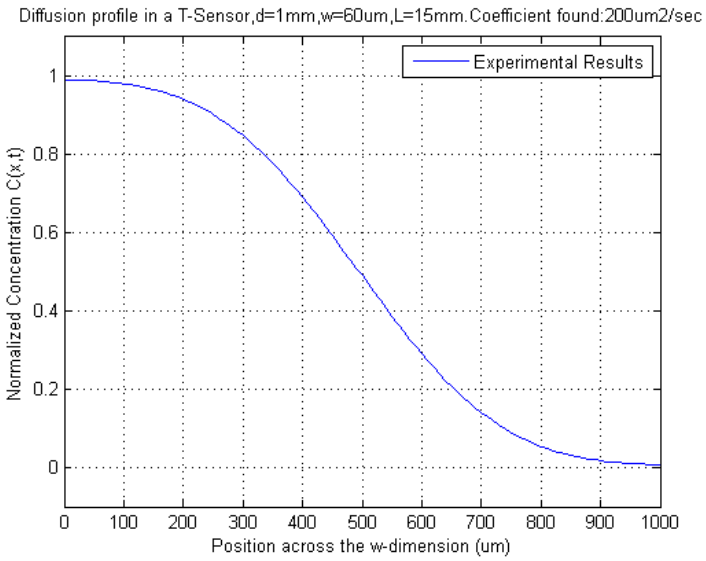

Putting the curve in the center of the graphic

In order to discriminate the channel edges, the method decide is to center the curve at the mean point. As the concentration at 500um has to be C=0.5, we center the profile at this point. For do that limit tell us how many pixels there are between the center and one of the walls. There are two possible results for limit, one for each wall, and sometime does not agree. In this case the minimum value is chosen

```
[valueCenter,posCenter]=min(abs(B-0.5));
Con=B((posCenter-limit):(posCenter+limit));
```

Plotting the normalize concentration curve

```
[sizeC,u]=size(Con);
y=0:1000/(sizeC-1):1000; %Vector with spatial information
y=y';

plot(y,Con,'r');
axis([0 1000 -0.1 1.1]);
grid on
hold on
```

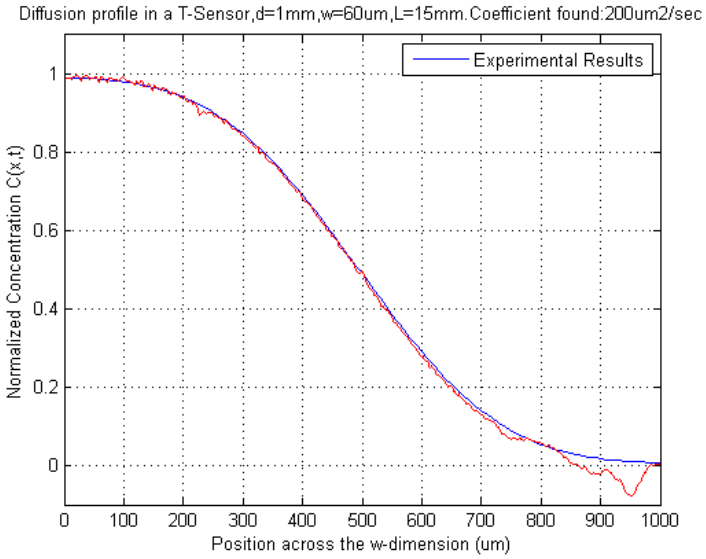

APPENDIX D

PDC image processing

This code pretends to process results coming from the experiments with PDC. Concentration profiles are extracted from the frames captured in a video at 24 fps.

```
clear all;
```

Get image from video

```
frames=video2frame;
```

Distances of each segment are defined in micrometers.

```
segmentAB=2300; %AB 3mm
segmentAD=3300; %AD 3.22mm
segmentAC=3860; %AC 3.86mm
```

Segment AB

Concentration profiles along of the segment AB. Five rows of pixels are taken from each capture and averaged in order to reduce the unwanted effects of shadows.

Initialization of variables

```
row=5;
col=46;
numFrames=13;
intensity=zeros(col,numFrames);
pixels=1:1:col;
arrayAB=0:segmentAB/(col-1):segmentAB;
```

Average of 5 rows of pixels

```
for i=1:9
    B(:,:,i)=frames(53:57,20:65,i);
    v=mean(B(:,:,i),1);
    intensity(:,i)=v';
end
```

Main loop AB

```
for i=1:9

    % In order to normalize all of these profiles the maximum concentration
    % is taken as the average of the first five points after the corner of the
    % microchannel.
    minavg=mean(intensity(30:35,i));
    aux=intensity(:,i)-minavg;

    lowmatrix=frames(34:69,19:22,i)-minavg;
    aux_mean0=mean(lowmatrix,1);
    mean0=mean(aux_mean0,2);

    maxavg=max(aux);

    intensityNorm_AB(:,i)=1-aux/mean0;

    % Intensity pfrofiles are smoothed.
    intensityNorm2_AB(:,i)=smooth(intensityNorm_AB(:,i),4);
end
```

Plotting normalizing concentration curves

```
figure(2)
plot(arrayAB,intensityNorm2_AB(:,2),'b');
hold on
axis([0 segmentAB -0.1 1.5]);
plot(arrayAB,intensityNorm2_AB(:,3),'g');
```

```
hold on

axis([0 segmentAB -0.1 1.5]);

plot(arrayAB,intensityNorm2_AB(:,4),'r');

hold on

axis([0 segmentAB -0.1 1.5]);

plot(arrayAB,intensityNorm2_AB(:,5),'c');

hold on

axis([0 segmentAB -0.1 1.5]);

plot(arrayAB,intensityNorm2_AB(:,6),'m');

hold on

axis([0 segmentAB -0.1 1.5]);

plot(arrayAB,intensityNorm2_AB(:,7),'y');

hold on

axis([0 segmentAB -0.1 1.5]);

plot(arrayAB,intensityNorm2_AB(:,8),'k');

hold on

axis([0 segmentAB -0.1 1.5]);

plot(arrayAB,intensityNorm2_AB(:,9),'-b');

hold on

axis([0 segmentAB -0.1 1.5]);

grid on

title('Normalized concentration along the segment AB');

xlabel('Distance (um)');

ylabel('Normalized concentration');

legend('30 seconds','60 seconds','90 seconds','120 seconds','150 seconds','180
seconds','210 seconds','240 seconds');
```

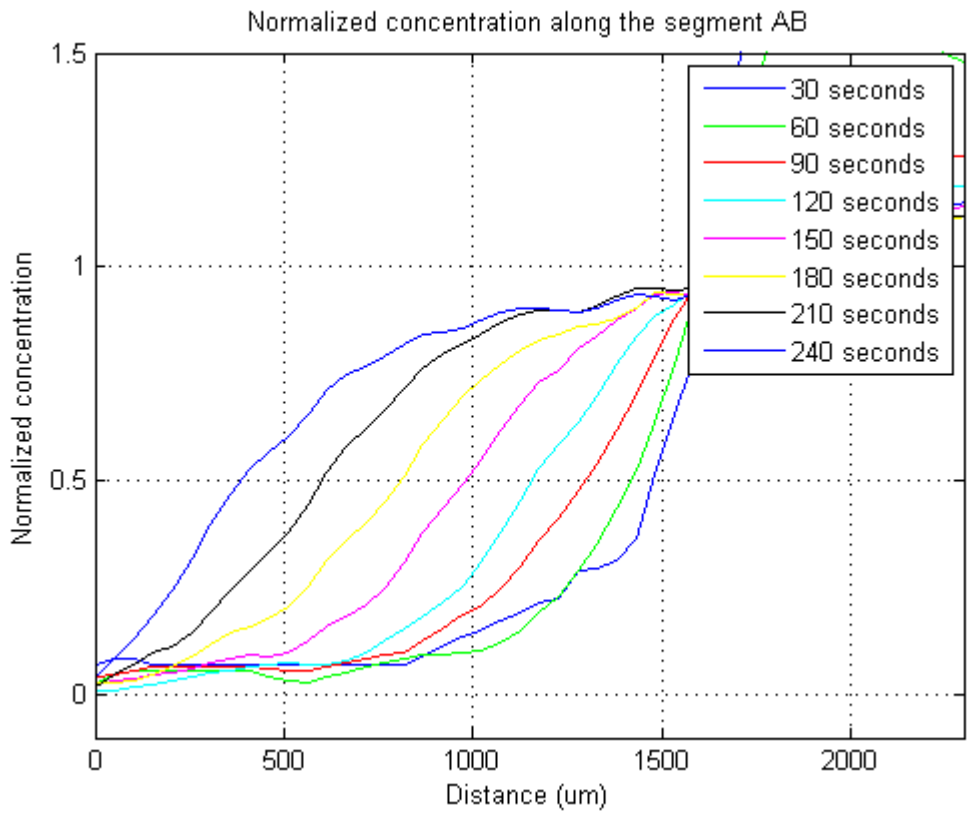

Segment AD

Concentration profiles along of the segment AD. Five columns of pixels are taken from each capture and averaged in order to reduce the unwanted effects of shadows.

Initialization of variables

```
row=46;
col=5;
numFrames=9;
intensity=zeros(row,numFrames);
pixels=1:1:row;
arrayAD=0:segmentAD/(row-1):segmentAD;
```

Average of 5 rows of pixels

```
for i=1:9
    C(:,:,i)=frames(20:65,52:56,i);
```

```
    v=mean(C(:,:,i),2);
    intensity(:,i)=v;
end
```

Main loop AD

```
for i=1:9

    % In order to normalize all of these profiles the maximum concentration
    % is taken as the average of the first five points after the corner of the
    % microchannel.
    minavg=mean(intensity(34:35,i));
    aux=intensity(:,i)-minavg;

    % Calculus of mean concentration around 0.
    lowmatrix=frames(22:25,39:66,i)-minavg;
    aux_mean0=mean(lowmatrix,1);
    mean0=mean(aux_mean0,2);

    maxavg=max(aux);

    intensityNorm_AD(:,i)=1-aux/mean0;

    % Curve smoothing.
    intensityNorm2_AD(:,i)=smooth(intensityNorm_AD(:,i),4);
end
```

Plotting concentration curves

```
figure(4)
plot(arrayAD,intensityNorm2_AD(:,2),'b');
hold on
axis([0 segmentAD -0.1 1.5]);
plot(arrayAD,intensityNorm2_AD(:,3),'g');
hold on
axis([0 segmentAD -0.1 1.5]);
plot(arrayAD,intensityNorm2_AD(:,4),'r');
```

```
hold on

axis([0 segmentAD -0.1 1.5]);

plot(arrayAD,intensityNorm2_AD(:,5),'c');

hold on

axis([0 segmentAD -0.1 1.5]);

plot(arrayAD,intensityNorm2_AD(:,6),'m');

hold on

axis([0 segmentAD -0.1 1.5]);

plot(arrayAD,intensityNorm2_AD(:,7),'y');

hold on

axis([0 segmentAD -0.1 1.5]);

plot(arrayAD,intensityNorm2_AD(:,8),'k');

hold on

axis([0 segmentAD -0.1 1.5]);

plot(arrayAD,intensityNorm2_AD(:,9),'-b');

hold on

axis([0 segmentAD -0.1 1.5]);

grid on

title('Normalized concentration along the segment AD');

xlabel('Distance (um)');

ylabel('Normalized concentration');

legend('30 seconds','60 seconds','90 seconds','120 seconds','150 seconds','180
seconds','210 seconds','240 seconds');
```

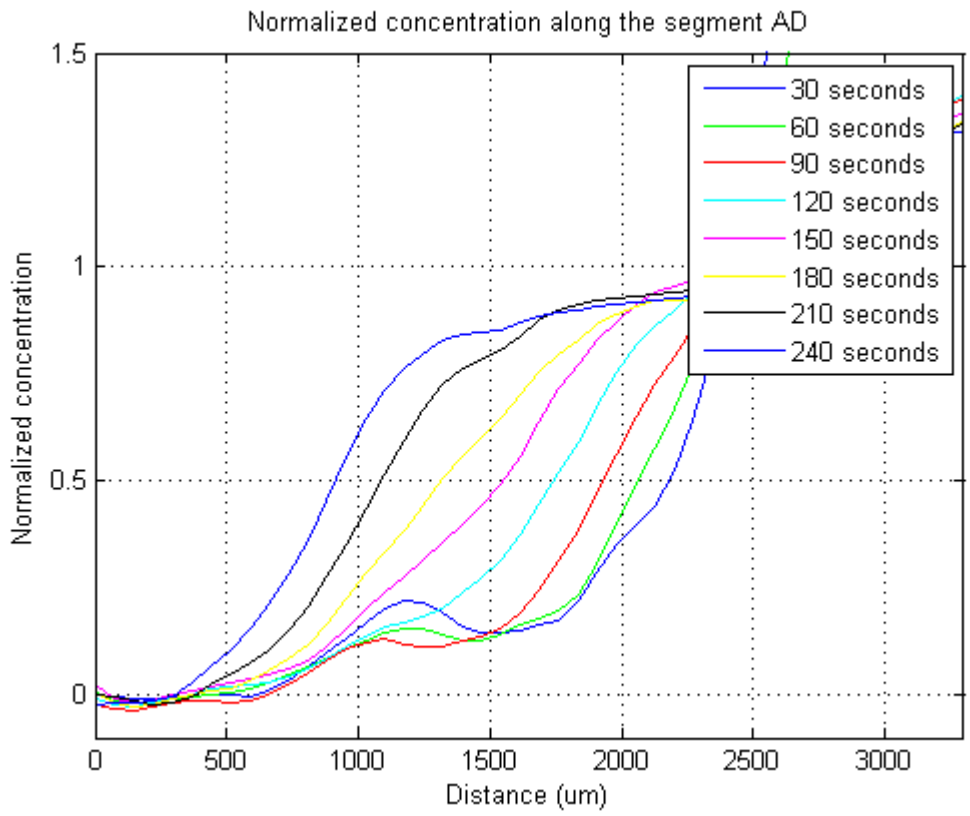

Segment AC

Concentration profiles along of the segment AC.

Initialization of variables

```
row=38;
col=38;
numFrames=9;
intensity=zeros(row,numFrames);
pixels=1:1:row;
arrayAC=0:segmentAC/(row-1):segmentAC;
```

Getting pixels in diagonal AC

```
for i=1:9
    D(:,:,i)=double(frames(20:59,20:59,i));
    for k=1:row
```

```
            diagonal(k,i)=D(k,k,i);
        end
    end
```

Main loop AC

```
    for i=1:9
        minavg=mean(diagonal(34:36,i));
        aux=diagonal(:,i)-minavg;

        maxavg=max(aux);

        intensityNorm_AC(:,i)=1-aux/maxavg;

        % Curve smoothing.
        intensityNorm2_AC(:,i)=smooth(intensityNorm_AC(:,i),5);
    end
```

Plotting concentration curves

```
    figure(6)
    plot(arrayAC,intensityNorm2_AC(:,2),'b');
    hold on
    axis([0 segmentAC -0.1 1.5]);
    plot(arrayAC,intensityNorm2_AC(:,3),'g');
    hold on
    axis([0 segmentAC -0.1 1.5]);
    plot(arrayAC,intensityNorm2_AC(:,4),'r');
    hold on
    axis([0 segmentAC -0.1 1.5]);
    plot(arrayAC,intensityNorm2_AC(:,5),'c');
    hold on
    axis([0 segmentAC -0.1 1.5]);
    plot(arrayAC,intensityNorm2_AC(:,6),'m');
    hold on
    axis([0 segmentAC -0.1 1.5]);
    plot(arrayAC,intensityNorm2_AC(:,7),'y');
```

```
hold on

axis([0 segmentAC -0.1 1.5]);

plot(arrayAC,intensityNorm2_AC(:,8),'k');

hold on

axis([0 segmentAC -0.1 1.5]);

plot(arrayAC,intensityNorm2_AC(:,9),'-b');

hold on

axis([0 segmentAC -0.1 1.5]);

grid on

title('Normalized concentration along the segment AC');

xlabel('Distance (um)');

ylabel('Normalized concentration');

legend('30 seconds','60 seconds','90 seconds','120 seconds','150 seconds','180
seconds','210 seconds','240 seconds');
```

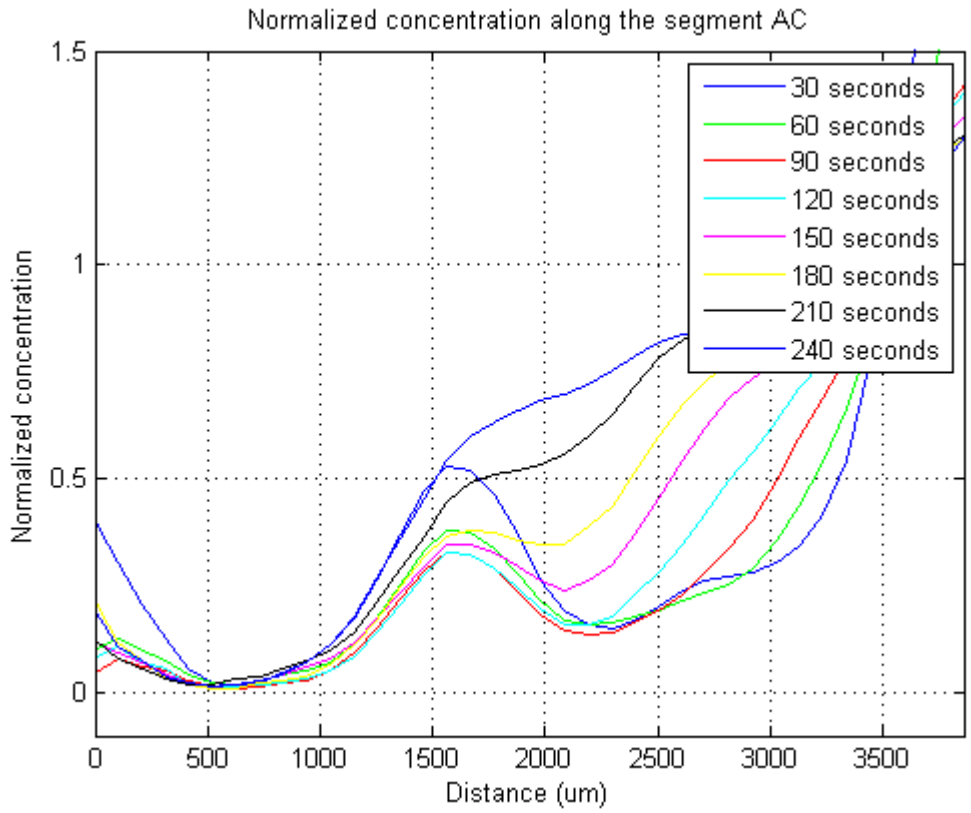

Video to Frame function

Function able to extract frames from an .avi video

```
function frames = video2frame


% Video is loaded on matalb
mov=mmreader('bona_difusio.AVI');
```

Definition of variables

```
fps=24;%frames per second
frame30sec=fps*30;

% The first image is taken at the second number 20. Three dimensional image
% RGB is modified in a new Gray scale image.
aux=rgb2gray(read(mov,480));
```

Cropping image

```
frames(:,:,1)=aux(205:280,284:359);
```

Erasing error

First frame is modified copying "cleaned" pixels onto "dirty" pixels.

```
frames(32:41,29:39,1)=frames(32:41,17:27,1);
```

Main loop

```
for i=1:8
    index=i*frame30sec;

    % Three dimensional images RGB are modified in a new Gray scale images
    aux=rgb2gray(read(mov,index));
```

```
    % Cropping images.
    frames(:,:,i+1)=aux(205:280,284:359);

    % Frames are modified copying "cleaned" pixels onto "dirty" pixels.
    if i<6
        frames(32:41,29:39,i+1)=frames(32:41,17:27,i+1);
    end
    if i==6
        frames(32:41,29:39,i+1)=frames(24:33,37:47,i+1);
    end
    if i==7
        frames(31:36,31:36,i+1)=frames(31:36,38:43,i+1);
    end
end
```

7 REFERENCES

[1] P. Carmeliet and R. K. Jain, "Angiogenesis in cancer and other diseases," *Nature,* vol. 407, pp. 249-257, 2000.

[2] J. Atencia*, et al.*, "The microfluidic palette: A diffusive gradient generator with spatio-temporal control," *Lab on a Chip,* vol. 9, pp. 2707-2714, 2009.

[3] A. B. Shrirao and R. Perez-Castillejos, "Simple fabrication of microfluidic devices by replicating Scotch-tape masters," *Lab on a Chip: Chips and Tips,* 2010.

[4] B. Alberts*, et al.*, *Molecular Biology of the Cell*, 2002.

[5] A. R. Asthagiri and D. A. Lauffenburger, "Bioengineering models of cell signaling," *Annual Review of Biomedical Engineering,* vol. 2, pp. 31-53, 2000.

[6] O. Traub and B. C. Berk, "Laminar shear stress - Mechanisms by which endothelial cells transduce an atheroprotective force," *Arteriosclerosis Thrombosis and Vascular Biology,* vol. 18, pp. 677-685, 1998.

[7] G. M. Walker*, et al.*, "Effects of flow and diffusion on chemotaxis studies in a microfabricated gradient generator," *Lab on a Chip,* vol. 5, pp. 611-618, 2005.

[8] C. Beta*, et al.*, "Chemotaxis in microfluidic devices-a study of flow effects," *Lab on a Chip,* vol. 8, pp. 1087-1096, 2008.

[9] P. F. Davies*, et al.*, "TURBULENT FLUID SHEAR-STRESS INDUCES VASCULAR ENDOTHELIAL-CELL TURNOVER INVITRO," *Proceedings of the National Academy of Sciences of the United States of America,* vol. 83, pp. 2114-2117, 1986.

[10] R. Weiss*, et al.*, "Genetic circuit building blocks for cellular computation, communications, and signal processing," *Natural Computing,* vol. 2, pp. 47-84, 2003.

[11] S. F. Bush, *Nanoscale Communication Networks*, 2010.

[12] I. F. Akyildiz*, et al.*, "Nanonetworks: A new communication paradigm," *Computer Networks,* vol. 52, pp. 2260-2279, 2008.

[13] R. A. Freitas, *Nanomedicine, Volume I: Basic Capabilities*, 1999.

[14] S. Hiyama*, et al.*, "Molecular Communication," in *Proceedings of the 2005 NSTI Nanotechnology Conference*, 2005, pp. 391 - 394.

[15] E. Carafoli, "Calcium signaling: A tale for all seasons," *Proceedings of the National Academy of Sciences of the United States of America,* vol. 99, pp. 1115-1122, February 5, 2002 2002.

[16] W. D. Kepseu and P. Woafo, "Intercellular waves propagation in an array of cells coupled through paracrine signaling: A computer simulation study," *Physical Review E,* vol. 73, 2006.

[17] C. Bustamante*, et al.*, "Mechanical processes in biochemestry," *Annual Review of Biochemistry,* vol. 73, pp. 705-748, 2004.

[18] P. Tabeling, *Introduction to Microfluidics*, 2003.

[19] G. M. Whitesides, "The origins and the future of microfluidics," *Nature,* vol. 442, pp. 368-373, 2006.

[20] M. Madou, *Fundamental of Microfabrication*, 2000.

[21] E. S. Koselar Jr and R. R. Reston, "Silicon micromachined gas chromatography system with a thin-film copper phthalocyanine stationary phase and its resulting performance," *Surface and Coatings Technology,* vol. 68-69, pp. 679-685, 1994.

[22] D. J. Harrison*, et al.*, "Capillary electrophoresis and sample injection systems integrated on a planar glass chip," *Analytical Chemistry,* vol. 64, pp. 1926-1932, 1992.
[23] B. Lindstedt*, et al.*, "OSMOTIC PUMPING RELEASE FROM KCL TABLETS COATED WITH POROUS AND NONPOROUS ETHYLCELLULOSE," *International Journal of Pharmaceutics,* vol. 67, pp. 21-27, 1991.
[24] A. E. Kamholz*, et al.*, "Quantitative analysis of molecular interaction in a microfluidic channel: The T-sensor," *Analytical Chemistry,* vol. 71, pp. 5340-5347, 1999.
[25] H. Z. Wang*, et al.*, "Mixing of liquids using obstacles in microchannels," *Biomems and Smart Nanostructures,* vol. 4590, pp. 204-212, 2001.
[26] M. U. Kopp*, et al.*, "Chemical Amplification: Continuous-Flow PCR on a Chip," *Science,* vol. 280, pp. 1046-1048, May 15, 1998 1998.
[27] D. E. Smith and S. Chu, "Response of Flexible Polymers to a Sudden Elongational Flow," *Science,* vol. 281, pp. 1335-1340, August 28, 1998 1998.
[28] S. C. Jacobson*, et al.*, "Precolumn Reactions with Electrophoretic Analysis Integrated on a Microchip," *Analytical Chemistry,* vol. 66, pp. 4127-4132, 1994.
[29] J. P. Abraham*, et al.*, "Heat transfer in all pipe flow regimes: laminar, transitional/intermittent, and turbulent," *International Journal of Heat and Mass Transfer,* vol. 52, pp. 557-563, 2009.
[30] C. Noakes and A. Sleigh, *An Introduction to Fluid Mechanics*, 2009.
[31] A. P. Wong*, et al.*, "Partitioning microfluidic channels with hydrogel to construct tunable 3-D cellular microenvironments," *Biomaterials,* vol. 29, pp. 1853-1861, 2008.
[32] A. Einstein, *Investigations on the Theory of the Brownian Movement*: Dover Publicatio, 1956.
[33] E. L. Cussler, *Diffusion: Mass Transfer in Fluid Systems*: Cambridge University Press, 2009.
[34] J. Philibert, "One and a Half Century of Diffusion: Fick, Einstein, Before and Beyond," *Diffusion Fundamentals,* vol. 4, pp. 1-19, 2006.
[35] R. B. Bird*, et al.*, *Transport Phenomena*, 2001.
[36] Z. Zhenrong*, et al.*, "Roughness characterization of well-polished surfaces by measurements of light scattering distribution," *Optica Applicata,* vol. 40, pp. 811-818, 2010.
[37] B. H. Chueh*, et al.*, "Leakage-free bonding of porous membranes into layered microfluidic array systems," *Analytical Chemistry,* vol. 79, pp. 3504-3508, 2007.
[38] A. E. Kamholz and P. Yager, "Theoretical analysis of molecular diffusion in pressure-driven laminar flow in microfluidic channels," *Biophysical Journal,* vol. 80, pp. 155-160, 2001.
[39] B. A. Finlayson, *Nonlinear analysis in chemical engineering*, 1980
[40] A. E. Kamholz and P. Yager, "Molecular diffusive scaling laws in pressure-driven microfluidic channels: deviation from one-dimensional Einstein approximations," *Sensors and Actuators B-Chemical,* vol. 82, pp. 117-121, 2002.
[41] S. A. Rani*, et al.*, "Rapid diffusion of fluorescent tracers into Staphylococcus epidermidis biofilms visualized by time lapse microscopy," *Antimicrobial Agents and Chemotherapy,* vol. 49, pp. 728-732, 2005.
[42] D. deBeer*, et al.*, "Measurement of local diffusion coefficients in biofilms by microinjection and confocal microscopy," *Biotechnology and Bioengineering,* vol. 53, pp. 151-158, 1997.

[43] N. Li Jeon*, et al.*, "Neutrophil chemotaxis in linear and complex gradients of interleukin-8 formed in a microfabricated device," *Nat Biotech,* vol. 20, pp. 826-830, 2002.
[44] M. A. Unger*, et al.*, "Monolithic microfabricated valves and pumps by multilayer soft lithography," *Science,* vol. 288, pp. 113-116, 2000.
[45] S. Johnson, *Stephen Johnson on Digital Photography*, 2006.
[46] D. C. Duffy*, et al.*, "Rapid Prototyping of Microfluidic Systems in Poly(dimethylsiloxane)," *Analytical Chemistry,* vol. 70, pp. 4974-4984, 1998.
[47] *http://www.microchem.com/*.